A METHODOLOGY FOR CHARACTERIZING PAVEMENT RUTTING CONDITION USING EMERGING 3D LINE LASER IMAGING TECHNOLOGY

A Dissertation
Presented to
The Academic Faculty

by

Feng Li

In Partial Fulfillment

of the Requirements for the Degree
Doctor of Philosophy in Civil Engineering

Georgia Institute of Technology

December 2012

A METHODOLOGY FOR CHARACTERIZING PAVEMENT RUTTING CONDITION USING EMERGING 3D LINE LASER IMAGING TECHNOLOGY

Approved by:

Dr. Yi-Chang James Tsai, Advisor
School of Civil and Environmental Engineering
Georgia Institute of Technology

Dr. Elliot Moore II
School of Electrical and Computer Engineering
Georgia Institute of Technology

Dr. James Lai
School of Civil and Environmental Engineering
Georgia Institute of Technology

Dr. Zhaohua Wang
Center for Geographic Information Systems
Georgia Institute of Technology

Dr. Michael D. Meyer
School of Civil and Environmental Engineering
Georgia Institute of Technology

Date Approved: June 11, 2012

ACKNOWLEDGEMENTS

First of all, I would like to thank my advisor, Dr. Yi-Chang James Tsai, for his endless support in the past five years. He has kept me on the right path toward completing my PhD, inspired me to think critically, and taught me to learn and work proactively, for which I am extremely grateful.

I would also like to thank Dr. James Lai, Dr. Michael D. Meyer, Dr. Elliot Moore II, and Dr. Zhaohua Wang sitting on my committee, and for their valuable advice. I am most grateful to Dr. Zhaohua Wang for his understanding, support, and friendship which always helped me to get through this tough process. Thanks also owe to Dr. Lai for his kindness and support. I would like to thank Dr. Elliot Moore II for advising me to use the overlapping-reducing method to solve large-scale problems, which is a brilliant idea. I would like to thank Dr. I-lin Wang for advising me to use the linear programming technique in solving engineering problems. Many thanks also owe to Dr. Michael Rodgers for many wonderful discussions.

I would like to acknowledge the support from Mr. Jim Leben and Mr. Eric Pitts in Georgia Department of Transportation. Their expert knowledge and support have been invaluable. I would also like to acknowledge Mr. Stephen Kollinger and staff from the Savannah Precision Machine for their dedicated service in delivering accurate CMM measurements.

Sincere thanks are also given to my colleagues and friends, Ye Lu, Chengbo, Rodger, Dr. Yi-shih Chung, Danjue, Weina, Chenglong, Ross, Zach, Sam, Thomas, and all others that I have not listed here.

Last, but no means least, I thank my husband Dapeng for his support and patience at all times. Special thanks also owe to my parents and sisters for their encouragement and unconditional trust and love.

TABLE OF CONTENTS

LIST OF TABLES

LIST OF FIGURES

SUMMARY

Pavement rutting is one of the major asphalt pavement surface distresses affecting pavement structure integrity and driving safety and is also a required performance measure specified in the Highway Performance Monitoring System (HPMS). Manual rutting measurement is still conducted by many state Departments of Transportation (DOTs), like Georgia DOT; however, it is time-consuming, labor-intensive, and dangerous. Although point-based rut bar systems have been developed and utilized by state DOTs to measure rutting conditions, they often underestimate rut depth measurements. There is an urgent need to develop an automated method to accurately and reliably measure rutting conditions. With the advance of sensing technology, emerging 3D line laser imaging technology is capable of collecting high-resolution 3D range data at highway speed (e.g., 100 km/h) and, therefore, holds a great potential for accurately and repeatedly measuring pavement rutting condition. The main contribution of this research includes a methodology, along with a series of methods and procedures, for the first time, developed utilizing emerging 3D line laser imaging technology to improve existing 1D rut depth measurement accuracy and repeatability and to measure additional 2D and 3D rutting characteristics. These methods and procedures include: (1) a threshold-based outlier removal method employing the multivariate adaptive regression splines (MARS) technique to remove outliers caused by non-rutting features, such as wide transverse cracks and potholes; (2) a modified topological-ordering-based segment clustering (MTOSC) method to optimally partition the continuous roadway network into segments with uniform rutting condition; (3) an overlapping-reducing heuristic method to solve large-scale segmentation problems; (4) a network-level rutting condition assessment procedure for analyzing 3D range data to statistically interpret the pavement rutting condition in support of network-level pavement management decisions; (5) an

isolated rut detection method to determine the termini, maximum depth, and volume of isolated ruts in support of project-level maintenance operations. Comprehensive experimental tests were conducted in the laboratory and the field to validate the accuracy and repeatability of 1D rut depth obtained using the 3D range data. Experimental tests were also conducted in the laboratory to validate the accuracy of 3D rut volume. Case studies were conducted on one interstate highway (I-95), two state routes (SR 275 and SR 67), and one local road (Benton Blvd.) to demonstrate the capability of the developed methods and procedures. The results of experimental tests and case studies show that the proposed methodology is promising for improving the rutting measurement accuracy and reliability. This research is one of the initial effort in studying the applicability of this emerging sensing technology in pavement management. And the outcomes of this research will play a key role in advancing state DOTs' existing pavement rutting condition assessment practices.

CHAPTER 1 INTRODUCTION

1.1 Background

Pavement rutting is one of the major asphalt pavement surface distresses affecting pavement structure integrity and driving safety. It is, also, a required performance measure specified in the Highway Performance Monitoring System (HPMS) (Federal Highway Administration, FHWA 2010). Manual rutting measurement is still conducted by many state Departments of Transportation (DOTs), like Georgia DOT; however, it is time-consuming, labor-intensive, and dangerous. Although point-based rut bar systems have been developed and utilized by state DOTs to measure rutting conditions (McGhee 2004), they often underestimate the rut depths. This is because point-based systems only sample a limited number of points in the transverse direction, which may not locate exactly on the peaks and valleys of ruts because of the wandering of the survey vehicle, varying lane widths, and varying rut shapes. There is an urgent need to develop an automated method to accurately and reliably measure the rutting condition data.

With the advancement of sensing technology, 3D range-based systems have been developed for pavement surface condition data collection. Some 3D range-based systems utilize a line laser and were developed based on the triangulation principle. They are also known as 3D line laser imaging systems (referred as 3D line laser systems hereafter). Examples of 3D line laser systems include a real-time 3D scanning system (Li et al. 2009; 2010), the VRUT by Texas DOT (TxDOT) (Huang et al. 2012), the PaveVision3D (Wang et al. 2011; 2012), the Pathway 3D Data Acquisition System by Pathway Services Inc. (2012), and the Laser Rut Measurement System (LRMS) and the Laser Crack Measurement System (LCMS) by INO (Laurent et al. 1997; Laurent et al. 2008; INO 2012). The 3D line laser systems are capable of acquiring high-resolution (as high as 1 mm in the transverse direction and 5 mm in the driving direction) 3D range data of the

pavement surface at highway speed (100 km/h), and, therefore, holds a great potential for accurately and repeatedly measuring pavement rutting condition. Research is needed to develop methods and algorithms to take advantage of this sensing technology to improve existing pavement rutting condition data collection and associated network-level and project-level pavement management practices and support new applications, such as project-level isolated rutting detection and cause diagnosis. A commercially-available 3D range-based system, LCMS, is used in this research to collect 3D range data for testing the developed methods and algorithms.

1.2 Research Objectives

The main objective of this research is to develop a methodology that utilizes the high-resolution 3D line laser imaging technology to improve existing 1D rut depth measurement accuracy and repeatability and to measure additional 2D and 3D rutting characteristics to support existing pavement management systems (PMSs). The outcomes of this research will play a key role in advancing state DOTs' existing pavement rutting condition assessment practices. The following are detailed objectives:

- Develop a sensor-based and spatially-enabled pavement rutting condition assessment methodology that utilizes the emerging 3D line laser imaging technology to improve existing 1D rut depth measurement accuracy and repeatability and to measure additional 2D and 3D rutting characteristics.
- Propose methods and procedures to substantiate the proposed methodology, including the following:
    - A method to remove outliers in the 1D rut depth measurements caused by non-rutting features, such as wide transverse cracks and potholes.
    - A method to partition a continuous roadway network into segments with uniform rutting condition to apply cost-effective treatments for each homogeneous segment.

    - A procedure to derive and report the network-level rutting information in support of the network-level pavement management. The proposed procedure will deliver a meaningful rutting representation that can be directly used in current GDOT's PMS. It will improve the accuracy and repeatability of the network-level rutting condition assessment.
    - A method to detect isolated ruts for project-level, low-cost, localized treatments. Isolated ruts are not recorded in current PMS because it is difficult to manually collect such detailed levels of information. A method will be proposed to detect isolated ruts and support project-level pavement maintenance operations.
- Validate the rutting measurement accuracy and repeatability of the 3D line laser system by conducting comprehensive experimental tests in the laboratory and in the field with established ground truths.
- Conduct case studies on actual roadways, including interstate highways, state routes, and city roads, to assess the applicability of proposed methods and procedures.

1.3 Organization of the Dissertation

This dissertation focuses on the development of a sensor-based and spatially-enabled pavement rutting condition assessment methodology that uses emerging 3D line laser imaging technology to accurately and repeatedly measure the 1D rut depth and additional 2D/3D rutting characteristics in support of various network-level and project-level pavement management decisions. The proposed methodology can be used to analyze the detailed level of data and aggregate them to multi-scales to support various pavement management decisions, such as network-level rutting condition assessment and identification of isolated rutting spots that a cost-effective localized treatment can be

applied. The proposed methodology, experimental tests, and case studies are discussed in the dissertation. The remainder of this dissertation is organized as follows.

Chapter 2 reviews manual and automated rutting measurement technologies, as well as the practices adopted by state DOTs to assess and report rutting conditions. Additionally, this chapter identifies issues with data used for rutting progression modeling and the potential benefits of using high-resolution rutting data collected with a 3D line laser system to improve rutting progression modeling. This chapter also reviews existing homogeneous segmentation methods to partition pavement condition data into uniform segments in order to apply cost-effective treatments to each of the uniform segments. Finally, research needs are identified.

Chapter 3 introduces a sensing vehicle, the Georgia Tech Sensing Vehicle (GTSV), assembled by integrating state-of-the-practice sensing systems, including a commercial 3D line laser system to collect 3D range data. Then, the assessment on the 3D range data quality is presented. Since studying the 3D range data quality is a very complicated subject in Electrical Engineering, this chapter does not intend to resolve all the issues associated with this subject. The focus of this chapter including various laboratory and field tests is to verify the 3D line laser system's range measurement uncertainty specified in the manufacture's manual and to identify potential irregular data points in the 3D range data. The test results will help remove specific uncertainties and irregular data points and improve rutting measurement accuracy and repeatability.

Chapter 4 presents experimental tests in the laboratory and in the field with established ground truths to validate the accuracy and repeatability of rutting measurements (including 1D rut depth, rut length, and 3D rut volume) obtained using the 3D range data collected by the 3D line laser system. Laboratory tests were conducted to validate the laser's performance under controlled environment, and field tests were performed to verify its performance under normal survey practices.

Chapter 5 outlines the concept of a sensor-based and spatially-enabled pavement rutting condition assessment methodology. Each of the six modules, including data acquisition, data processing, data segmentation, statistical analysis, data visualization, and decision support, in the proposed methodology is described. Methods and applications proposed to substantiate the methodology are presented in Chapter 6.

Chapter 6 introduces methods and algorithms proposed to substantiate the sensor-based and spatially-enabled pavement rutting condition assessment methodology. First, a threshold-based outlier removal method employing the multivariate adaptive regression splines (MARS) technique is proposed in the data processing module. Then, a modified topological-ordering-based segment clustering (MTOSC) method is proposed in the data segmentation module to optimally partition the continuous roadway network into segments with uniform rutting conditions. In addition, an overlapping-reducing heuristic method is proposed to solve large-scale segmentation problems. Third, a network-level rutting condition assessment procedure is proposed in the decision support module to support the data items, statistical analyses, and reports needed in GDOT's PMS using the 3D line laser system. Finally, a method is proposed in the decision support module to detect isolated ruts in support of project-level pavement management.

Chapter 7 presents case studies on one interstate highway, two state routes, and one city road to demonstrate the applicability of the proposed methods and procedures. In addition, case studies were performed to observe the rutting progression behavior and to explore the potential benefits of using the 3D line laser system to improve pavement rutting progression modeling.

Chapter 8 summarizes the main findings of current research and presents recommendations for future studies.

Appendix A presents experimental tests using synthetic datasets and real datasets to assess the validity of the proposed homogenous segmentation method, MTOSC, and the overlapping-reducing heuristic method.

CHAPTER 2 LITERATURE REVIEW

Rutting is a major asphalt pavement distress that affects pavement structure integrity and driving safety (Kamplade 1990; Start et al. 1998). It is a permanent longitudinal depression that mainly forms because of traffic loadings in the wheel paths of a road. Rut depth is a 1D rutting characteristic commonly used to indicate the severity level of rutting. This chapter reviews manual and automatic rutting measurement technologies and the practices adopted by state DOTs to measure and report rutting condition. Additionally, the chapter identifies issues with data used for existing rutting progression models and the potential benefits of using high-resolution rutting data collected with a 3D line laser system to improve rutting progression modeling. This chapter also reviews existing homogeneous segmentation methods to partition a roadway network into segments with uniform pavement condition in order to apply cost-effective treatments to each of the uniform segments. Finally, research needs are identified.

Figure 2-1 Rutting holding water

2.1 Rutting Measurement Technologies

To obtain accurate and repeatable network-level pavement rutting measurements, practitioners and researchers have developed manual and automated rutting measurement

technologies. This section reviews those technologies, most of which focus on measuring 1D rut depth.

2.1.1 Manual Methods

The traditionally-used manual method for measuring 1D rut depth is a straightedge method, suggested in the ASTM 1703 Standard (2010). To measure the rut depth, a surveyor places a straightedge, preferably spanning half of the traffic lane, across one of the wheel path, and then measures the maximum distance between the pavement surface and the straightedge. The maximum distance is determined as the rut depth for the wheel path. The straightedge method was commonly used by highway agencies. Some state DOTs still assess the pavement rutting condition manually using the straightedge method, like GDOT. Other manual methods are static profiling technologies, such as the rod and level method (ASTM E-1364 2005) and the Dipstick profiler, which were mostly used in research studies to measure rutting. Because the manual methods are time-consuming, labor-intensive, and unsafe, especially on highways with high traffic volume, they are gradually being phased out and replaced with automated methods.

2.1.2 Point-based Rut Bar Systems

A point-based rut bar system typically utilizes 3 or more point lasers to profile the pavement surface in the driving direction and uses the collected data to calculate the rut depth in the transverse direction. Usually, a rut bar system is limited to being no longer than 3.0 m for the sake of survey safety (McGhee 2004). Figure 2-2 shows the configuration of a 5-point rut bar system. To cover the full-lane width (typically 12 ft or 3.6 m), the two sides of a rut bar system are mounted with point lasers that are tilted to a certain angle in the vertical direction as illustrated in Figure 2-2.

According to a survey conducted in 2003 (see Table 2-1), point-based rut bar systems are commonly used by North American highway agencies (McGhee 2004). The

number of sensors that are used in a point-based rut bar systems varies from 3 to 37. Thirty-two agencies were equally divided over the 3-point and 5-point rut bar systems; another 14 agencies adopted a rut bar system with 7 to 37 sensors. Some agencies that claimed to be using a 37-point system were actually using a 31-point system.

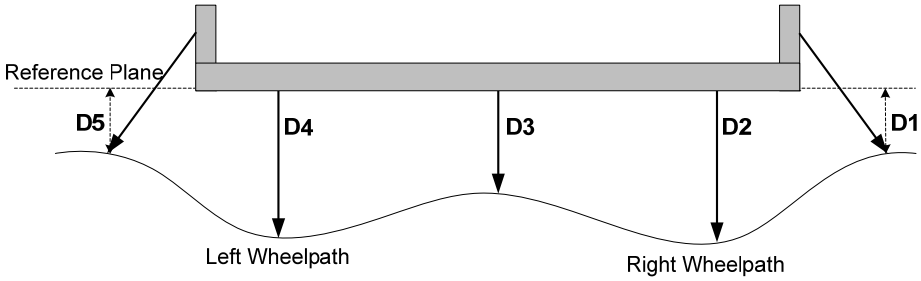

Figure 2-2 Configuration of a 5-point rut bar system

Table 2-1 Survey in 2003 (McGhee 2004)

Point-based Rut Bar System	3-point	5-point	7-point to 37-point
Number of Highway Agencies	16	16	14

Potential errors exist in these point-based rut bar systems because they only sample a limited number of points (e.g., 3 to 31 points) in the transverse direction to determine the maximum rut depth. Because of the wandering of a survey vehicle, the variation of lane widths, and the variation of rut shapes, the laser sensors may not capture the peaks and valleys of ruts and the maximum rut depths were often underestimated. Existing studies show that rut depth measurement errors exist in point-based rut bar systems. For example, Ksaibati (1996) evaluated the rut depths measured by 3-sensor and 5-sensor profilometers and found significant differences between the non-contact and direct-contact measurements. HTC (2001) compared the rut depths from a 30-sensor ROMDAS profilometer with field measurements using a 1.5-m straightedge method and identified a bias. Mallela and Wang (2006) assessed the sampling bias of the profilometers (with 13 to 30 sensors) operated in New Zealand and concluded that rut depth measurement of point-based rut bar systems is underestimated. Simpson (2001)

determined that the correlation of rut depths measured by a 5-point rut bar and a rod and level method is approximately 0.4. Thus, the 5-point rut bar system is not reliable with regard to rut depth measurement. In summary, past studies have shown that 3-point and 5-point rut bar systems have poor rut depth measurement accuracy. This underestimation negatively impacts the development of a reliable rutting progression model and the determination of timely preventive maintenance to ensure roadway safety.

In addition, the major issues of the aforementioned studies on establishing the ground truth transverse profiles are 1) the sample size of the ground truth transverse profiles is very small and 2) it is labor-intensive and time-consuming to acquire ground truth transverse profiles. Simpson (2001) used the transverse profiles collected by the rod and level method as the ground truth transverse profile, each of which consists of only 25 points. Also, only 30 transverse profiles were analyzed. Data Collection Ltd. (DCL) used Transverse Profile Beam (TPB) with a transverse resolution of 3 mm to establish the ground truth transverse profiles (Mallela and Wang 2006). Only 64 profiles were collected. There is a need to develop an alternative method to cost-effectively acquire ground truth transverse profiles for quantitatively assessing the rut depth measurement errors of point-based rut bar systems. Moreover, there is a need to develop a method to more reliably and accurately measure rut depths.

2.1.3 3D Range-based Systems

Besides point-based rut bar systems, 3D range-based systems, employing a point laser or a line laser, have been developed for pavement surface condition data collection. Table 2-2 and Table 2-3 summarize the specifications of six 3D range-based systems.

Of six 3D systems, only the PPS, developed by the Phoenix Scientific Inc., uses a point laser. The PPS is usually integrated with an inertial/GPS navigation system and is capable of acquiring 3D point cloud data of the pavement surface in Geodetic coordinates (Phoenix Scientific Inc. 2004; 2010). This 3D range-based system can acquire 4.6-m

wide profiles, each of which consists of 943 points spaced at a constant angle, 1,000 times per second. The average transverse spacing between points is 5 mm. The average depth resolution is 0.15 mm.

The other five range-based systems were built using the 3D line laser imaging technology based on the triangulation principle. They are referred as 3D line laser systems in this dissertation. A real-time 3D scanning system was developed by Li et al. (2010) from the University of Texas at Austin for pavement distortion inspection. The 3D scanning system consists of two laser profiling units, each of which collects 1.83-m wide transverse profiles consisting of 1,024 data points. The maximum profiling rate is 200 profiles per second. The system specifications are shown in Table 2-2. A rut measurement system called VRUT was designed and implemented by a TxDOT team in 2009 (Huang et al. 2012). Different from other 3D line laser systems, VRUT consists of only one sensing profiler to cover 4.267-m field of view in the transverse direction. The transverse resolution is around 2.8 mm. Wang et al. (2011; 2012) presented another 3D line laser system, named PaveVision3D, which is capable of acquiring both 2D intensity and 3D range data from pavement surfaces. It has a higher transverse resolution and maximum profiling rate than the real-time 3D scanning system and the VRUT.

INO in Canada developed the LRMS to measure rutting (INO 2012). This system consists of two laser profilers; each can cover a 2 m width and collect 640 data points per transverse profile. It can operate at a speed up to 100 km/h. Its depth accuracy is +/-1 mm. However, this system sheds the laser light onto the pavement surface at a small angle. The transverse profile collected is different from the one collected when the laser is aimed straight downward. It may potentially overestimate the rut depth, especially for severe rutting. Another commercial product from INO is the LCMS, which has a similar transverse resolution and maximum profiling rate as the PaveVision3D. The LCMS is

used for data collection in this dissertation. A detailed description will be presented in Section 3.2.

Table 2-2 Specifications for 3D Range-based Systems

	PPS	VRUT	Real-time 3-D Scanning System
Sample Points (points/profile)	943	1,536	1,024
Field of View (m/profile)	4.3	4.267	1.83
Transverse Resolution (mm)	5 (average)	2.8	1.79
Depth Resolution (mm)	0.15 (average)	0.75	2
Depth Range of Operation (mm)	N/A	± 203	N/A
Maximum Profiling Rate (profiles/s)	1,000	4,900	200
Maximum Vehicle Speed (km/h)	100	112	112
Profile Spacing at 100 km/h (mm)	28	5.7	139

Table 2-3 Specifications for 3D Range-based Systems (Continued)

	LRMS	LCMS	PaveVision3D
Sample Points (points/profile)	640	2,080	>2,000
Field of View (m/profile)	2	2	2
Transverse Resolution (mm)	2	1	1
Depth Accuracy (mm)	1	0.5	1
Depth Range of Operation (mm)	500 @ 30 Hz or 450 @ 150 Hz	± 125	N/A
Maximum Profiling Rate (profiles/s)	30 or 150	5,600	6,000
Maximum Vehicle Speed (km/h)	100	100	100
Profile Spacing at 100 km/h (mm)	926 or 185	5	5

Because of the high-resolution and high-speed of 3D line laser systems, they have attracted researchers' and practitioners' attention. However, since these 3D line laser systems only emerged in the past several years, the application of these new systems for pavement condition assessment is still in its infancy. Research is needed to develop methodologies and algorithms to take advantage of the emerging 3D line laser systems to improve pavement condition assessment practices. This dissertation is a part of this

research effort with a special focus on pavement rutting condition assessment. Although only the 3D range data collected by LCMS was tested in this dissertation, the developed methodologies and algorithms to convert the high-resolution 3D range data into useful rutting information in support pavement management decisions are still valid for other 3D line laser systems. Therefore, the main contribution of this study is not limited to the specific 3D line laser system. It can be transferred and applied to other 3D line laser systems and other 3D technologies with higher resolution coming in the future.

2.1.4 Summary

In summary, the manual straightedge method is labor-intensive, time-consuming, and unsafe. The point-based rut bar systems, although commonly used by state DOTs, are not accurate and repeatable because of the limited number of laser sensors used to capture the maximum rut depth. Therefore, there is a need to improve the accuracy and repeatability of 1D rut depth measurements. The emerging high-resolution 3D line laser imaging technology can potentially be used to improve the accuracy and repeatability of 1D rut depth measurements and to provide additional 2D and 3D rutting characteristics.

2.2 Rutting Condition Assessment Practices by State DOTs

Current pavement rutting condition assessment carried out by highway agencies is mainly for network-level pavement maintenance and rehabilitation. Different practices have been adopted by different highway agencies. This section summarizes the rutting condition assessment protocols, including indicators and definition of severity levels, and the rutting aggregation methods applied by Federal and several state DOTs.

2.2.1 Long-term Pavement Performance (LTPP) Rutting Condition Assessment (FHWA 2003)

For Specific Pavement Studies (SPS)-3, the rut depths are measured using a 1.2-m straightedge and are recorded to the nearest millimeter at 50 ft (15.25 m) intervals for each wheel path. For all other LTPP sections, transverse profiles are measured with a Dipstick® profiler at 50 ft (15.25 m) intervals.

2.2.2 GDOT Rutting Condition Assessment (GDOT 2007)

GDOT performs an annual survey of the pavement surface condition, including rutting, on its 18,000 centerline miles of state-maintained highways. The entire pavement network is partitioned into segments, each of which is typically 1 mile long, for the survey purpose. During the survey, a rater first drives through the entire segment to examine the general pavement condition, and then, identifies a representative 100-ft (30.5-m) sample section upon which a walking survey is performed.

As one of ten types of predefined pavement distresses, the average rut depth for the left and right wheel path within the100-ft sample section is recorded to the nearest 1/8 in. If the rut depth is less than 3/8 in., the rater usually visually estimates it; if the rut depth is 3/8 in. or greater, actual measurement using a straightedge is required. Rut depth measurements will not be taken from locations where potholes, wide cracks, or loss of section exist. The deduct values for rutting are listed in Table 2-4. According to the treatment criteria used by the GDOT, rutting is usually treated with slurry seal if its depth is less than 1/4 in.; if its depth is between 1/4 in. and 3/8 in., micro seal or level and overlay can be applied; if its depth is greater than 3/8 in., mill and inlay is suggested (Gao 2004).

Table 2-4 Deduct Values for Rutting in the GDOT's Survey Manual

Depth (1/8 in.)	1	2	3	4	5	6	7	8
Deduct	2	5	12	16	20	24	24	24

2.2.3 Oregon DOT (ODOT) Rutting Condition Assessment (ODOT 2010)

ODOT measures the rut depths for both wheel paths automatically using a 5-point rut bar system. This automated rutting condition survey is conducted separately from the manual survey of other surface distresses for every 0.1 mile survey section. The rut bar system measures rut depths at 6 in. intervals and reports the average rut depth and standard deviation for each wheel path for every 0.1 mile. The rut depth measurements are categorized into four severity levels: zero (0 - 1/4 in.), low (1/4 - 1/2 in.), moderate (1/2 - 3/4 in.), and high (≥ 3/4 in.).

2.2.4 Pennsylvania DOT (PennDOT) Rutting Condition Assessment (PennDOT 2010)

PennDOT adopts the Automatic Road Analyzer (ARAN) to automatically collect pavement condition data. Each evaluation section is typically 0.5 mile long. Within an evaluation section, the rut depth measurements are taken at an interval of no greater than 30 ft. Then, each measurement is assigned to one of the three severity levels. They are low (rut depth between 1/4 in. and 1/2 in.), medium (rut depth between 1/2 in. and 1 in.), and high (rut depth equal or greater than 1 in.). After that, the length for each severity level is recorded and reported for each wheel path.

2.2.5 Kansas DOT (KDOT) Rutting Condition Assessment (Gisi 2011)

KDOT uses a 3-point rut bar method to automatically measure the rut depths for each pavement management section (typically 1 mile long). According to Rick Miller (Chair of the FHWA/ASHHTO Pavement Rutting and Cracking Expert Task Group), the detailed rut depths are recorded at 1-ft intervals, the average rut depth for each wheel path is reported for every 0.1 mile, and, finally, the average and maximum rut depths for each wheel path are reported for every 1 mile.

2.2.6 TxDOT Rutting Condition Assessment (TxDOT 2009)

A Pavement Management Information System (PMIS) data collection section defined by TxDOT is usually 0.5 mile in length. A 5-point rut bar system is used to measure the rut depth throughout each PMIS section. Based on the rut depth measurements, the rutting is rated by area and severity. Severity of rutting is described in terms of rut depth. Shallow rutting is defined as 0.25 in. to 0.49 in. deep. Deep rutting is referred to rutting from 0.5 in. to 0.99 in. Severe rutting is 1.0 in. to 1.99 in. and failure rutting is 2.0 in. or deeper. The area of rutting is measured as the percent of a section's total wheel path area that exhibits certain severity level of rutting. For example, the area of shallow rutting equals the total feet of shallow rutting of both wheel paths divided by the section length.

2.2.7 Summary

Based on the literature review, the rutting indicator commonly used by state DOTs is the 1D rut depth. Some highway agencies also define the severity level of rutting, although the definitions are slightly different. Table 2-5 summarizes the definitions of rutting severity levels in the ODOT, PennDOT, and TxDOT. Table 2-6 summarizes the aggregation methods used on the continuous rut depth measurements by state highway agencies. As shown in Table 2-6, the sampling interval varies among different agencies. The smallest sampling interval is 6 in., which is used by the ODOT. AASHTO (2010) suggests that the sampling interval should not be more than 3 m for the network-level rutting survey and not be more than 0.5 m for project-level survey. The aggregation interval also varies from 0.1 mile to 1 mile for state DOTs. Statistical indicators, including the average, maximum, and standard deviation of 1D rut depths, are usually reported for every aggregation interval. Additionally, PennDOT and TxDOT report the linear percentages of different severity levels (low, medium, and severe) of rutting.

Table 2-5 Rutting Severity Levels Defined by ODOT and PennDOT

Severity Level	Low	Medium	Severe
ODOT	≥ 1/4 in. and < 1/2 in.	≥ 1/2 in. and < 3/4 in.	≥ 3/4 in.
PennDOT	≥ 1/4 in. and < 1/2 in.	≥ 1/2 in. and < 1 in.	≥ 1 in.
TxDOT	≥ 1/4 in. and < 1/2 in.	≥ 1/2 in. and < 1 in.	≥ 1 in.

Table 2-6 Aggregation Methods for Rutting Survey

Agency	Method	Aggregation Interval	Sampling Interval	Data Aggregation
GDOT (2007)	Manual	1 mile	--	Representative rut depth for each wheel path
ODOT (2010)	5-point	0.1 mile	6 in.	Average rut depth and standard deviation for each wheel path
PennDOT (2010)	ARAN Profiler	0.5 mile	<30 ft	Length for each severity level for each wheel path
KDOT (mails with Rick Miller)	3-point	0.1 mile	1 ft	Average rut depth for each wheel path
TxDOT	5-point	0.1 mile	1 ft	Average, maximum, length for each severity level for each wheel path

In addition, it is observed that although some state DOTs, including GDOT and KDOT (Gisi 2011), requires surveyors to record isolated spots with severe rutting problems; the isolated rut information is not recorded in existing PMSs because it is difficult to manually collect such detailed levels of information. There is a lack of data acquisition technology and an automated detection method to detect isolated ruts efficiently. The emerging 3D line laser systems collect high-resolution rutting measurements and, thus, provide an opportunity to detect isolated ruts. Research is needed to develop an automated method to process 3D range data and detect isolated ruts.

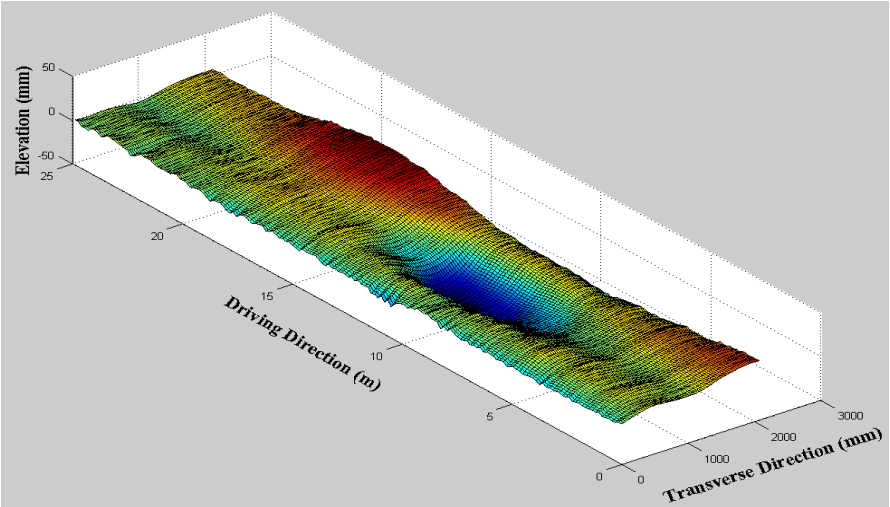

Figure 2-3 An isolated rut in the 3D range data

2.3 Rutting Progression Modeling

Pavement performance modeling and prediction is the core of a PMS. The importance of a reliable performance model can never be overemphasized. Over the past decades, serious effort has been directed at developing reliable rutting progression models. This section reviews the existing rutting progression models with a special focus on the data used for rutting progression modeling. Issues of existing data were identified and the potential benefits of the high-resolution rutting measurements collected by a 3D line laser system in improving rutting progression modeling were explored.

Most rutting progression models were developed using rutting data collected from purposely-built pavement test roads. Some models were developed using data from test roads subjected to the accelerated action of traffic (e.g., Heavy Vehicle Simulator) and environmental conditions (e.g., application of UV radiation), such as the AASHO and WesTrack test sections (Archilla and Madanat 2000; Archilla 2000; Prozzi 2001). Some other models used data from test roads that were subjected to the action of actual highway traffic and environment, such as long-term pavement performance program (LTPP) (Ali and Tayabji 1998) and Virginia's Smart Road. Since the experimental tests

cover limited types of pavements and limited weather conditions, the developed rutting progression models usually have limited prediction capability when used to predict rutting progression of other types of pavements or pavements located in other climate areas (Chu and Durango-Cohen 2008).

Few progression models have used the historical data from in-service pavements, since those data are of poor quality (Rada et al. 1999; Stoffels et al. 2001; Selezneva et al. 2004; Tsai et al. 2011). The issues of those data are 1) poor data integrity (missing data points), 2) subjective rating depending on raters' experiences, and 3) large data variance that the actual deterioration behavior cannot be well separated. The variance may result from the change of sampling location, the change of raters, and minor/routine maintenance activities (e.g., slurry seal).

Improvements in the quality of historical data are highly desirable to ensure that they serve their intended purposes, e.g., developing reliable rutting progression models. The 3D line laser systems are potentially capable of improving the rutting measurement accuracy and repeatability, and, consequently, may be used to develop more reliable rutting progression models. In addition, the 3D line laser systems can be used to derive 2D and 3D characteristics (such as 2D rut cross-sectional area), which can capture both rut depth and rut shape change. The new 2D and 3D rutting characteristics can potentially be used to develop more reliable rutting progression models.

2.4 Homogeneous Segmentation Methods

This section reviews existing homogeneous segmentation methods used to partition a roadway network into segments with uniform pavement condition in order to apply cost-effective treatments to each of the segments with uniform pavement condition.

Partitioning a roadway network into segments with uniform pavement condition is a vital step for pavement management because most analyses (e.g., performance modeling) and decisions (e.g., inspection and maintenance planning) are made based on

the homogeneity assumption (Haas et al. 1994; Shahin 1994; Kerali et al. 1988; Bennett 2004). Studies have shown that whether the homogeneity assumption will hold or not has significant engineering and economic implications (Bennett 2004; Latimer et al. 2004). Latimer et al. (2004) revealed that the improper consideration of the variability within an analysis segment tends to obscure extreme cases (such as localized road sections in poor condition) and results in loss of accuracy in recognizing the needs for maintenance work, in recognizing the benefits of maintenance, and in estimating the level of deterioration across the network.

Previous studies have proposed a variety of methods to solve this homogeneous segmentation problem. Some researchers have treated the segmentation problem as a two-dimensional clustering problem. They have used 2D spatial data analysis methods to cluster pavement sections based on condition uniformity for let project determination (Yang et al. 2009) and for performance-based contracting (Kim et al. 2010). However, the majority of existing methods handle the segmentation problem as a one-dimensional clustering problem. Some researchers have applied Bayesian Information Criterion (BIC) (Xia and Chen 2007) to analyze freeway operating conditions, and they have applied the minimum message length (MML) reference (Byrne et al. 2009) to recognize the pattern of seasonal variation in pavement roughness. Among existing one-dimensional clustering methods, those methods that have been developed in the context of pavement condition assessment are presented below.

The first and most popular method is the cumulative difference approach (CDA) specified in AASHTO (1986) and AASHTO (1993). It detects the points where the sign of the slope of the cumulative difference between the input data and the mean value changes. Based on this concept, CDA can always separate the input data into at least two homogeneous segments unless the measurements in the input data are all identical to each other (Misra and Das 2003). Since in the closely-spaced pavement condition data (e.g. rut

depth measurements at 5 mm intervals) adjacent values are essentially always different, CDA is not suited to deal with this jagged data. Accordingly, Divinsky et al. (1997) preprocessed the input data by applying a moving average before performing CDA. However, the moving average smoothes out minor changes and blurs significant, big changes. Instead of smoothing out the input data, Ping et al. (1999) proposed a variation of CDA by adding exogenous restrictions, e.g., the minimal length of a homogeneous segment and the minimal difference between means of adjacent homogeneous segments. Tejeda et al. (2008) proposed a data segmentation procedure and employed the accumulated sum (CUSUM) method, a generalized version of CDA, for segmenting the skid resistance data.

The French Laboratory of Roads and Bridges developed the LCPC method (Lebas et al. 1981; Thomas 2004). It uses a dichotomist technique to recursively identify partition points where the mean changes. A method with a similar concept is the absolute differences in sliding mean values method (ADS) (Rübensam and Schulze 1996; Thomas 2004). The only difference is that ADS locates partition points sequentially from the start to the end of the input data. Instead of setting a constraint on the change of mean values, El Gendy et al. (2005; 2008) applied the absolute difference approach (ADA) and C-chart method to resolve the segmentation problem. Both approaches limit the variation of data within a homogeneous segment. The methods either set a maximum range of response (El Gendy et al. 2005) or upper and lower control limits based on the estimated standard deviation (El Gendy et al. 2008). Misra and Das (2003) extend the methods developed by Gey and Lebarbier (2002) and propose the classification and regression tree (CART) plus an exhaustive search method. This method first builds a classification and regression tree by recursively dividing the parent segment into two child segments and minimizing the sum of the squared differences within each segment until reaching a predefined limit, e.g., the minimum length of a homogeneous segment. Then it searches the tree

exhaustively and selects the best sub-tree with the specified number of segments and the minimum sum of the squared differences. Thomas (2001; 2003) proposed an AMOC algorithm (the at-most-one-change assumption), which is based on the Bayesian concept. It is different from previous homogenous segmentation methods, since it takes into account the correlation in the measurements of IRI or rutting. Because the AMOC algorithm only locates one partition point at a time, Thomas (2005) proposed a heuristic scheme which uses the AMOC algorithm as a building block and identifies multiple partition points recursively. Cuhadar et al. (2002) presented a wavelet-based algorithm for automated segmentation of pavement condition data. The algorithm first detects the singularities of the smoothed waveform. Those singularities that are not isolated are used as border points to segment the pavement condition data.

Although a number of methods and algorithms have been proposed, these methods are heuristic methods. They can neither provide the optimal homogeneous segmentation nor guarantee near-optimal solution. To optimally identify uniform spatial regions for performance modeling, Mishalani and Koutsopoulos (2002) developed a methodology based on nonparametric cluster analysis and dynamic programming. Under the given stopping criterion (e.g., the incremental contribution of an additional partition point to the reduction in the total variance), the methodology can provide the optimal solution. However, it does not incorporate crucial engineers' knowledge, such as the minimal segment length and the minimal mean difference. Therefore, there is a need to develop a segmentation method which not only provides the optimal segmentation solution but also has the flexibility to incorporate engineering considerations.

2.5 Summary

The following summarizes the findings of the literature review and the research needs:

- The manual straightedge method is labor-intensive, time-consuming, and unsafe. It is virtually impossible to conduct rutting measurement manually on highways (e.g., I-285 near Atlanta, Georgia) with heavy traffic flow. There is a need to develop an automated pavement rutting measurement method.
- The point-based measurement technology is still commonly used by state DOTs. It underestimates the rut depth measurement, since the measurement technology uses a limited number of laser points (e.g., 3 to 37 lasers) to capture the rut shape and the maximum rut depth. There is a need to quantify the rut depth measurement errors of point-based rut bar systems so that transportation agencies can use the derived information confidently to support their pavement management decisions.
- The emerging 3D line laser imaging technology can capture more than 4,000 laser points on each transverse profile at highway speed. Because of its high resolution, the 3D line laser imaging technology holds a great potential for improving the rutting measurement accuracy and repeatability.
    - **Network-level Rutting Measurement**: there is a need to develop methodologies and algorithms to accurately extract 1D rut depth from the 3D range data collected using a 3D line laser system in support of the existing PMS (e.g., the Georgia Pavement Management System, GPAM). Algorithms or methods are needed to 1) remove noises, irregular data points, and non-rutting features in the 3D range data; 2) to extract 1D, 2D, and 3D rutting measurements; 3) to meaningfully aggregate the detailed rut measurements and result in useful statistical representation of the network-level and project-level rutting condition that can directly support pavement management decisions.

    - **Isolated Rut Detection**: there is a need to develop a method to automatically detect isolated ruts using a 3D line laser system for applying low-cost and localized treatments.
- Experimental tests with established ground truths are needed to validate the accuracy and repeatability of rutting measurements (including 1D rut depth, rut length, and 3D rut volume) obtained using the 3D line laser system studied in this dissertation.
- The 3D line laser system may potentially be used to improve the 1D rut depth measurement accuracy and derive additional 2D and 3D rutting characteristics. Hence, it can potentially improve the pavement rutting progression modeling. There is a need to explore the feasibility of improving pavement rutting progression modeling using a 3D line laser system.

CHAPTER 3 3D LINE LASER IMAGING SYSTEM

The objective of this research is to improve pavement rutting condition measurement accuracy and repeatability utilizing emerging 3D line laser imaging technology. For this purpose, a sensing vehicle, the Georgia Tech Sensing Vehicle (GTSV), was assembled by integrating the state-of-the-practice sensing systems, including a commercial, downward 3D line laser system, i.e., the LCMS, and the Trimble Geography system by Geo3D, consisting of one downward-view camera, one side-view camera, a LiDAR system, a differential GPS, an inertial measurement unit (IMU), and a distance measurement instrument (DMI). The GTSV is used to acquire high-resolution 3D range data of the pavement surface in support of rutting measurement.

This chapter first introduces the 3D line laser system and the GTSV. Then, the quality of the 3D range data collected by the 3D line laser system is assessed by characterizing the range measurement uncertainty (also known as 3D noise) and irregular data points. Since studying the range measurement uncertainty is a very complicated subject in Electrical Engineering, mainly because the uncertainty depends on the design of the measurement system (Kwang-Ho et al. 2009). This chapter does not intend to resolve this subject. Instead, the focus of this chapter including various laboratory and field tests is to verify the range measurement uncertainty of the 3D line laser system specified in the manual (INO 2012) and identify potential irregular data points that may impact the 3D range data quality. The test results will help to remove specific uncertainty and irregular data points and improve rutting measurement accuracy and repeatability.

3.1 System Introduction

The 3D line laser system, also known in available literature as the camera-laser-based 3D scanner, is based on the triangulation principle, which is presented in Figure 3-

1. Typically, a 3D line laser system consists of a laser projector and a digital area scan camera with a charge coupled device (CCD) or complementary metal oxide semiconductor (CMOS) sensor. The camera is placed at a known distance and an oblique angle (ɵ) with respect to the projector. When collecting the 3D range data, the laser projector sheds a structured light, i.e., a laser line in the 3D line laser system, onto an object's surface. And the camera captures the laser line as an image. A sub-pixel peak detection algorithm is then employed to analyze the laser line image, find the sub-pixel location of the laser line, and convert the distortion of the laser line to the unevenness of the object's surface. Meanwhile, corresponding 2D intensity data are obtained. Up to this point, a single range profile and a single intensity profile of the object's surface are obtained. To acquire the essentially continuous 3D range data and 2D intensity data, the 3D line laser system is mounted onto a survey vehicle and coupled with a DMI, which is a wheel-mounted rotary shaft encoder that measures travelled linear distance. When the survey vehicle is moving, the 3D line laser system continuously scans the pavement surface and acquires range and intensity transverse profiles. The intensity profiles are used to restore the 2D intensity image of the pavement surface, and the range profiles are used to reconstruct an essentially continuous 3D pavement surface. The measurement range of such a 3D line laser system is determined by the intersection between the emitted laser line and the field of view of the digital camera. The LCMS's measurement range is +/-125 mm.

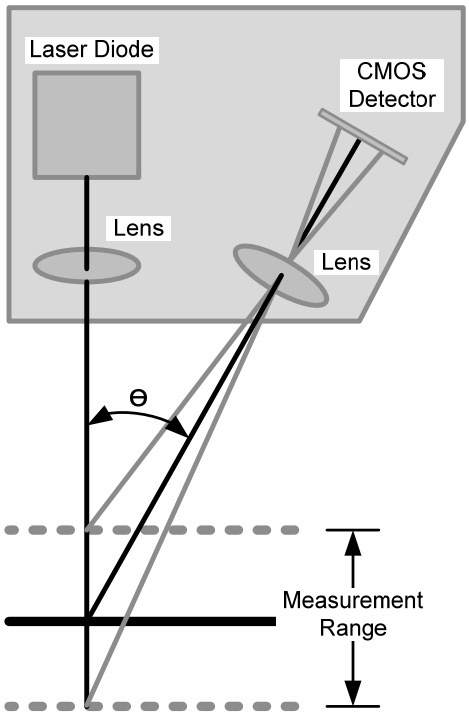

Figure 3-1 Illustration of the optical triangulation principle

3.2 Georgia Tech Sensing Vehicle

A sensing vehicle, the GTSV, has been integrated at the Georgia Institute of Technology for 3D pavement surface data collection. The GTSV is equipped with the 3D line laser system, which consists of two high-performance laser profiling units. These two units are mounted on the vehicle 2 m away from each other in the horizontal direction and about 2.25 m above the ground, as shown in Figures 3-2 and 3-3. To prevent the left and right scanning regions from cross-talking with each other, both laser profiling units were installed parallel to each other and with a 15° yaw angle (i.e., 75° to the driving direction) with respect to the vehicle, as shown Figure 3-3.

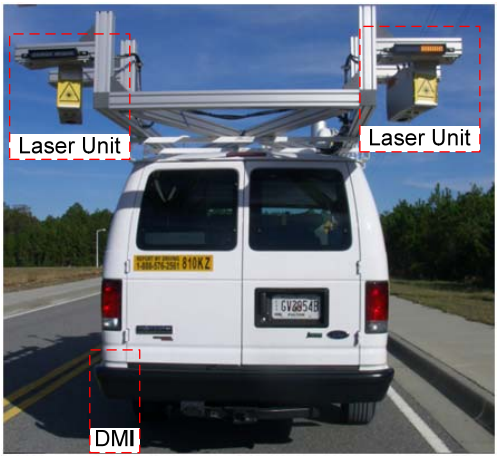

Figure 3-2 A sensing vehicle integrated at the Georgia Institute of Technology

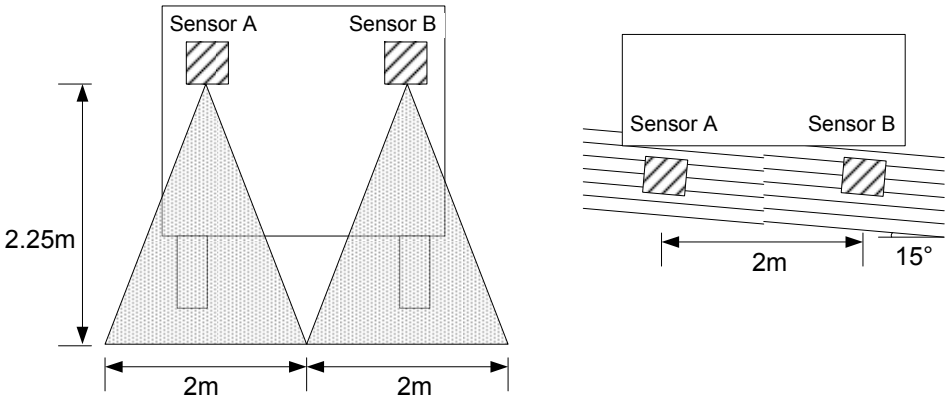

(a) Rear view (b) Birdseye view

Figure 3-3 3D line laser system and the GTSV

The following describes the resolutions of the 3D range data in x (transverse), y (longitudinal), and z (elevation) directions. With a two-unit setup, the 3D line laser system produces 4,160 3D data points per profile (2080 points * 2 units) and covers a 4-m pavement width. Therefore, the resolution in x direction (transverse profile direction) is about 1 mm (4 m / 4096 points). The elevation quantization level is 0.25 mm in the z direction. The elevation accuracy, which is the dispersion of the z coordinates of 3D points from their theoretical positions, is 0.5 mm. The resolution in the y direction depends on the DMI encoder. In the GTSV, a DMI encoder with 10,000 pulses per revolution was installed to trigger the acquisition of transverse profiles. When using the

encoder, the interval between two transverse profiles can be 1 mm or even smaller. The 3D line laser system equipped on the GTSV can collect transverse profiles at 5 mm intervals at a speed of 100 km/h. The 3D pavement range data can then be acquired for pavement rutting condition assessment. Figure 3-4 visualizes the 3D pavement range data and provides a close look at a crack line.

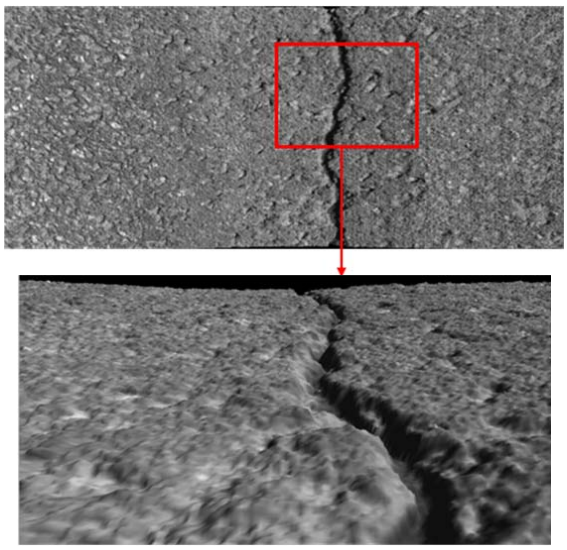

Figure 3-4 Visualization of 3D pavement surface data

The basic concept of the 3D line laser system, including the structured light and the triangulation principle, has existed for decades. However, with the advances in sensor technology, the newer system presented in this dissertation can produce data with better granularity and can operate at highway speed, and, thus, has a great practical potential for better detecting pavement distresses.

3.3 Quality of the 3D Range Data

The section is to assess the quality of the 3D range data by characterizing the range measurement uncertainty (or 3D noise) and irregular data points in the 3D range data.

3.3.1 Range Measurement Uncertainty

The range measurement uncertainty is defined as the dispersion of the 3D range data from its theoretical value, which is here given by the point on the corresponding fitted primitive (Guidi et al. 2010). The standard deviation is used as a measure of the range measurement uncertainty. The remainder of this subsection will present first the potential sources of the range measurement uncertainty when the 3D line laser system is either stationary or moving and then experimental tests to quantify the range measurement uncertainty.

3.3.1.1 Uncertainty in the Static Mode

Researchers have identified various sources of the range measurement uncertainty when both the 3D line laser system and the survey object are stationary (Linares et al. 2000). One main contributor to the uncertainty in the 3D range data is the speckle noise (Forest Collado 2004; Dorsch et al. 1994). The phenomenon of speckle, caused by interference of waves of the same frequency, is inherent to the use of laser light (Wikimedia 2012). Another potential source of the range measurement uncertainty is the intensity variation of the survey object's surface (Whaite and Ferrie 1990). When the intensity of the pavement surface varies, the intensity of the laser line image on the CCD sensor becomes non-uniform with dark and bright regions. The non-uniform laser line image introduces measurement uncertainty in the range data. This uncertainty has not been emphasized in the available literature, since most 3D line laser systems are applied to machine surfaces with uniform intensity. However, pavement surfaces, especially the asphalt pavement surfaces, have significant intensity variation. Therefore, this uncertainty may become a major source of the range measurement uncertainty.

3.3.1.2 Uncertainty in the Moving Mode

When the 3D line laser system is moving, the overall measurement uncertainty may be smaller than that in the static mode. The reasons are the following. First, the survey vehicle's vibration does not introduce additional uncertainty into the 3D range data, because the profiling frequency of the 3D line laser system, which is up to 5600 Hz (INO 2012), is much higher than the frequency of vehicle body vibration, typically ranging from several Hz to several hundred Hz (Aoki et al. 1998). The exposure time of the camera, which captures the laser line, is approximately 36.5 us (INO 2012). This time is very short compared to the time in which the position of the survey vehicle changes. Consequently, it can be assumed that the vehicle was not moving during the capturing time and the vehicle vibration has minimal impact on the quality of the 3D range data. Second, because the vehicle movement removes some of the spatial coherence of the laser light, the speckle noise in the 3D range data is reduced (Chellappan et al. 2010) and, therefore, the range measurement uncertainty is reduced.

3.3.1.3 Experimental Tests

To quantify the range measurement uncertainty, experimental tests were conducted using a surface plate with known ground truth. As shown in Figure 3-5(a), it is a Grade B surface plate made of granite. The tolerance of flatness for a Grade B surface plate is 0.0002 inches; that is, the difference between the lowest point and the highest point on the plate will be no more than 0.0002 inches. Because the surface plate is made of granite, its surface intensity is non-uniform, as shown in Figure 3-5(b). To test the impact of material on the measurement uncertainty, both the bare surface plate and the plate covered with blue tapes, as shown in Figure 3-5(c), were tested. In addition, to eliminate the impact of ambient lighting, all the tests were completed in the laboratory and in a short time period. The tests and results are presented below.

Static Test

In the static test, the test object and the 3D line laser system were set in stationary position. Four cross-sections (locations A and B on the bare surface and locations C and D on the taped surface) on the test object were selected. Each cross-section was tested twice. In each test, the 3D line laser system scanned the object surface 1,000 times without interruption. Table 3-1 summarizes the static test.

(a) Grade B surface plate

(b) Zom-in view

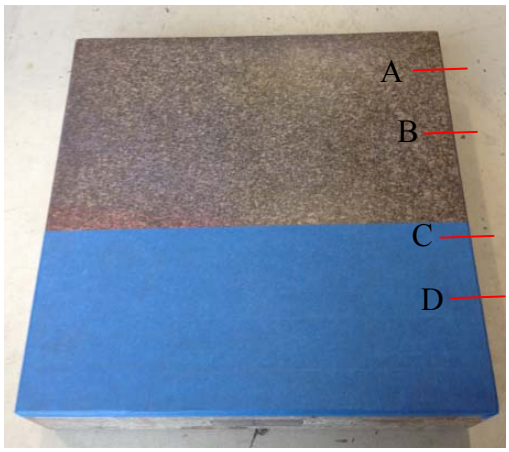

(c) Birdseye view

Figure 3-5 Grade B surface plate and a zoom-in view of its surface

A transverse profile example is the zigzag profile shown in Figure 3-6(a). Since the test object is absolutely flat, a straight line was obtained through robust linear regression analysis and used to fit the transverse profile. The straight line was used as the true surface of the plate. Deviations of the range measurements from the straight fitting line were defined as the range measurement uncertainties. Figure 3-6(b) shows the deviations of the range data from the straight line for the given example. It is denoted as an uncertainty profile in this dissertation.

Table 3-1 Summary of Static Tests

Material	Location	Test ID	Note
Stone	A	1	Repeated for 1,000 times
		2	Repeated for 1,000 times
	B	1	Repeated for 1,000 times
		2	Repeated for 1,000 times
Tape	C	1	Repeated for 1,000 times
		2	Repeated for 1,000 times
	D	1	Repeated for 1,000 times
		2	Repeated for 1,000 times

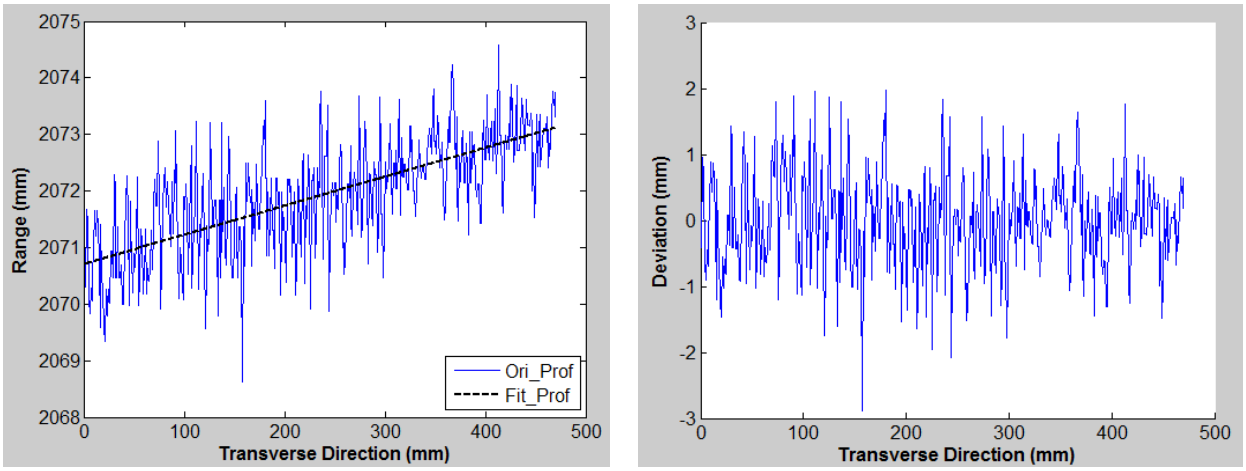

(a) Original profile and fitted profile (b) Uncertainty profile

Figure 3-6 Example of 3D range data and uncertainty profile

Figures 3-7, 3-8, and 3-9 show uncertainty profiles for four transverse profiles repeatedly collected in Test A-1, Test B-1, and Test C-1, respectively. All profiles were randomly selected. As shown in Figures from 3-7 to 3-9, the uncertainty profiles collected in the same test repeated each other very well. This high repeatability implies that the majority of the range measurement uncertainty is time-invariant. In addition, the uncertainty in Figure 3-9 ranges from -1 mm to 1 mm, which is much smaller than the range measurement uncertainty in Figures 3-7 and 3-8. This is consistent with previous studies that granite, a partially translucent material, in which the laser may penetrate part

way into the surface, affects the accuracy of range measurements (Beraldin et al. 2003; MacKinnon et al. 2008).

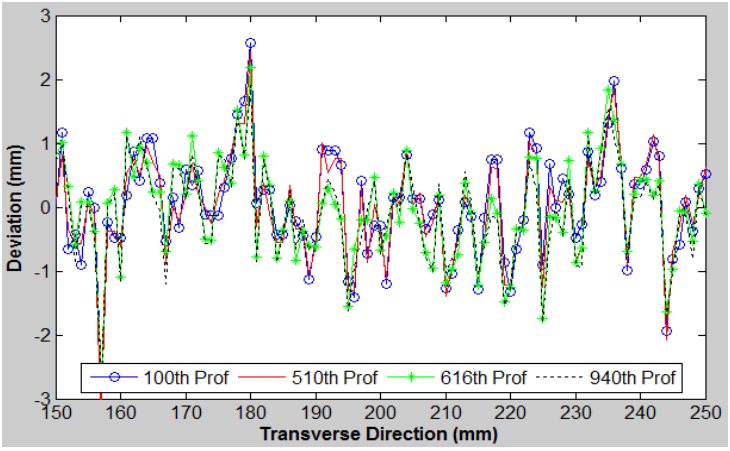

Figure 3-7 Repeatability of the range measurement uncertainty (Test A-1)

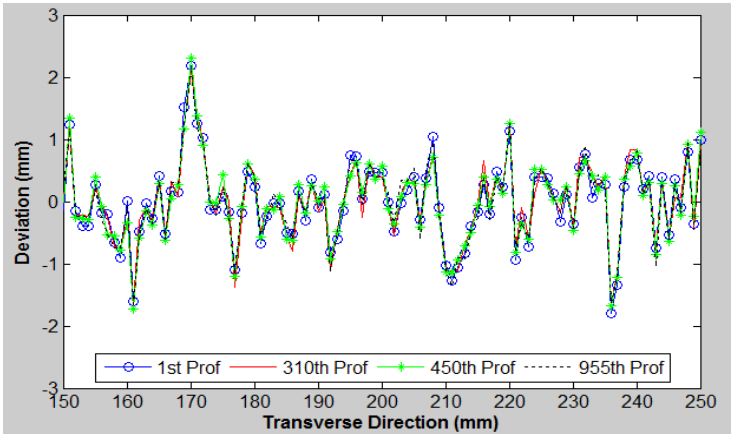

Figure 3-8 Repeatability of the range measurement uncertainty (Test B-1)

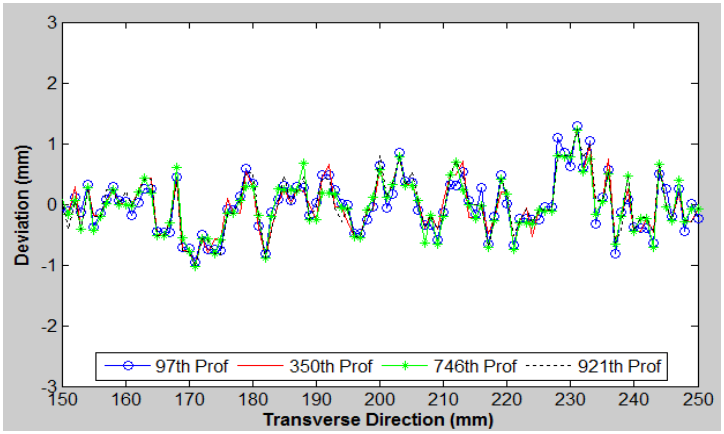

Figure 3-9 Repeatability of the range measurement uncertainty (Test C-1)

Figures 3-10 and 3-11 compare the uncertainty profiles for data collected from the same location during different tests. The only change from one test (e.g., A-1) to another (e.g., A-2) is that the 3D line laser system was turned off after the first test and then turned on. As shown in Figure 3-10, the two upper profiles, i.e., uncertainty profiles from Test A-1 and Test A-2, are analogous. The bottom profile is the difference between two uncertainty profiles. Most of the difference is within +/-1 mm. Figure 3-11 shows the comparison of uncertainty profiles from Test C-1 and Test C-2. Similarly, two profiles follow a similar trend. The majority of the absolute differences are no more than 0.5 mm. Both figures show that the repeatability between two tests, although still high, is inferior to that between two repetitions within one test. This might be because the environment (e.g. temperature) between two tests changed slightly.

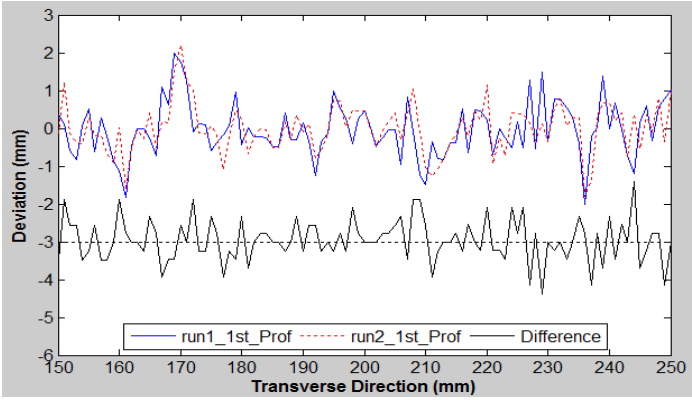

Figure 3-10 Comparison of the range measurement uncertainties in tests A-1 and A-2

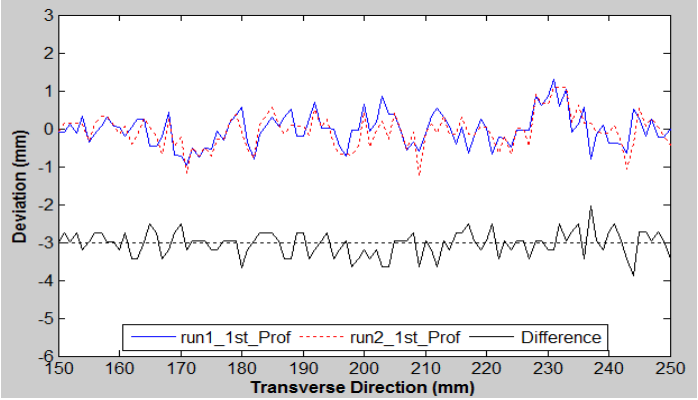

Figure 3-11 Comparison of the range measurement uncertainties in tests C-1and C-2

Further, the uncertainty profile collected from one location was compared with the one from another location. The comparison in Figures 3-12 and 3-13 shows that the uncertainty profiles do not repeat each other. This evidence supports the idea that the range measurement uncertainty is location dependent. Even Locations C and D seem to have similar surface color and reflectivity; their uncertainty profiles are dissimilar. This might be caused by features (e.g., texture) on the object's surface, which human eyes cannot differentiate but the 3D line laser system can.

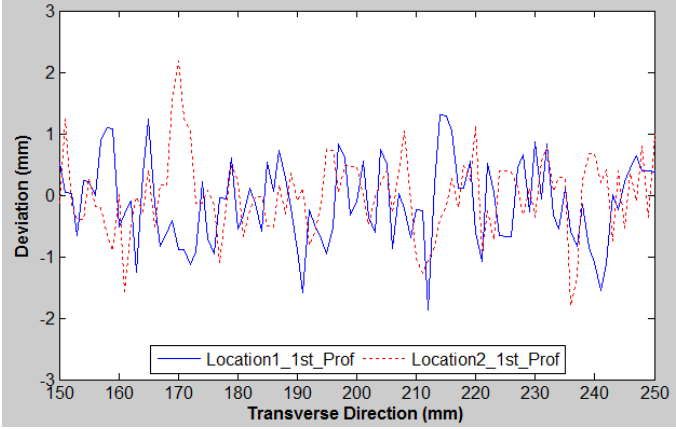

Figure 3-12 Comparison of the range measurement uncertainties at locations A and B

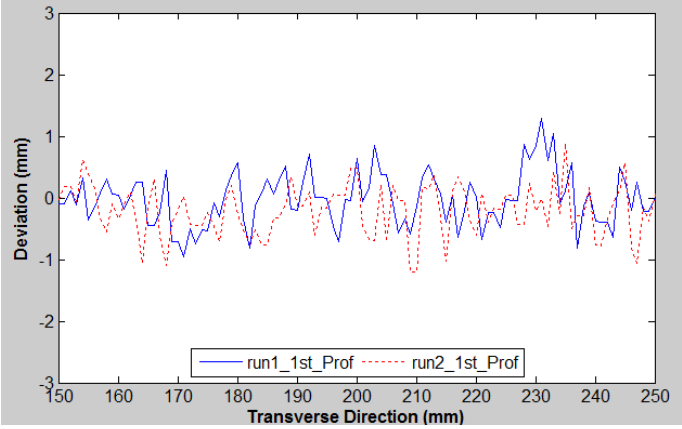

Figure 3-13 Comparison of the range measurement uncertainties at locations C and D

Figure 3-14 shows the histogram of the range measurement uncertainty for Test A-1 and Test C-1. The histogram was plot based on 1,000 profiles collected in each test. Table 3-2 tabulates the standard deviations for all tests. The average standard deviation

for the bare surface and taped surface is 0.73 mm and 0.43 mm, respectively. Therefore, based on limited tests, for surfaces made of opaque materials and with solid color, the range measurement uncertainty is 0.43 mm. This is consistent with manufacture's specification that the depth accuracy is 0.5 mm. The range measurement uncertainty is greater for surfaces made of partly-translucent materials, e.g., granite. Additional tests are needed to quantify (1) how much additional uncertainty will be introduced for surfaces made of partly-translucent materials and (2) how much additional uncertainty will be introduced for surfaces with varying colors or intensities.

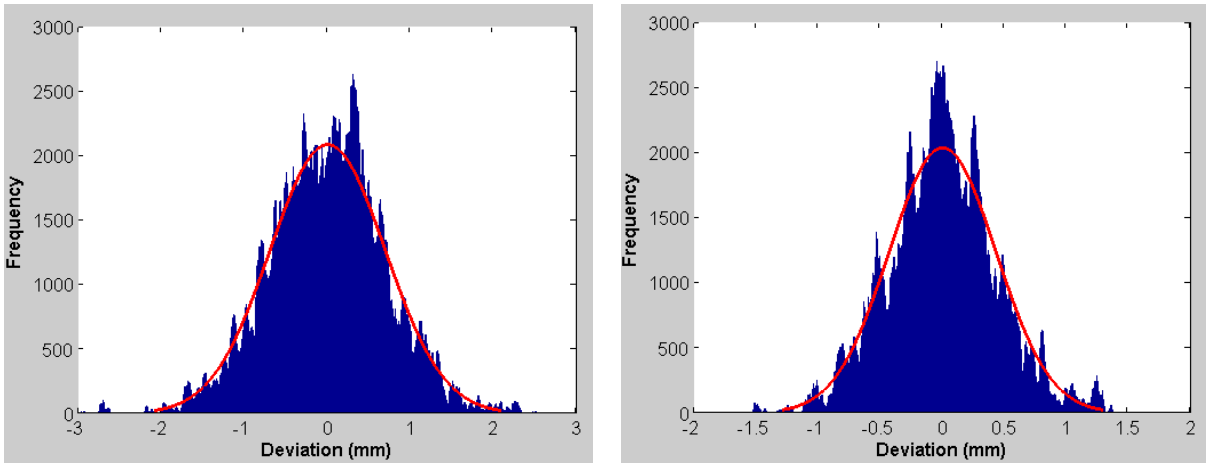

(a) Location A (b) Location C

Figure 3-14 Histogram of the range measurement uncertainty

Table 3-2 Standard Deviation of the Range Measurement Uncertainty (mm)

Test ID	A	B	C	D
1	0.70	0.75	0.43	0.44
2	0.77	0.70	0.43	0.43

Moving Test

In the moving Test, range data of the test object's surface was collected by moving the survey vehicle at a low speed. Since the test object is absolutely flat, straight lines can be used to fit collected transverse profiles. The deviation of points from the fitting straight line is the range measurement uncertainty. The uncertainty profiles are

aligned and presented in Figure 3-15(a). It is clear that the range data collected from the bare surface contains much more uncertainty compared to data from the taped surface.

Figure 3-16 shows the histogram of range measurement uncertainty for data from the bare surface and the taped surface. The standard deviations of data from the bare surface and the taped surface are 0.66 mm and 0.43 mm, respectively. The scale of this uncertainty is slightly smaller than the scale of the uncertainty captured in the static test. This shows that the vehicle moving removes some of the speckle noises and, thus, reduces the range measurement uncertainty.

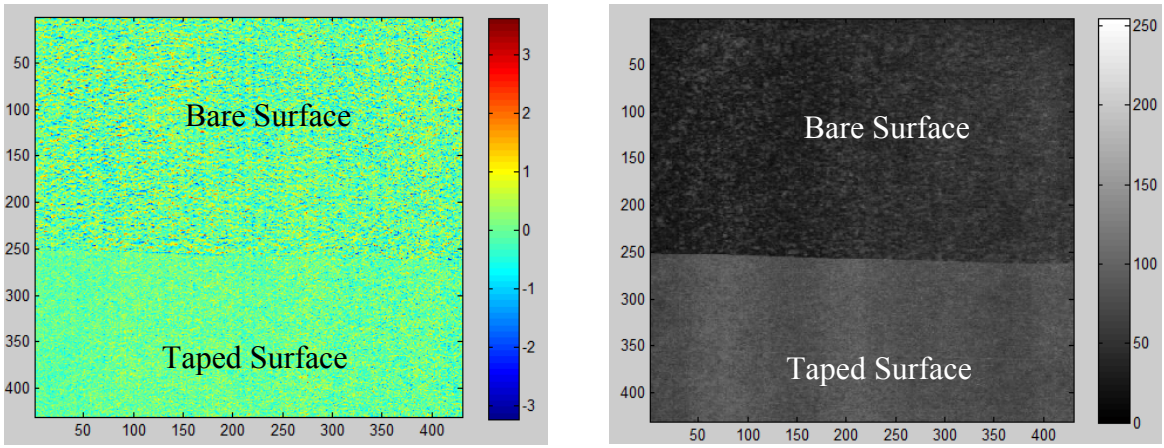

(a) Range measurement uncertainty (b) 2D intensity data

Figure 3-15 Range measurement uncertainty and intensity on the test object's surface

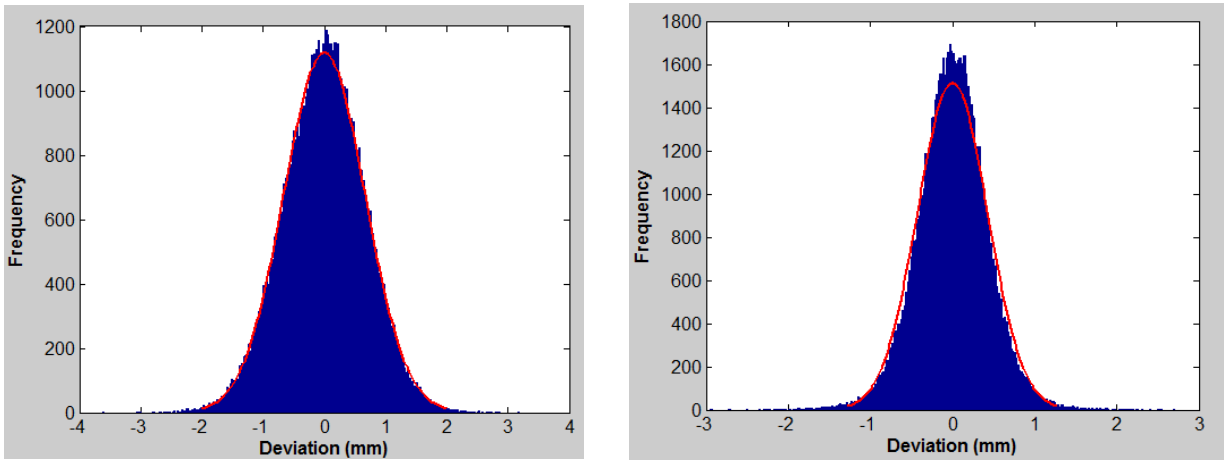

(a) Bare surface (b) Taped surface

Figure 3-16 Histogram of range measurement uncertainty

3.3.2 Missing Points

If the 3D line laser system could not obtain a valid range measurement, the 3D range value was set as -10,000. Those 3D laser points whose range value equals -10,000 are therefore denoted as missing points. There are three possible causes for missing points:

- ***The object surface gets out of the measurement range***.

As introduced in Section 3.2, the measurement range of the 3D line laser system is +/-125 mm from the calibrated ground surface. Any object, e.g., curb on the roadside, that is higher or deeper than 125 mm, will fall out of the region of interest on the CCD camera. Thus, it becomes "invisible" to the 3D line laser system, and the 3D line laser system cannot provide a valid range measurement for the object.

- ***Occlusion.***

Because of the sensor configuration (angle between the laser and the camera), some points are invisible to the camera. This phenomenon is named occlusion (Mavrinac et al. 2010) and it is an intrinsic limitation of the 3D line laser system using structured lighting and a single camera. As shown in Figure 3-17, the edge part was occluded by the object above, i.e., a curved wood board. Those regions were invisible to the 3D line laser system. Thus, the range value for those regions was set as -10,000.

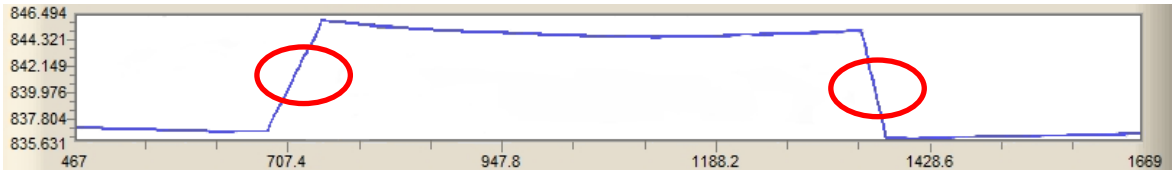

Figure 3-17 Missing data points due to occlusion

- ***Dim laser point.***

If the laser line looks dim on the CCD camera, it can be difficult to differentiate it from the background and, therefore, a reliable range value cannot be obtained. Ideally, the infrared laser line will be the brightest object on the CCD image. However, because

of the sunlight or the infrared reflection from the pavement surface, the background of the CCD image is not fully dark (Li et al. 2010). When extracting the laser line, a threshold is set in the 3D line laser system to remove those background pixels. For any portion of the laser line that looks dim, i.e., the maximum intensity is lower than the predefined threshold, -10,000 will be assigned as the range value. For example, when the object surface is very dark, most energy of the input lighting may be absorbed by the surface, sufficient light cannot be captured by the camera, and thus, missing points may be present in the 3D range data.

3.3.3 Unseemly Points

Besides missing points, unseemly points are also observed in the 3D range data. Unseemly points are defined as spikes abnormally higher or lower than the surrounding range data. Figure 3-18 gives an example. The single-point spike is around 35 mm higher than the surrounding data points, which is unlikely part of the actual pavement surface.

Figure 3-18 Example of unseemly point

3.3.3.1 Causes of Unseemly Points

To verify the cause of the unseemly points, tests have been conducted. The following summarizes the tests and test results.

- ***Effect of the Pavement Type***

Most unseemly points are found on asphalt pavement surfaces and only a few are found on concrete pavement surfaces. Hence, it is likely that some features that are common on the asphalt pavement surfaces are causing the unseemly points.

- ***Effect of Loose Rocks***

A test at Georgia Tech Savannah campus was conducted to verify whether unseemly points might be caused by loose rocks on the pavement surfaces. Approximately 40 rocks, with different colors (e.g., black or white) and varying sizes, were placed on the pavement surface, as shown in Figure 3-19. The size of the rocks ranged from 2 mm to more than 10 in. Then, the rocks were scanned using the 3D line laser system. The 3D range data was examined. The examination results show that none of the rocks, regardless of the size or color, caused unseemly points.

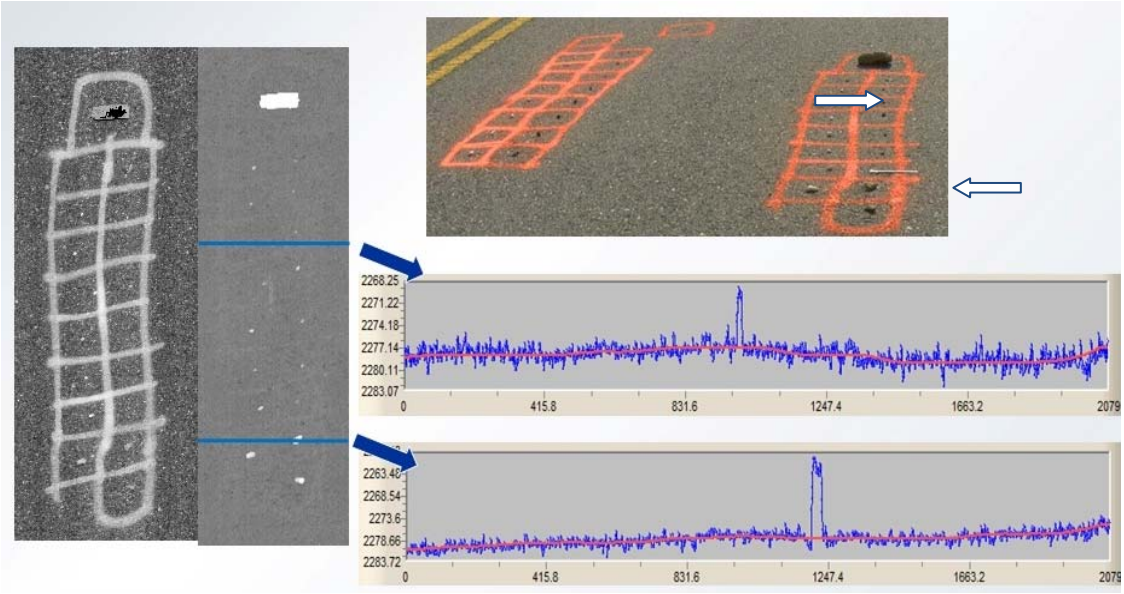

Figure 3-19 Effect of loose rocks

- ***Effect of Selected Road Surface Characteristics***

Several characteristics, including small holes, white rocks, smooth rocks, and oil stains, that could potentially result in unseemly points were identified through

visual inspection on asphalt pavements. Figure 3-20 shows the selected characteristics. These characteristics were marked on the road, and data was collected using the 3D line laser system. The 3D range data was visually examined. None of the suspected characteristics was found to actually cause any of the unseemly points.

(a) Small holes (b) White rocks (c) Smooth stones (d) Oil stains

Figure 3-20 Surface characteristics suspected to cause unseemly points

- ***Effect of Vegetation***

By examining the 3D range data, it was determined that some unseemly points, as shown in Figure 3-21, were caused by the vegetation that grew in the cracks between the asphalt surface and the concrete curb and gutter.

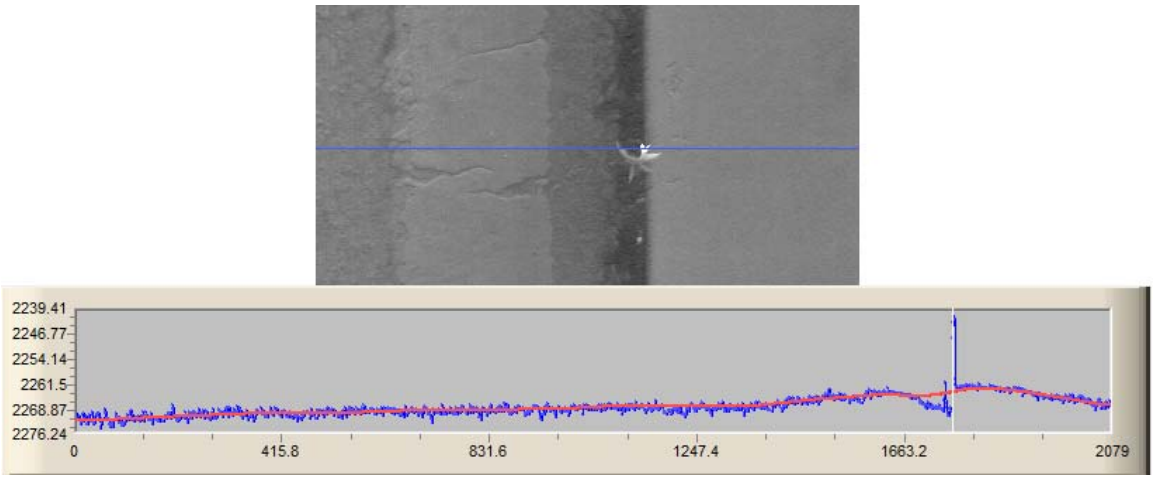

Figure 3-21 Unseemly points caused by vegetation

- ***Reflective Surface Test***

Specular components on the pavement surface may cause unseemly points. Because of the specular component, noisy reflections of the laser line may appear in the images observed by the camera. These reflections can be easily confused with the primary signal, in which case false 3D range values will result (Trucco et al., 1994). The floor, painted with reflective materials, of the laboratory located in the ELAB building at the Georgia Tech Savannah campus was tested to confirm this.

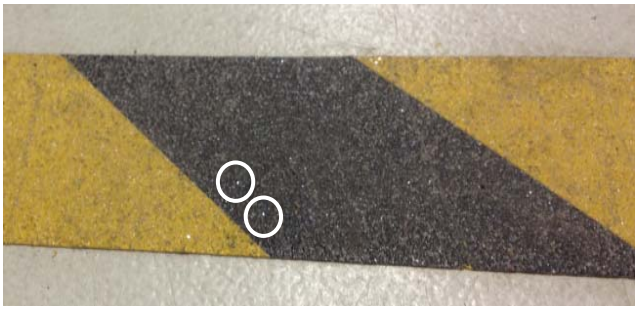

Figure 3-22 Reflective surface

Three runs of data were collected and inspected. The inspection results indicate that few unseemly points were present in the 3D range data, although a number of specular components were observed on the physical surface. Also, for some runs of data collection, unseemly points repeatedly occurred in some locations, but no unseemly points were observed in the same location for the third run. Figure 3-23 shows the location that had an unseemly point in one run but not in the other runs. This may be because the 3D line laser system may sample the pavement surface slightly differently in different data collection runs. The specular components, i.e., small glass beads in the painting material, were too small to be captured by the 3D line laser system in every run of data collection. Thus, unseemly points may be caused by the specular components on the pavement surface, and their occurrence may appear to be random.

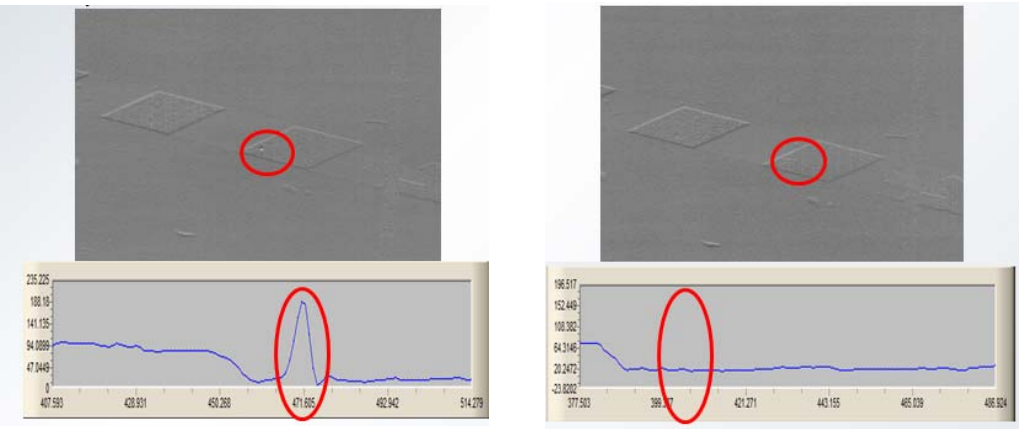

(a) Run 1 (b) Run 3

Figure 3-23 Results from the reflective surface test

3.3.3.2 Amount of Unseemly Points

Because the unseemly points adversely impact the 3D range data quality, it is desired to estimate how frequently the points appear and how much is their impact to the data quality. The amount of unseemly points in the 3D range data was estimated by randomly inspecting 3 data files that were collected by the 3D line laser system. The number of unseemly points was determined by counting spikes that were 10 mm or higher. 10 mm is selected as the conservative threshold to count changes in the 3D range data that are unlikely caused by pavement surface texture. The results from this analysis are shown in Table 3-3. The amount of unseemly points varies from file to file. However, compared to 4.16 million (= 2000 profiles * 2080 points) 3D range data points within one file, the average 90 unseemly points are only a trivial portion. Further review on hundreds of 3D range data files has confirmed this finding. Thus, the unseemly points, although present, are only a trivial portion of the whole 3D range data, and they have limited impact on the overall data quality.

Table 3-3 Amount of Unseemly Points

File #	Sensor	# of Unseemly Points	Sensor	# of Unseemly Points	Summary
1	Left	47	Right	27	74
2	Left	92	Right	65	157
3	Left	19	Right	21	40
Average	--				90

In summary, test results show that the unseemly points are possibly caused by reflective components, vegetation, and maybe other features on the pavement surfaces. The occurrence of unseemly points may appear somehow random since the 3D line laser system samples the pavement surface differently in different data collection runs. The number of unseemly points is limited, and their impact on the data quality and the repeatability of derived rutting information is expected to be minimal. Additional tests should be conducted to obtain more conclusive results.

3.3.4 Location Uncertainty (X and Y Coordinates)

An important aspect of the quality of the 3D range data is the location uncertainty of the 3D range data points in the 2D plane. Figure 3-25 illustrates how vehicle movement, including raw, pitch, and roll, changes the location of the laser line from its expected location on the pavement surface. It may shift the laser line from the expected location to a partially or totally new location, and it may pick up a paritially new transverse profile, as shown in Figure 3-25(a), or a totally new transverse profile, as shown in Figure 3-25(b), (c), and (d). Consequently, the 3D line laser system does not take equal-spacing samples of the roadway surface, as described in Figure 3-24(a), because of vehicle movement. This is the uncertainty in the location (X and Y coordinates) of the 3D range data. An extreme case of the location uncertainty because of vehicle movement is shown in Figure 3-24(b). The location uncertainty in the driving direction is ignorable compared to the scale of smallest pavement inspection unit, e.g.,

0.1 mile. However, the location uncertainty in the transverse direction may become critical when the 3D line laser system is used to measure the rut depth. This issue will be further discussed in Chapter 7.

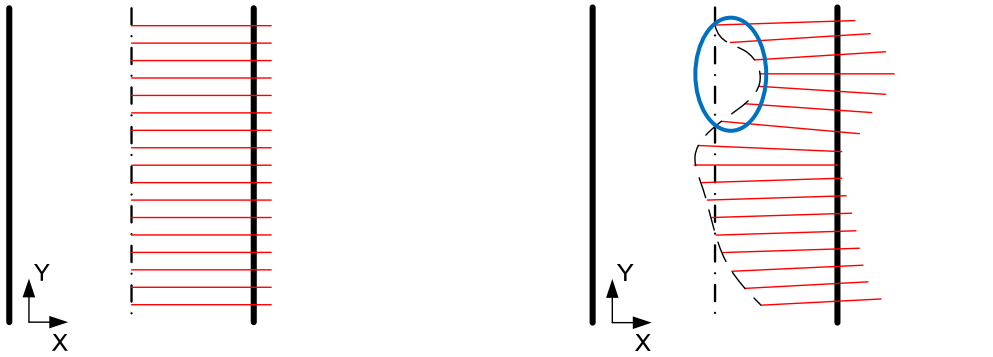

(a) Ideal case (b) Data collected when vehicle moves

Figure 3-24 Location uncertainty due to vehicle wanders and rotates

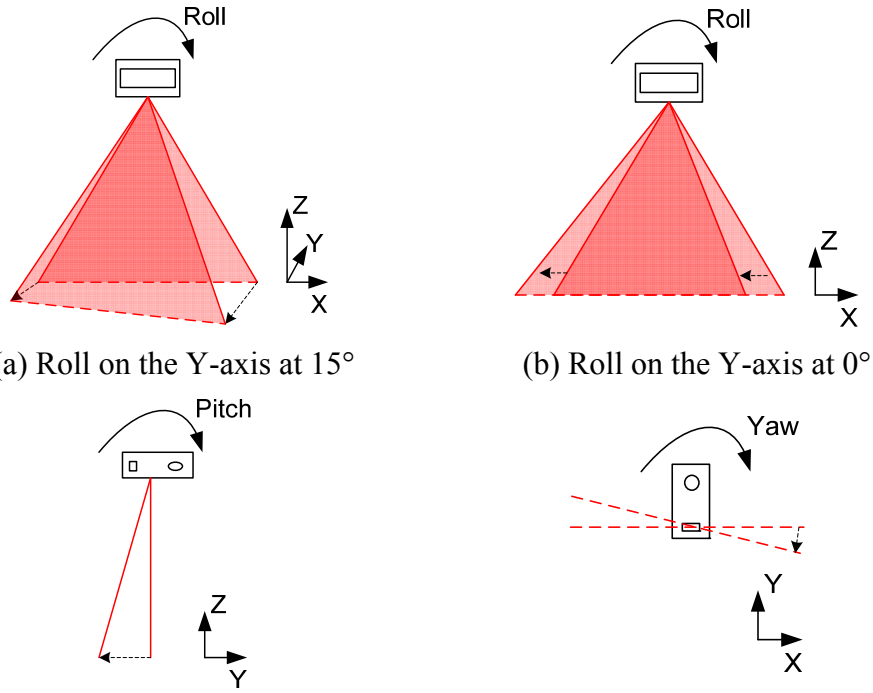

(a) Roll on the Y-axis at 15° (b) Roll on the Y-axis at 0°

(c) Pitch on the X-axis (d) Yaw on the Z-axis

Figure 3-25 Change of the laser line location when vehicle moves

3.3.5 Other Cases

3.3.5.1 Bump Test

Bumps are usually used as a safety counter measurement on city streets to calm moving traffic (Pat Noyes & Associates 1998). The presence of bumps, however, will adversely impact the quality of 3D range data collected by the sensing vehicle. To assess this impact, bump tests have been conducted on the Osprey Point Circle near Savannah, Georgia. Figure 3-26 shows the typical 3D range data collected when there is a bump. As observed in the data, when the front wheel crosses a bump, it has ignorable impact on the 3D range data quality; however, when the rear wheel crosses the bump, it leaves a dark band before the bump in the 3D range data, as shown in Figure 3-26. It looks like that the road surface before the bump was depressed, which, in reality, it is not. Missing points are also present in the 3D range data, since the portion of bump got out of the measurement range.

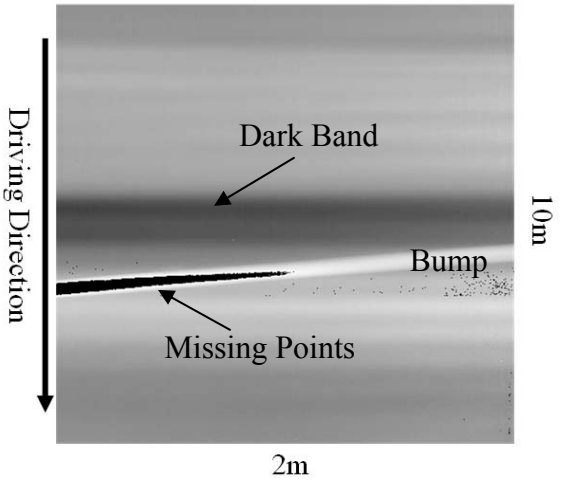

Figure 3-26 Data collected when there is a bump

Figure 3-27 explains the cause of the dark band. When the rear wheel crosses the bump, it is pushed upwards by the bump, as is the 3D line laser system. Thus the distance between the laser emit point and the road surface is elongated and, thereby, the measured range data gets increased. In other words, the increase of the range data is caused by the

position change of the laser profiler, not a depression in the road surface. However, the current 3D line laser system is not coupled with a sensor unit, such as an inertial measurement unit (IMU), to detect its own position change. Any change in the range data is simply assumed to be caused by features on the road surface. Consequently, the increase in the 3D range data because of lifted profilers is "wrongly" recognized as a depression in the road surface. In the future, this can be improved by integrating an IMU and the 3D line laser system.

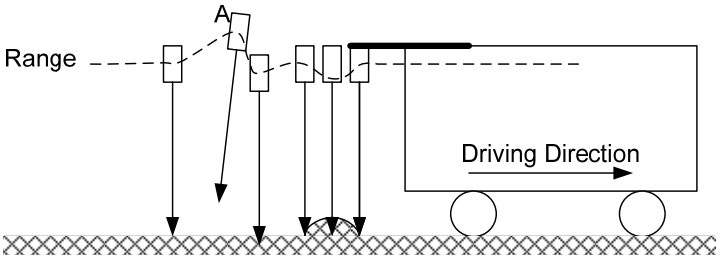

Figure 3-27 Range data change when there is a bump

3.3.5.2 Data collection on New Pavements

The 3D range data collected from newly-paved open graded friction course (OGFC) contain a significant number of missing points and unseemly points, since its surface is dark and specular. Figure 3-28 shows an example. The black points observed in Figure 3-28 are missing points and unseemly points that are abnormally lower than surrounding range data, and the white points are unseemly points that are abnormally higher than surrounding range data. A 3D transverse profile highlighted with a blue straight line in Figure 3-28(a) is shown in Figure 3-28(b). As shown in Figure 3-28(b), the 3D transverse profile which is the blue one contains a number of spikes that are unlikely part of the actual pavement surface. The red line is the smoothed transverse profile obtained after applying some low-pass filter to the blue profile. In summary, the quality of the 3D range data collected from newly-paved OGFC using a 3D line laser system is inferior to the quality of 3D range data collected from aged pavements.

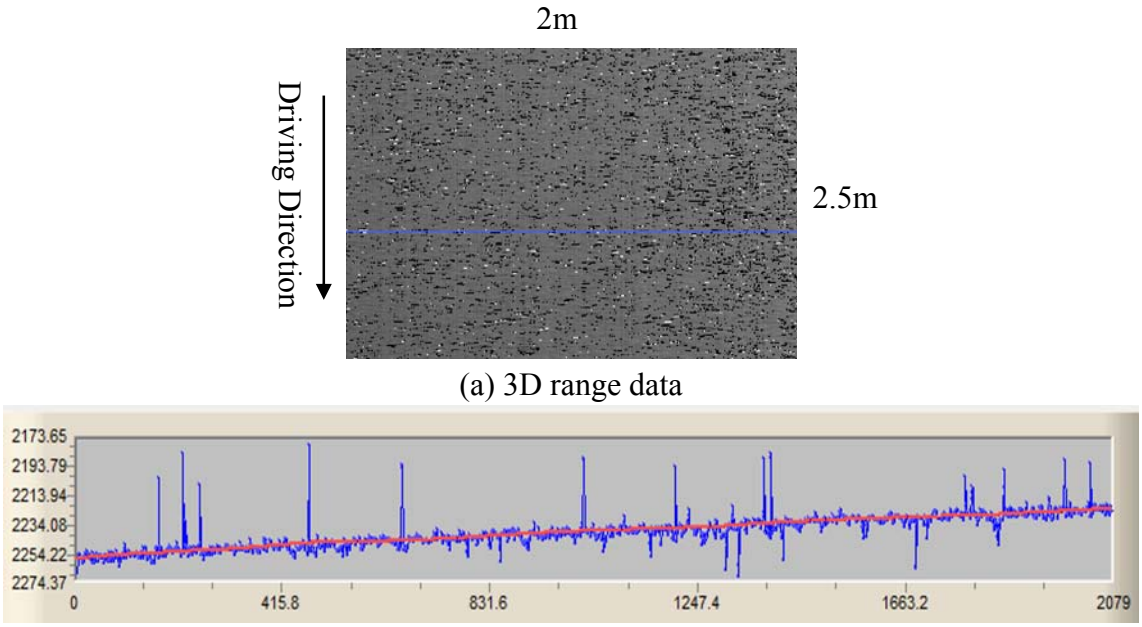

(a) 3D range data

(b) 3D transverse profile

Figure 3-28 3D range data collected on newly paved OGFC

3.4 Summary

The GTSV, developed by the Georgia Tech research team, was integrated with one of the commercial 3D line laser systems. The 3D line laser system is capable of collecting high-resolution (i.e., 1 mm in transverse direction and 5 mm in longitudinal direction) 3D range data at highway speed (e.g., 100 km/h). Because of its high-resolution, the 3D system can provide essentially 100% coverage of the pavement surface. It is potentially capable to collect various pavement surface distresses through a single data collection run in the future. Additional findings through laboratory and field tests are the following.

- Static and moving tests show that the standard deviation of the range measurement uncertainty is around 0.43 mm for the taped surface (with uniform intensity). This confirms the specification that the measurement uncertainty of the 3D line laser system is no more than 0.5 mm. In addition, the test results show that the majority of the range measurement uncertainty is not random.

- Irregular data points, including missing points and unseemly points, were observed in the 3D range data. Missing points occur when the pavement surface gets out of the measurement range of the 3D line laser system, when the pavement surface is occluded, or when the laser line on the CCD sensor looks dim. Unseemly points are possibly caused by reflective components present on asphalt pavement surfaces. Nevertheless, the amount of unseemly range data is limited compared to the enormous amount of data collected by the 3D line laser system. Consequently, they have minimal impact on the quality of the 3D range data.

In summary, this preliminary study confirmed that the 3D line laser system is capable of providing quality 3D range data consistently for the majority of pavement surfaces. More thorough experimental tests and assessment are recommended in the future research.

CHAPTER 4 EXPERIMENTAL TESTS FOR ASSESSING RUTTING MEASUREMET ACCURACY AND REPEATABILITY USING THE 3D LINE LASER SYSTEM

According to Chapter 2, there is a need to validate the accuracy and repeatability of rutting measurements (including 1D rut depth, rut length, and 3D rut volume) extracted from the 3D range data collected using the 3D line laser system. To address this need, experimental tests were conducted in the laboratory and in the field with established ground truths. The experimental test design and results are presented in this chapter.

4.1 Rut Depth Measurement Accuracy

This section presents the laboratory and field tests that were conducted to validate the rut depth measurement accuracy of the 3D line laser system. In these tests, 3D range data, consisting of 3D continuous transverse profiles, were first acquired using the 3D line laser system; the simulation straightedge methods (presented in Section 4.1.1) were used to process the transverse profiles and obtain rut depth measurements. The laser-profile-measured rut depths were compared to manually-measured ground truths to quantify the rut depth measurement accuracy of the 3D line laser system. The remainder of this section introduces the simulated straightedge methods and then the laboratory and field tests.

4.1.1 Simulated Straightedge Methods

A simulated straightedge method, which is based on the manual method suggested in the ASTM 1703 Standard (2010), was provided by the manufacture to measure the rut depths from 3D range data (Laurent et al. 1997; INO 2010). However, the manufacture-

developed method cannot be customized for laboratory tests. Therefore, another simulated straightedge method employing the Discrete Cosine Transform (DCT) was developed in this study. A comparison was made to ensure that both the DCT-based method and the manufacture-developed method are providing similar rut depth measurements. Both simulated straightedge methods are presented and compared in this subsection.

4.1.1.1 Manufacture-Developed Simulated Straightedge Method

A simulated straightedge method was implemented by the manufacture of the 3D line laser system used in this study (INO 2010). The method is shown in Figure 4-1. The curve is a pavement surface transverse profile. The straight line simulates the straightedge, and the rectangular block simulates the gauge that is used to read the rut depth measurement in the field. The gauge width is adjustable. In this study, 5 mm was used. The simulated straightedge method is implemented as follows. First, a median filter is used to smooth the transverse profile, and the smoothed profile is then fit with straight lines. Second, the rut support point pairs, (x_L, z_L) and (x_R, z_R), are identified and justified. Third, the rutting characteristics (including the rut depth, rut width, rut shape, and rut cross-section area) are measured for both wheel paths.

- Rut depth is given by: $Depth = \sqrt{(x_B - x_T)^2 + (z_B - z_T)^2}$.
- Rut width is given by: $Width = \sqrt{(x_R - x_L)^2 + (z_R - z_L)^2}$.
- Rut cross-sectional area is the cross-sectional area of the detected rut under the straightedge.

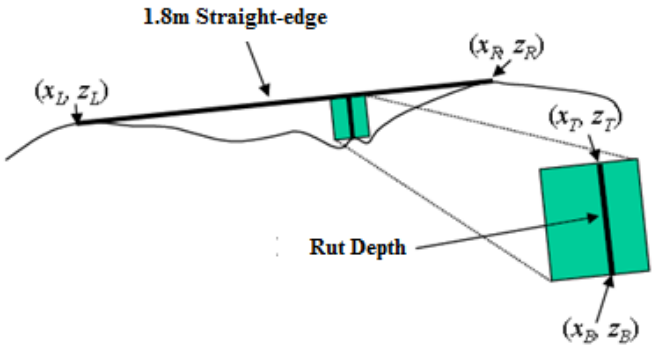

Figure 4-1 Rut depth computation (INO 2010)

4.1.1.2 DCT-based Simulated Straightedge Method

Another simulated straightedge method was developed by the Georgia Tech research team. The algorithm employed the Discrete Cosine Transform (DCT) to smooth out the high-frequency variations resulting from the pavement surface texture and the 3D noises. The DCT coefficients were selected to preserve 99.9% of the total signal energy. The smoothed transverse profile is shown in Figure 4-2(a). Due to the significant end effect of DCT, as seen in Figure 4-2(a), which will impact the accuracy of rut depth measurement, a stepwise linear interpolation was used at the two ends of the transverse profile. The improved, smoothed transverse profile can be seen in Figure 4-2(b). After the transverse profiles were smoothed, a 1.8-m straightedge was simulated to calculate the rut depths. The computation procedure is as follows:

- Identify the highest points at both ends of a transverse profile that are the support points of the straightedge;
- Connect the two support points;
- The maximum distance between the simulated straightedge and the transverse profile is the rut depth, as shown in Figure 4-3.

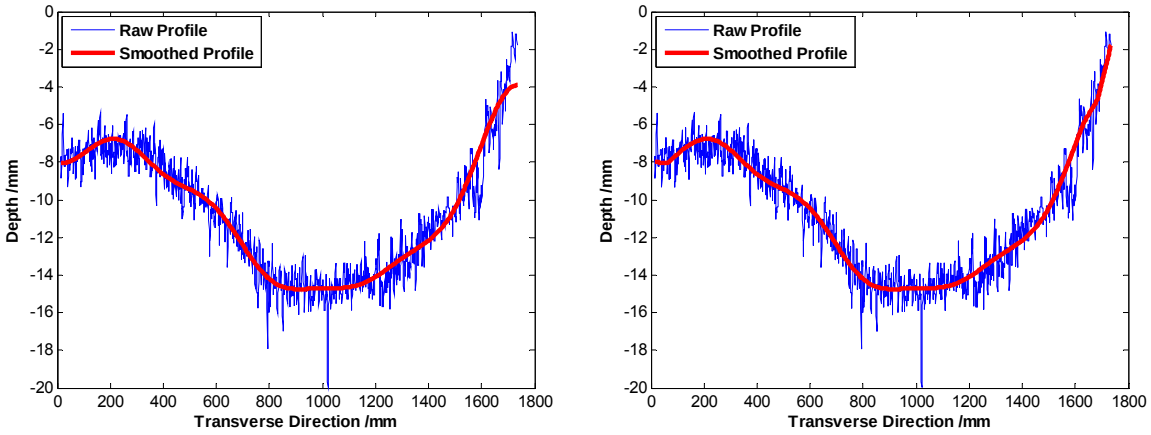

(a) DCT only (b) DCT plus stepwise linear interpolation

Figure 4-2 Smoothed transverse profiles

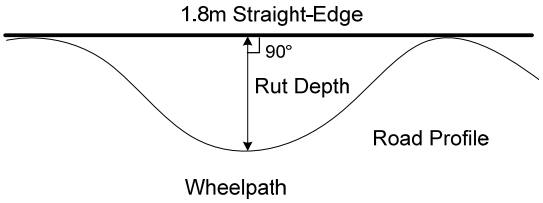

Figure 4-3 1.8-m straightedge method

4.1.1.3 Comparison between Manufacture-Developed and DCT-based Straightedge Methods

To ensure that the manufacture-developed and the DCT-based methods deliver similar rut depth measurements, both methods were used to process 10 transverse profiles collected from county roads in the field test (which will be presented in Section 4.1.3). The results are tabulated in Table 4-1. According to the comparison, the absolute difference between the manufacture-developed and DCT-based methods is less than 1 mm, which indicates that both methods can provide essentially similar rut depth measurements.

Table 4-1 Comparison between Manufacture-Developed and DCT-based Methods

Profile #	Manufacture-Method-Measured				DCT-Method-Measured				Average Difference
	Run 1	Run 2	Run 3	Average	Run 1	Run 2	Run 3	Average	
1	12.1	14	13.5	13.2	12.4	14.4	13.3	13.3	-0.1
2	13.4	14.6	12.8	13.6	13.9	14.8	14.0	14.2	-0.6
3	10.7	10.8	10.3	10.6	10.6	10.5	10.2	10.5	0.1
4	12.9	12.1	11.3	12.1	12.6	12.4	11.2	12.1	0.0
5	6	6.7	7.6	6.8	6.5	7.2	8.4	7.4	-0.6
6	7.3	7.2	7.1	7.2	7.8	7.4	7.1	7.5	-0.3
7	5.9	6	6.6	6.2	6.4	5.9	6.4	6.2	-0.1
8	7.2	7.1	7.2	7.2	7.8	7.6	7.6	7.7	-0.5
9	19.8	20.8	20.3	20.3	20.3	20.4	20.4	20.3	0.0
10	5.7	4.7	5.3	5.2	5.7	4.8	5.5	5.4	-0.1

4.1.2 Laboratory Test

To validate the laser's rut depth measurement accuracy under controlled environment, laboratory test was conducted. Different severity levels of rutting were simulated in the laboratory using a curved wood board and a curved metal bar, as shown in Figure 4-4(a) and (b). On the wood board, 10 profiles were marked with blue tape. The rut depths of those profiles vary from several millimeters to several centimeters. The curved metal bar was used to simulate a rut of the high severity level. Thus, there were 11 profiles fabricated in the laboratory to simulate ruts with different severity levels.

The ground truth was established by using the straightedge method specified in ASTM Standard E1703 (2010). As shown in Figure 4-4(a), a steel angle bar was used as the straightedge. The rut depth was measured using a vernier caliper with a precision of 0.02 mm. During the measurement, the vernier caliper was set perpendicular to the steel bar. To identify the maximal distance between the steel bar and the wood board surface, sufficient measurements were made at different locations along the steel bar. The

measurement for each profile was repeated three times. The average rut depth of these three times was used as the ground truth.

The 3D line laser system was set up in the laboratory as shown in Figure 4-5(b). Because the length of the simulated pavement profiles was less than half a lane, only one laser profiling unit was installed. The infrared camera shown in Figure 4-5(b) was used to observe the invisible laser line. The data collection procedure for each profile was repeated twice. During each procedure, the wood board or the metal bar was placed under the laser profiling unit, and its position was fine-tuned until the laser line was right on the marked profile. Then, 2,000 repetitive data profiles were collected. For testing the 11 simulated ruts, a total of 44,000 (=11*2*2,000) profiles were obtained. The rut depth for each profile was calculated using the DCT-based simulated straightedge method presented in Section 4.1.1.2. Figure 4-6 shows typical transverse profiles collected by the 3D line laser system. The collected profiles were not very smooth. Due to the relatively smooth surface of the simulated ruts in the laboratory, the data variation in Figure 4-6 could come from the noise of the sensing device.

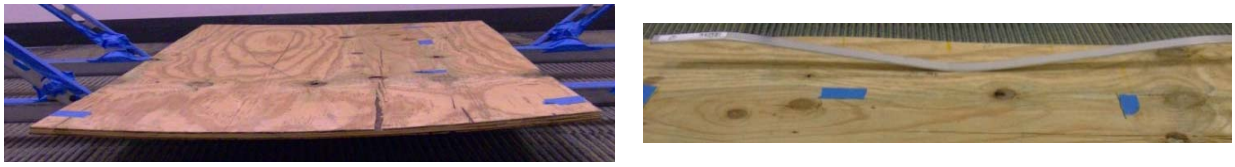

(a) Wood board (b) Metal bar

Figure 4-4 Simulated ruts in the laboratory

(a) Straightedge method (b) 3D line laser system setup in the laboratory

Figure 4-5 Laboratory test setup

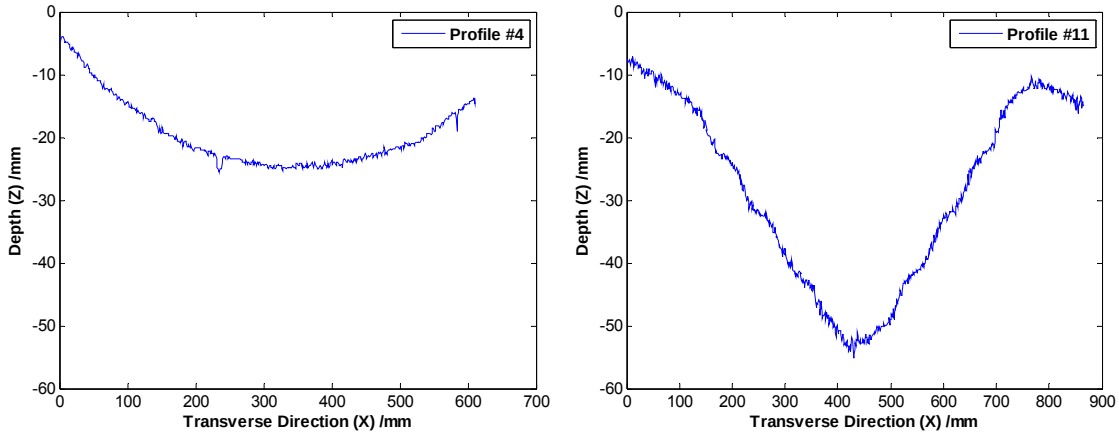

(a) Wood board (b) Metal bar

Figure 4-6 Typical transverse profiles measured in the laboratory

Table 4-2 shows the rut depth measurement results of the 11 simulated ruts. The average manual measurements vary from 8.0 mm to 43.4 mm covering the low to high severity levels and were used as the ground truth. Two runs of 3D range data collection were performed to evaluate the repeatability of the 3D line laser system. The difference between these two runs ranges from 0.1 mm to 1.3 mm, which is comparable to the manual measurement error. The absolute difference between the DCT-method-measured results and the ground truth varies from 0.0 mm to 0.7 mm, which is less than 1 mm. Figure 4-7 shows the correlation of rut depth measurements between the two runs. In

accordance with the standard ASTM C670-03 (2010), the average coefficient of variance is about 4.4%, which indicates good measurement repeatability.

Table 4-2 Laboratory Testing Results

Profile #	Severity Level	Rut Depth (mm)					
		Ground Truth	DCT-Method-Measured				Absolute Difference to Ground Truth
			Run 1	Run 2	Difference between Runs	Average	
1	Low	8.0	8.3	7.1	1.2	7.7	0.3
2	Low	7.9	8.2	8.0	0.2	8.1	0.2
3	Low	7.9	6.8	7.6	0.8	7.2	0.7
4	Medium	13.2	13.2	13.1	0.1	13.2	0.0
5	Low	12.3	12.3	11.5	0.8	11.9	0.4
6	Medium	14.2	13.8	14.0	0.2	13.9	0.3
7	Medium	15.5	15.0	14.8	0.2	14.9	0.6
8	Medium	16.2	15.4	16.7	1.3	16.1	0.1
9	Medium	17.5	17.6	17.1	0.5	17.4	0.1
10	Medium	10.0	11.0	9.7	1.3	10.4	0.4
11	High	43.4	43.2	N/A	N/A	43.2	0.2

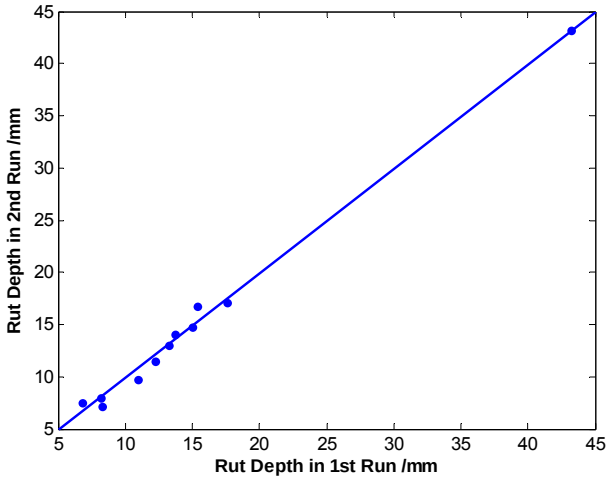

Figure 4-7 Correlation of DCT-method-measured rut depths in two runs in the laboratory

4.1.3 Field Test

Two local roadway sections were selected in Pooler, Georgia, for the sake of manual survey safety. As shown in Figure 4-8(a), a 725-m roadway section was chosen on Benton Blvd., and a 45-m roadway section was selected on Towne Center Ct., as shown in Figure 4-8(b). Six test transverse profiles, which are visible on the laser intensity data, were marked on Benton Blvd. On the Towne Center Ct., 4 test profiles were marked. To establish the rut depth ground truth of the 10 test profiles, a 1.8-m straightedge method was performed as shown in Figure 4-8(c). The same measurement procedure was followed as in the laboratory test, which was repeated three times for each test profile. The average rut depth of those three times was used as the ground truth.

(a) Roadway section on Benton Blvd.

(b) Roadway section on Towne Center Ct.

(c) 1.8-m straightedge method

(d) Data collection vehicle

Figure 4-8 Field test setup

The GTSV, as shown in Figure 4-8(d), collected 3D range data, consisting of transverse profiles, three runs for each roadway section. Typical transverse profiles are shown in Figure 4-9. The collected transverse profiles were then processed using the DCT-based straightedge method presented in Section 4.1.2 to compute the corresponding rut depth.

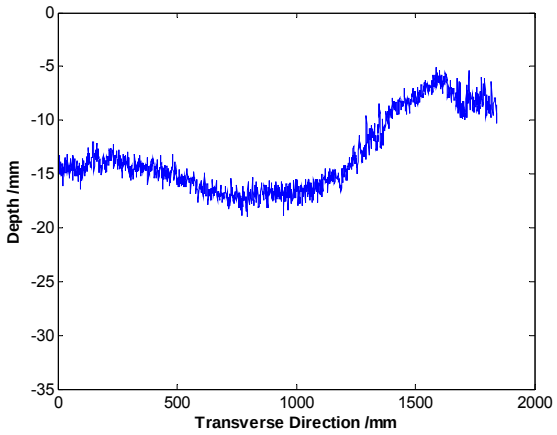

(a) Low severity level rutting

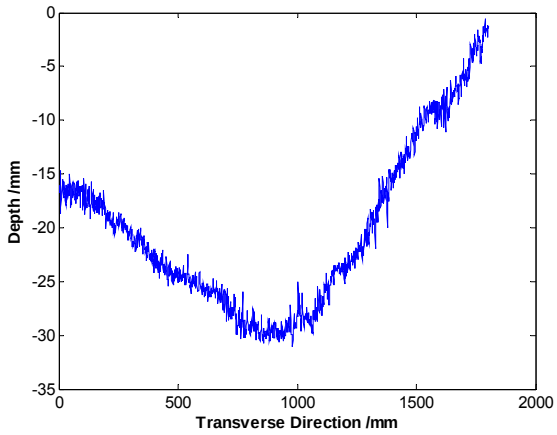

(b) Medium severity level rutting

Figure 4-9 Typical transverse profiles obtained by the 3D line laser system

The field test results on the local roads are summarized in Table 4-3. Ten manually marked profiles on the test roadway sections were examined. The manually measured rut depths, which are considered as the ground truth, vary from 6.4 mm to 21.1 mm. They correspond to the low to high severity rutting. The absolute difference

between the manual measurements and the average of DCT-method-measured results varies from 0.8 mm to 2.1 mm, which is higher than the one in the well-controlled laboratory test. Several factors could contribute to this. First, for a profile-based comparison, it is very critical to make sure that the location of each extracted profile from 3D range data is exactly the same as the manually marked and measured one. In the harsh field testing environment, it is very difficult to make this happen. Second, unlike the well-controlled laboratory test, vehicle wandering is inevitable in a field test, which impacts the rut depth measurement.

Table 4-3 Field Testing Results

Profile #	Severity Level	Rut Depth (mm)					
		Ground Truth	DCT-Method-Measured				Absolute Difference to Ground Truth
			Run 1	Run 2	Run 3	Average	
1	Medium	14.5	12.4	14.4	13.3	13.3	1.2
2	Medium	15.8	13.9	14.8	14.0	14.2	1.6
3	Low	9.6	10.6	10.5	10.2	10.5	0.9
4	Medium	14.2	12.6	12.4	11.2	12.1	2.1
5	Low	8.5	6.5	7.2	8.4	7.4	1.1
6	Low	9.5	7.8	7.4	7.1	7.5	2.0
7	Low	7.8	6.4	5.9	6.4	6.2	1.6
8	Low	9.4	7.8	7.6	7.6	7.7	1.7
9	High	21.1	20.3	20.4	20.4	20.3	0.8
10	Low	6.4	5.7	4.8	5.5	5.4	1.0

From the test results listed in Table 4-3, the absolute rut depth measurement difference is around 1.6 mm, which is the average of "difference to ground truth." Also, this difference is random and independent of the rut depth, which indicates that the relative error decreases with the increase of rut depth. For example, though the relative error for profile #10 is around 19%, the one for profile #9, which has the largest rut depth, is just 4%. This will assure the accuracy of rut depth measurement for more severe rutting, which is of the most concern in transportation agencies' practices. In addition, for the network level rutting survey, profile-based rutting measurements are normally aggregated at a fixed interval, such as 1 m, which will further reduce the random measurement error.

Figure 4-10 shows the correlation of DCT-method-measured rut depths for three runs. The average coefficient of variance is about 5.3%, which shows good measurement repeatability.

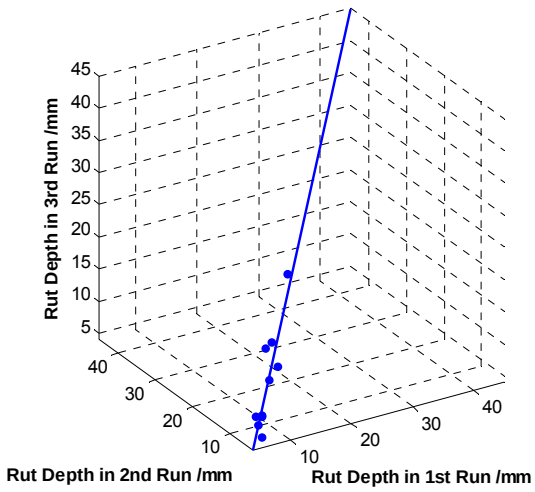

Figure 4-10 Correlation of DCT-method-measured rut depths in three runs in the field

4.1.5 Summary

The assessment on the rut depth measurement accuracy using the 3D line laser system is presented in this section. Eleven laboratory-simulated profiles and 10 field-

selected profiles (from two county routes) were tested in a well-controlled laboratory environment and in a practical field environment. The ground truth for each testing profile was established by using the manual straightedge method. The rut depths of acquired transverse profiles were calculated using a DCT-based simulated straightedge method. Both laboratory and field tests show promising results.

Laboratory testing results show that the absolute difference between DCT-method-measured rut depths and the ground truth varies from 0.0 mm to 0.7 mm. Due to the uncontrolled environment, such as vehicle wandering, the results from both field tests are inferior to the ones in the laboratory. However, the absolute difference, which ranges from 0.8 mm to 2.1 mm, still satisfies the rut depth measurement requirement, which is +/-3 mm, for multiple transportation agencies (ADOT 2002; McGhee 2004). More importantly, the testing results indicate the difference is random and has no dependence on the rut depth, which means the relative measurement error would decrease for more severe rutting.

4.2 Rut Depth Measurement Repeatability and Reproducibility

To use the 3D line laser system to assess the network-level pavement rutting condition and monitor the long-term pavement performance, the 3D line laser system should be capable of producing accurate rut depth measurements consistently. However, many factors, such as the measurement uncertainties intrinsic to the 3D line laser system, vehicle wandering, and roadway environment, contribute to the variability of the rut depth measurements. To quantify the consistency of the 3D line laser system, both repeatability and reproducibility, commonly used for describing the variability of a measurement method (ISO 5725-1 1994), were assessed. The repeatability was determined based on repeated independent tests conducted by the same surveyor and the same device within short interval of time. The reproducibility was determined based on

repeated independent tests conducted by different surveyors and the same device within short interval of time.

Experimental tests were carried out in both the laboratory and the field to assess the repeatability and reproducibility of the 3D line laser system. In the laboratory, fabricated ruts shown in Figure 4-4 were tested when both the laser profiling unit and the test profile were in stationary position. In the field, multiple surveyors were employed to survey two selected roadway sections, which have different roadway environments (e.g., pavement surface distresses, pavement surface mixtures, lane widths, and speed limits). This is because the extent of vehicle wandering varies if the surveyor or the roadway environment changes. This section presents the experimental test design and test results.

4.2.1 Laboratory Test

In the laboratory, transverse profiles were collected by the 3D line laser system repeatedly for each fabricated rut (as shown in Figure 4-4) when both the laser profiling unit and the fabricated rut were in stationary position. Totally, 2,000 profiles were collected for each rut uninterruptedly. These 2,000 profiles were used to assess the repeatability of the 3D line laser system. The potential factor that impacts the repeatability is the range measurement uncertainty intrinsic to the 3D line laser system. Table 4-4 summarizes the analysis results with regard to the standard deviation of rut depths of 2,000 profiles for each fabricated rut. It shows that the standard deviation varies from 0.1 mm to 0.3 mm, which indicates satisfactory repeatability of the 3D line laser system.

Table 4-4 Standard Deviation of Rut Depths of 2,000 Profiles

Profile #		1	2	3	4	5	6	7	8	9	10	11
Standard Deviation (mm)	Run 1	0.1	0.2	0.2	0.1	0.1	0.2	0.1	0.2	0.1	0.2	0.3
	Run 2	0.2	0.1	0.1	0.2	0.2	0.2	0.2	0.2	0.1	0.2	N/A

4.2.2 Field Test

Table 4-5 summarizes experimental design of the field test. Two roadway sections, which are straight and have no horizontal or vertical curvature, were selected for the field test. One test section is located on Benton Blvd. (an 11-ft wide city road with gutter and curb) and the other one is on I-95 (a 12-ft wide interstate highway). The lane markings in both test sections were in good condition. The speed limit is 45 miles/hour for Benton Blvd. and 65 miles/hour for I-95. In the field test, three surveyors were employed to survey those two test sections. For each test section, the 3D range data were collected using the GTSV at 5 mm intervals in the driving direction for 5 runs. In addition, to control the vehicle wandering due to surrounding traffic to a minimum level, the data collection was conducted during non-peak hours. The data collection on I-95 was carried out on a Sunday, when there was minimum truck traffic. Moreover, all the surveyors were required to drive as straight as possible with minimal meandering. To further assure this requirement, the collected 3D range data were reviewed and only data with both left and right lane marking visible were used for repeatability assessment.

The manufacture-developed straightedge method presented in Section 4.1.1.1 was used to process the collected 3D range data and calculate 1D rut depths. The 1D rut depth measurements were then aligned into longitudinal rut depth profiles in the driving direction. Qualitative and quantitative analyses were conducted on aligned longitudinal rut depth profiles to assess the repeatability and reproducibility of the 3D line laser system. The remainder of this subsection presents the analyses and the analysis results.

Table 4-5 Experimental Test Design

Test Section	Section Length (ft)	Lane Width (ft)	Speed Limit (miles/hour)	Surveyor 1	Surveyor 2	Surveyor 3
I-95	510	12	65	N/A	N/A	Repeated for 5 runs
Benton Blvd.	320	11	45	Repeated for 5 runs	Repeated for 5 runs	N/A

4.2.2.1 Multi-run Data Registration

It is observed that the longitudinal rut depth profiles collected repeatedly usually do not match each other since the survey vehicle could not follow exactly the same route repeatedly. As shown in Figure 4-11(a), an obvious shift is observed between the Run 2's profile and the other runs. This shift might lead to underestimation of the rut depth measurement repeatability of the 3D line laser system. Therefore, the shift needs to be compensated for and longitudinal rut depth profiles collected from different runs need to be registered before assessing the repeatability and reproducibility of the 3D line laser system.

Obviously, the shift is not constant, but accumulates as the survey vehicle travels. The shift is zero at the start of the test section and reaches its maximum at the end of the test section. The accumulation rate may vary across different test sections and different surveyors. Therefore, it is challenging to register repeatedly collected longitudinal rut depth profiles. However, the multi-time registration can be simplified by assuming the accumulation rate is constant across the test section. This assumption is acceptable given that the test section is up to 510 ft long and the total accumulated vehicle wandering for these test sections is no more than 5 ft. Under this assumption, a simplified method is proposed to remove the accumulated shift. The method (a) fixes the start and end point of the test section; (b) selects the shortest longitudinal rut depth profile out of the 5 repeatedly collected profiles; (c) compresses other 4 rut depth profiles to have the same length as the shortest one; (d) reports the average rut depth per foot. As shown in Figure 4-11(b), the proposed method has effectively removed the accumulated shift.

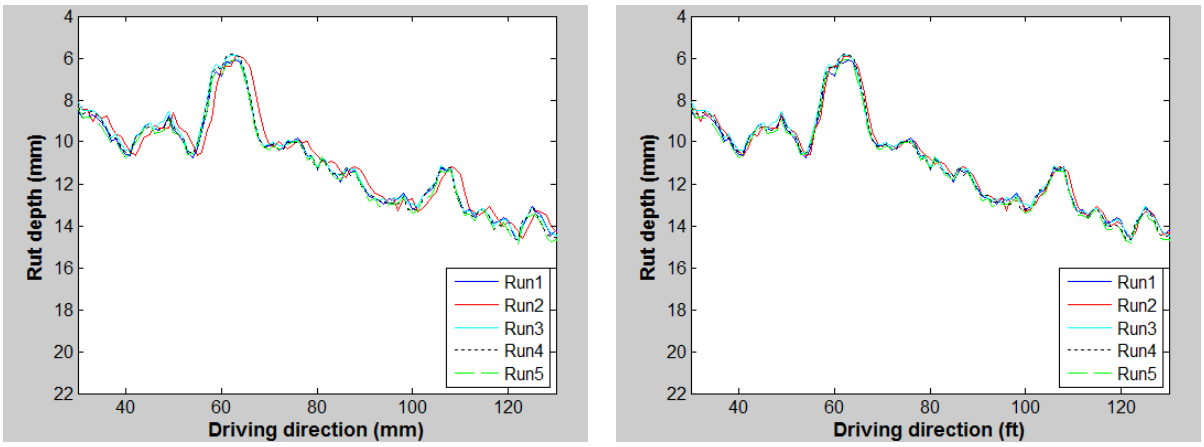

(a) Before adjustment (b) After adjustment

Figure 4-11 Shift adjustment to align rut depth Profiles

4.2.2.2 Test Results

Visual Inspection

This subsection compares longitudinal rut depth profiles collected in different runs of the survey. Visual inspection of profile plots was used as a diagnostic tool to qualitatively assess the agreement between profiles and identify potential factors that result in rut depth measurement inconsistency.

Figure 4-12 shows all the longitudinal rut depth profiles from I-95 test section. Figure 4-13 are the profiles collected by Surveyor 1 from the Benton Blvd. test section and Figure 4-14 are by Surveyor 2. It is observed that the rut depths collected during different runs are very close to each other, which indicates a high repeatability of the 3D line laser system.

Moreover, it is found that the profiles from I-95 (in Figure 4-12) have a better agreement between different runs; the agreement between profiles collected from Benton Blvd. is much inferior, although the texture of the OGFC surface layer on I-95 is rougher than the texture on Benton Blvd. The poor agreement could be contributed by the following factors: a) the survey vehicle wanders less when running on the interstate highway at highway speed; b) the rut on I-95 is narrower than the one on Benton Blvd.; c) the I-95 test section does not have much cracking; d) the impact of surface texture has been eliminated in the process of computing rut depths; e) the true profile might have slightly changed between runs because of temperature and other environmental effects. Specifically, for the Benton Blvd. test section, vehicle wandering is identified as the prominent contributor to the inferior agreement. Figure 4-15 gives an example to illustrate the impact of vehicle wandering.

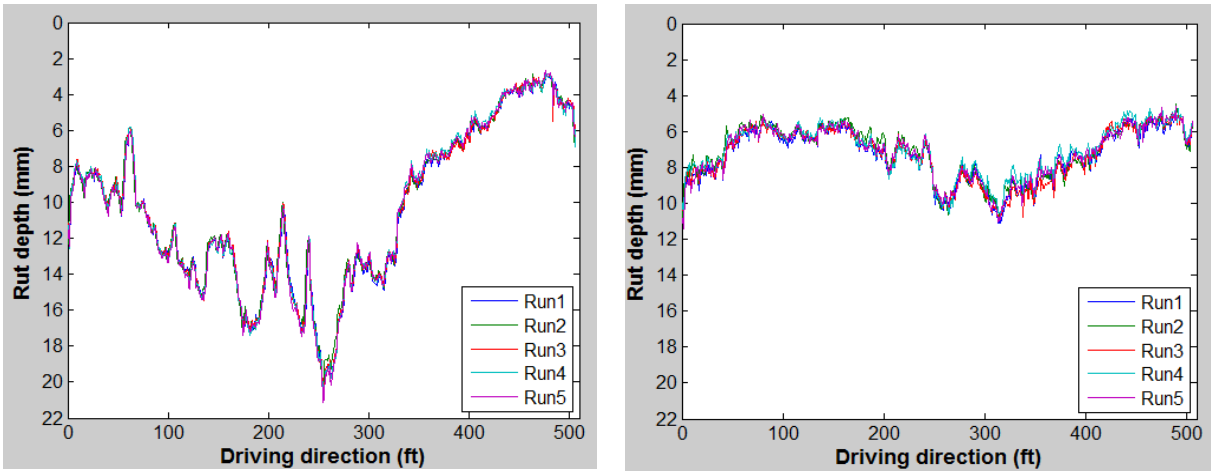

(a) LWP (b) RWP

Figure 4-12 Distribution of rut depths (I-95)

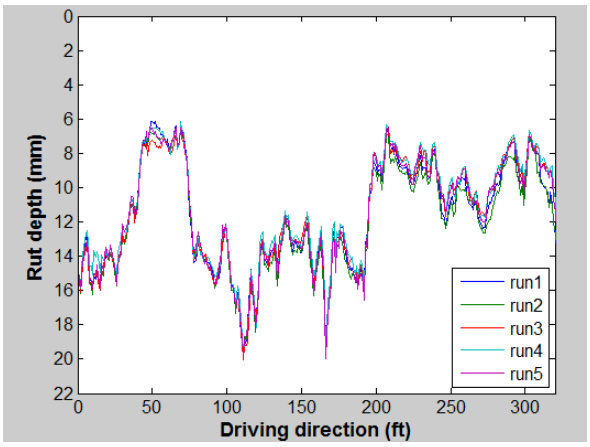

(a) LWP

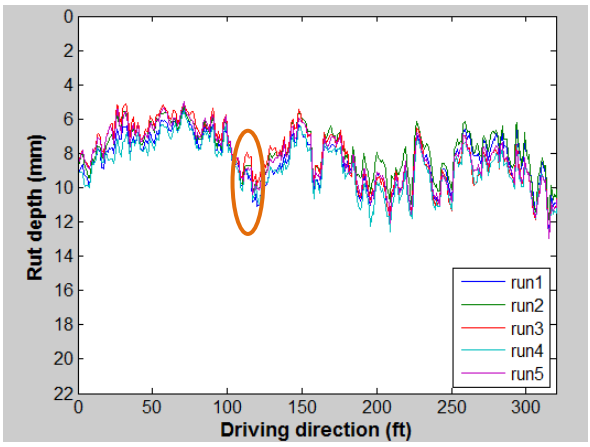

(b) RWP

Figure 4-13 Distribution of rut depths (Benton Blvd., Surveyor 1)

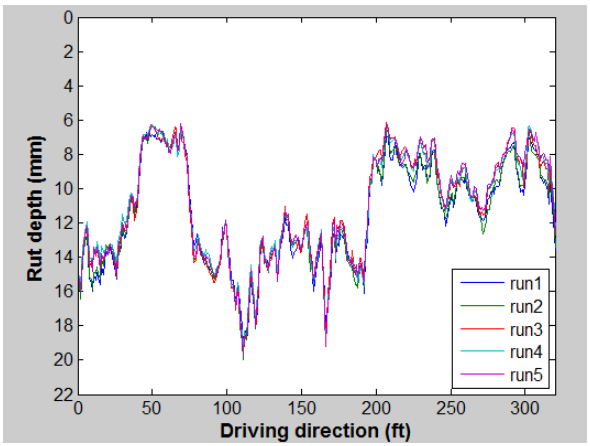

(a) LWP

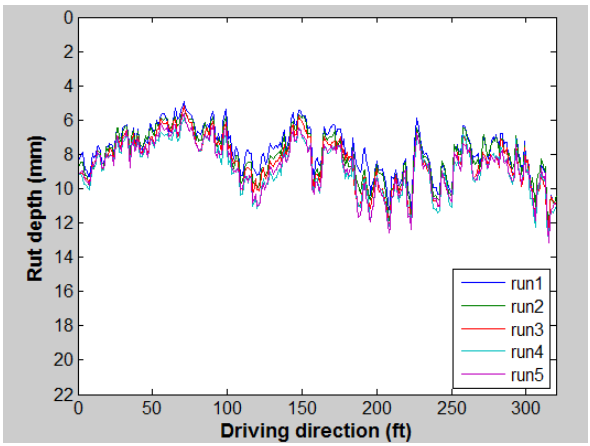

(b) RWP

Figure 4-14 Distribution of rut depths (Benton Blvd., Surveyor 2)

The roadway section highlighted with a red circle in Figure 4-13 is used to illustrate the rut depth measurement inconsistency caused by vehicle wandering. Within this short roadway section, the RWP rut depths collected in the Run 3 are, in average, approximately 1 mm smaller than those collected in the other runs. According to the intensity data shown in Figure 4-15, the vehicle in the Run 3 of data collection moved to the right. Thus, the right profiling unit of the 3D line laser system covered more portion of the gutter and less portion of the pavement. Two half-lane transverse profiles taken from the location (marked with blue lines in Figure 1-17) are shown in Figure 4-16. Obviously, the half-lane transverse profile in Figure 4-16(b) failed to cover a complete

rut. Moreover, since current simulated straightedge methods computed rut depths based on half-lane profiles only, the rut depths collected in the Run 3 were underestimated. In the future, it is suggested to combine the left and right half-lane transverse profiles to reduce the impact of vehicle wandering and improve rut depth measurement repeatability.

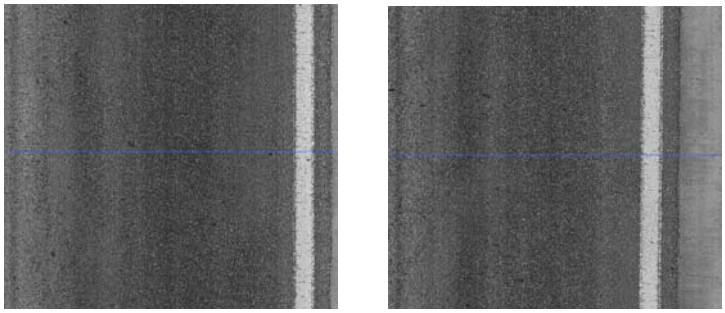

(a) Run1 (b) Run3

Figure 4-15 Intensity data from Benton Blvd. (Surveyor 1)

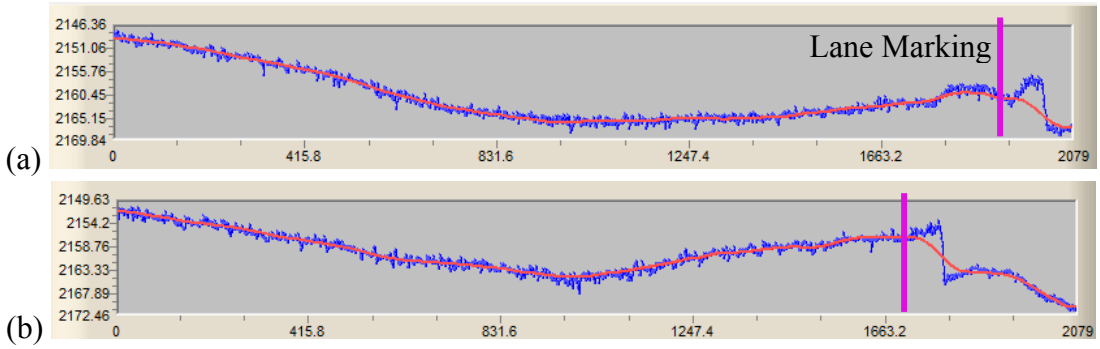

Figure 4-16 Transverse profiles from Benton Blvd. (Surveyor 1)

Rut Depth Measurement Repeatability

The rut depth measurement repeatability is quantitatively evaluated based on the standard deviation of repeated rut depth measurements collected at the same location by the same surveyor using the same survey vehicle. A large standard deviation indicates less repeatability.

The repeatability of rut depths collected from the test sections are listed in Table 4-6. The median of standard deviations of rut depths ranges from 0.1 mm to 0.5 mm, which indicates that the 3D line laser system has a high repeatability. The comparison

also shows that the medians of standard deviations of rut depths for the I-95 test section are smaller than those for the Benton Blvd. test section. The percentage of standard deviations that are smaller than 0.5 mm is close to 100% for the I-95 section, and it is around 85% for LWP and 65% for RWP on the Benton Blvd. Therefore, the repeatability of the 3D line laser system does not degrade for the interstate highway test section, although it has coarse-textured surface layer.

Table 4-6 Repeatability of Rut Depths Measured using the 3D line laser system

Statistics	I-95		Benton Blvd.					
			Surveyor 1		Surveyor 2		Mean	
	LWP	RWP	LWP	RWP	LWP	RWP	LWP	RWP
Std Median (mm)	0.1	0.2	0.3	0.4	0.3	0.5	0.3	0.5
Std Mean (mm)	0.1	0.2	0.3	0.5	0.3	0.5	0.3	0.5
Std 67th Percentile (mm)	0.2	0.2	0.4	0.5	0.4	0.5	0.4	0.5
Std 90th Percentile (mm)	0.2	0.4	0.6	0.7	0.6	0.7	0.6	0.7
Percentage (< 0.5 mm)	100%	98%	83%	70%	86%	59%	85%	65%

Rut Depth Measurement Reproducibility

Reproducibility is a measure of how well two different surveyors are able to obtain the same rut depth measurement at the same location. This is important, since highway agencies or contractors may have different surveyors across different regions and different inspection times. In the field test, since only two surveyors were employed for the same test section, the test data is insufficient to support a quantitative assessment on the reproducibility based on ISO 5725. Consequently, only a qualitative analysis on the reproducibility of the 3D line laser system was carried out. The analysis includes the following steps:

- Obtain the average rut depth profile for each surveyor by averaging the five runs of longitudinal rut depth profiles;

- Plot the average rut depth profiles on the same figure;
- Compute statistics, e.g., cross-correlation and mean difference, to describe the agreement between profiles.

According to Figure 4-17 and Table 4-7, different surveyors have produced highly similar longitudinal rut depth profiles. The cross-correlation of two rut depth profiles for the LWP and RWP is 0.983 and 0.997, respectively. The mean of the difference between rut depths measured at the same location is around 0.3 mm, and 90% of the differences are smaller than 0.6 mm. Given that the depth measurement accuracy of the 3D line laser system used in this study is specified as 0.5 mm, this preliminary test results indicate that the 3D line laser system has a high reproducibility across different surveyors.

Table 4-7 Reproducibility of the 3D line laser system

	Correlation Coefficient	Mean Difference (mm)	Median Difference (mm)	67th Percentile Difference (mm)	90th Percentile Difference (mm)
LWP	0.983	0.2	0.2	0.3	0.5
RWP	0.997	0.3	0.3	0.4	0.6

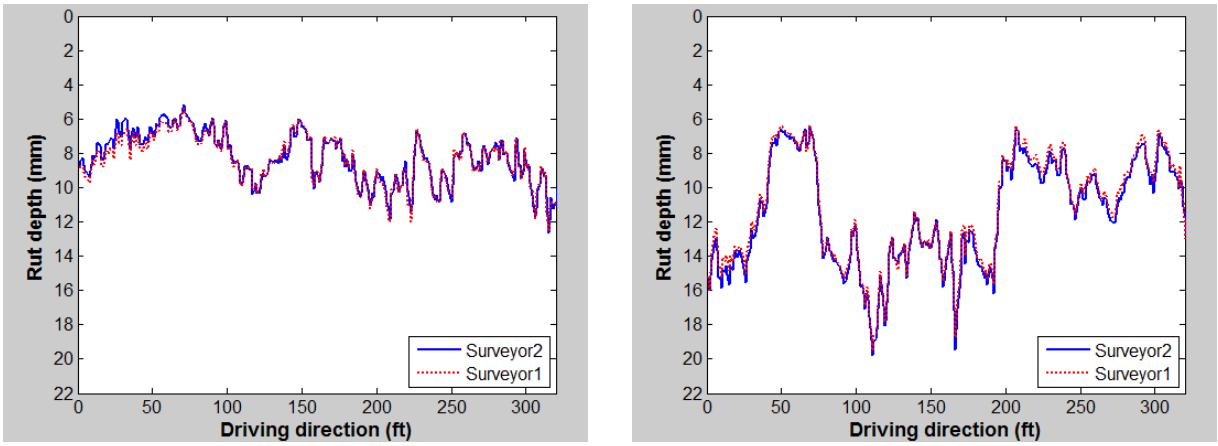

(a) LWP (b) RWP

Figure 4-17 Reproducibility of the 3D line laser system

A Case with Poor Rut Depth Measurement Repeatability

The previous test sections were required to have both left and right lane marking in good condition, and the test results show high repeatability and reproducibility. However, the 3D line laser system may have poor repeatability for roadway sections with missing lane markings. A roadway section on Benton Blvd. is given as an example. Figure 4-18 shows the rut depth profiles collected repeatedly from this roadway section. According to Figure 4-18, the rut depths, although collected repeatedly from the same roadway section by the same surveyor in a short period of time, can be quite different from each other. For the spot highlighted with an arrow, the maximum difference between the rut depth in Run 1 and the one in Run 2 is close to 50 mm. Figure 4-19 explains the cause of this poor repeatability. Since both sides of the lane marking are missing for this short roadway section, the position of lane marking is set as default by assuming there is no vehicle wandering. For the data collected in the Run 1, there is no vehicle wandering. So the default position of lane marking is close to its true position. However, for the data collected in the Run 2, the vehicle was moved laterally to the right and thus the default lane marking position is no longer appropriate. A portion of the gutter was counted as the pavement surface, resulting in the extraordinary high rut depth measurements obtained in Run 2. Therefore, when the survey vehicle makes significant lateral movement (either to the right or left), it is no longer appropriate to set the lane marking position as default. An enhanced lane marking detection algorithm is desired to handle this issue and improve the rut depth measurement accuracy and repeatability.

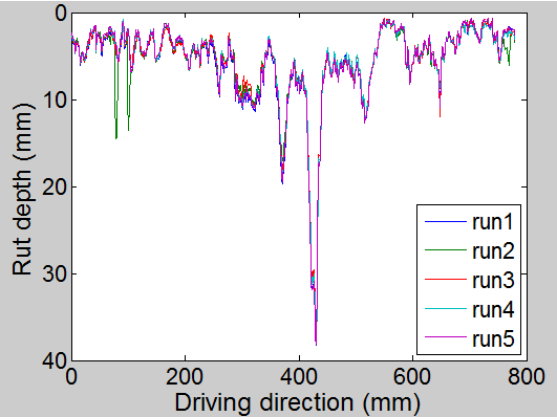

(a) LWP

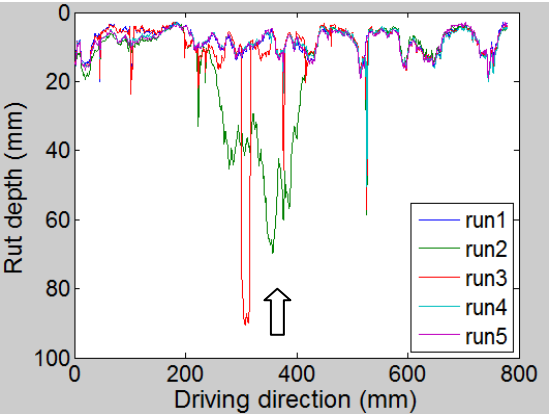

(b) RWP

Figure 4-18 Distributions of rut depths from Benton Blvd. (Surveyor 1)

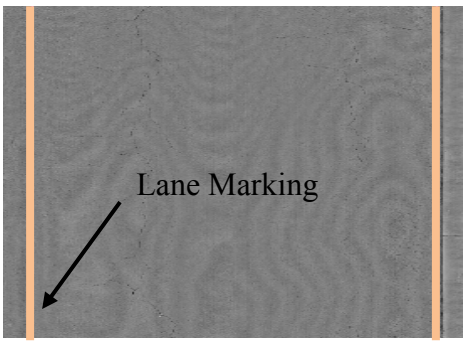

(a) Run 1

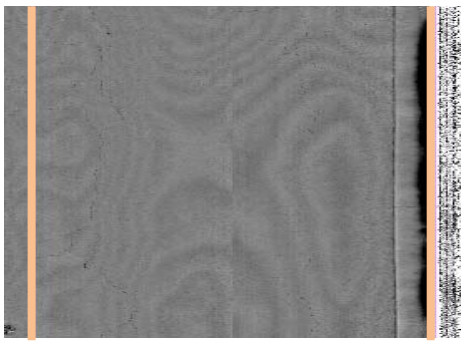

(b) Run 2

Figure 4-19 Lane marking detection results

4.2.3 Summary

Both laboratory and field tests were conducted to assess the repeatability and reproducibility of rut depths measured using the 3D line laser system. Two roadway sections, one on a city road and the other one on an interstate highway, were selected for testing. For each roadway section, 5 runs of data were collected repeatedly. A simplified method was proposed to register multiple runs of rut depth measurements. Visual inspections and statistical analyses were conducted to qualitatively and quantitatively assess the repeatability and reproducibility of the 3D line laser system. The test results show that the 3D line laser system has satisfactory repeatability and reproducibility for the majority of a roadway network.

- The laboratory test shows that the standard deviation of rut depths collected repeatedly for 2,000 times is no more than 0.3 mm.
- The field test shows that the median standard deviation of rut depths collected repeatedly at the same location from I-95 ranges from 0.1 mm to 0.2 mm; and the median standard deviation of rut depths from Benton Blvd. ranges from 0.3 mm to 0.5 mm. This repeatability is acceptable given that the depth accuracy of the 3D line laser system studied in this dissertation was specified as 0.5 mm.
- The 3D line laser system may have a better repeatability on interstate highways because the vehicle wandering on interstate highways is likely to be less than that on county roads.
- The 3D line laser system has a high reproducibility across different surveyors. The cross-correlation of longitudinal rut depth profiles collected by two different surveyors for the LWP and RWP is 0.983 and 0.997, respectively. The mean difference of rut depths measured at the same location is around 0.3 mm.

In addition to the aforementioned two test sections, a roadway section with the both sides of lane marking missing was also tested. Test results show that the repeatability of the 3D line laser system for this roadway section is poor. The rut depths, although collected repeatedly from the same roadway section by the same surveyor in a short period of time, are quite different from each other. This is because although the survey vehicle made significant lateral movement (to the right), the lane marking position was still set as default. This setting is inappropriate especially when the survey vehicle is wandering significantly. Although this setting won't be an issue when the 3D line laser system is applied to interstate highways and the majority of state routes, this will be a concern when the 3D line laser system is applied to the whole roadway network. In the future, an enhanced algorithm is desired to improve the repeatability of the 3D line laser system on roadway sections with missing lane marking.

4.3 Rut Length and Volume Measurement Accuracy

To assess the rut length and rut volume measurement accuracy of the 3D line laser system, an experimental test was conducted in the laboratory using a regular bowl shown in Figure 4-20. The ground truth establishment was outsourced to a local machine shop, Precision Machine of Savannah, which owns a Zeiss Eclipse coordinate-measuring machine (CMM). Meanwhile, the GTSV was used to scan the bowl, which was put right beneath the laser profiler to avoid the occlusion issue, and collect 3D range data for 5 runs. In each run, the 3D range data were collected at 1 mm intervals (in the transverse direction) and 5 mm intervals (in the driving direction). The DCT-based straightedge method, presented in Section 4.1.1.2, was used to process the 3D range data and obtain rut length and rut volume measurements. The rut length and volume measured using the 3D range data were then compared with the ground truth to determine the rut length and rut volume measurement accuracy of the 3D line laser system.

(a) Bowl in the laboratory (b) Bowl in the 3D range data

Figure 4-20 Test bowl

4.3.1 Ground Truth Establishment

The ground truth was established by a local machine shop using a Zeiss Eclipse CMM, as shown in Figure 4-21. A CMM is a device for measuring the 3D physical geometrical characteristics of an object. The measuring uncertainty of this Zeiss CMM is around six decimals of an inch. The bowl volume ground truth was measured as follows:

Figure 4-21 CMM machine and working staff

- **Step 1**. Make four sets of measurements from the bowl's sidewall, as shown in Figure 4-22 (a). Each set contains 5 to 7 measurements (x, y, and z coordinates).
- **Step 2**. Create a sphere (denoted as Sphere 1) that fits these sidewall measurements best. The radius of Sphere 1 is denoted as *R*.
- **Step 3**. Measure four points on the bowl's top surface, as shown in Figure 4-22(b). Find the plane (denoted as Plane 1) that fits those four measurements best. Next, get the circle which is the intersection curve of Plane 1 and Sphere 1. The elevation and radius of the circle are denoted as h_{top} and r_{top}, respectively.
- **Step 4**. Measure four points on the bowl's inside bottom surface, as shown in Figure 4-22(d). Find the plane (denoted as Plane 2) that fits those four measurements best. Next, get the circle which is the intersection curve of Plane 2 and Sphere 1. The elevation and radius of the circle are denoted as h_{buttom} and r_{buttom}, respectively.
- **Step 5**. The bowl's height is calculated as h_{top} -h_{buttom}, by assuming that Plane 1 is parallel to Plane 2.
- **Step 6**. The bowl's width equals the diameter of the top circle, which is 2* r_{top}.
- **Step 7**. The bowl's volume equals the volume difference between the top sphere cap and the buttom sphere cap, i.e., $V_{cap\_top} - V_{cap\_bottom}$. The volume of a sphere

cap is calculated using this equation $V_{cap} = \frac{PI * h^2}{3}(3R - h)$, where h is the height of the cap and R is the radius of the sphere.

Table 4-8 summarizes the measurement results, including width, depth, and volume of the bowl. The calculated bowl volume is 264.6379 in^3 (4336.64 ml).

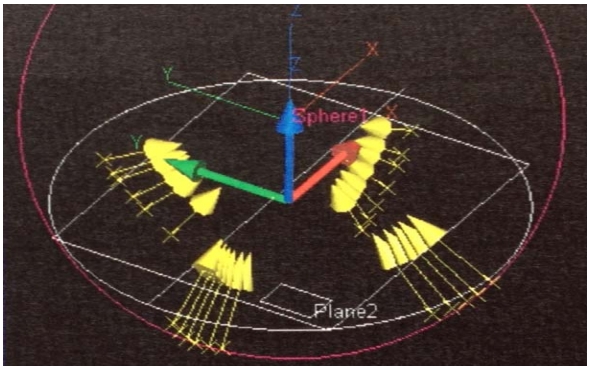

(a) Measurements on the bowl's sidewall

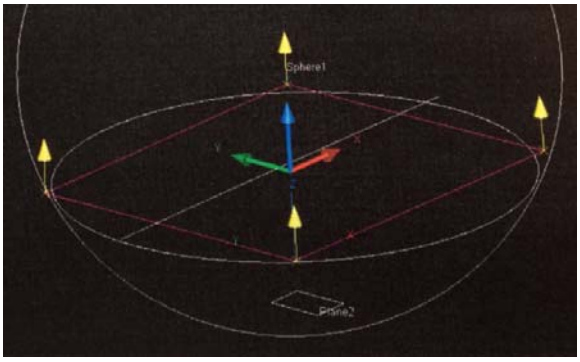

(b) Measurements on the bowl's top

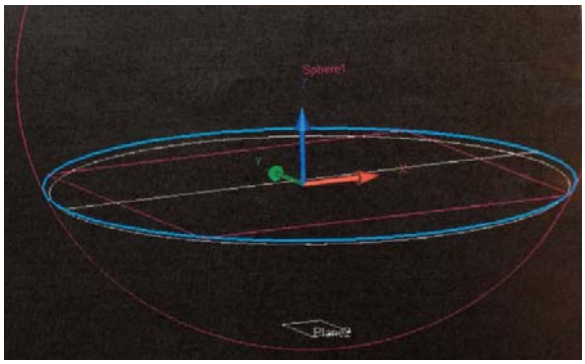

(c) Intersecting Plane 1 with the sphere

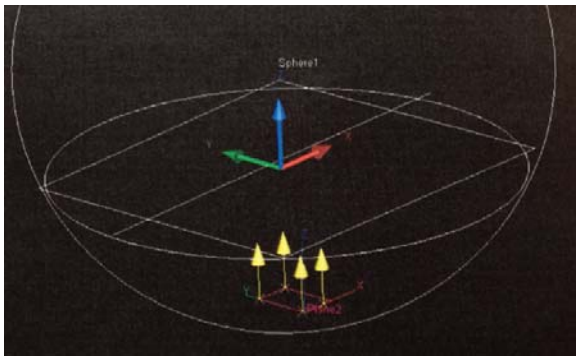

(d) Measurements on the bowl's insidebottom

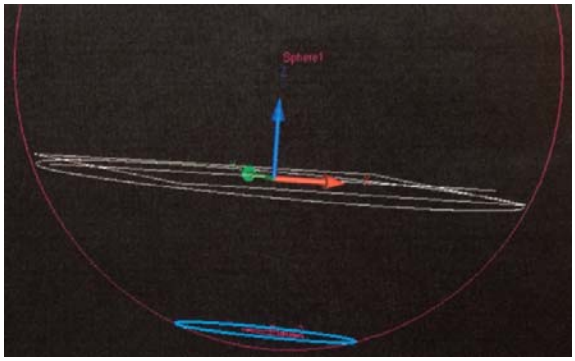

(e) Intersecting Plane 2 with the sphere

Figure 4-22 CMM measurements

Table 4-8 Bowl Volume Calculation

	R (in.)	*r* (in.)	*h* (in.)	Cap Volume (in^3)
Top	6.77695	6.15865	3.94886	267.5094
Buttom	6.77695	2.2105	0.37065	2.8715
Bowl Width		12.3173	--	
Bowl Height			3.57821	--
Bowl Volume				264.6379

4.3.2 Test Results

The test results are summerized in Table 4-9. Accroding to the test results, the difference between the DCT-method-measured rut volume and the ground truth is 164.7 ml, which is close to the measurement standard deviation.The relative rut volume measurement error is around 3.8% for the test bowl. The rut length measurement error is approximately 10 mm, 3.1% of the ground truth (i.e., 313 mm); it was mainly contributed by the DMI calibration error and the fixed-interval data collection. Both the rut length and volume measurement errors are satisfatory for engineering use.

Table 4-9 Validation of Rut Length and Volume Measurement

	99th Percentile Depth (mm)	99th Percentile Width (mm)	Length (mm)	Volume (ml)
Run 1	90.2	317.8	323.0	4541.0
Run 2	91.0	308.1	321.0	4331.6
Run 3	91.5	311.6	323.0	4434.6
Run 4	92.2	309.7	322.0	4461.1
Run 5	92.2	324.9	325.0	4738.5
Mean	91.4	314.4	322.8	4501.3
Standard Deviation	0.8	6.9	1.5	152.3
Ground Truth	90.8	313	313	4336.6
Difference	0.6	1.4	9.8	164.7
Difference (%)	0.7%	0.5%	3.1%	3.8%

4.4 Rut Depth Measurement Errors with Point-based Systems

According to the literature review in Chapter 2, there is a need to quantify the rut depth measurement errors of point-based rut bar systems so that transportation agencies can use the derived information confidently to support their pavement management decision making, since point-based rut bar systems are still commonly used by state DOTs. The 3D line laser system, which has been validated to have sufficient rutting measurement accuracy and repeatability through laboratory and field tests, was used as the reference device to characterize and quantify the rut depth measurement errors of point-based rut bar systems.

The objective of this section is to use 3D continuous transverse profiles collected by the 3D line laser system as reference profiles and quantitatively assess the rut measurement errors of various point-based rut bar systems, including 3-point, 5-point, and 7- to 31-point rut bar systems. In addition, roadway test sections with various rut shapes were tested because rut shape is an important factor that affects the rut depth measurement accuracy.

4.4.1 Rut Depth Computation Methods for Point-based Systems

Given that each 3D continuous transverse profile can be considered as a ground truth transverse profile, a point-based rut bar system can be simulated by down-sampling the ground truth transverse profile. For example, a 3-point laser bar can be simulated by selecting 3 specifically-configured points on each ground truth transverse profile. The following briefly introduces the configuration of each point-based rut bar system and the corresponding rut depth computation methods.

Figure 4-23 illustrates the configuration of a 3-point rut bar system. The 3 sensors were equally spaced at an 860 mm interval with the left and right sensors on top of left and right wheel path. Each sensor measured the distances from the reference plane to the

corresponding pavement surface, which are D_1, D_2 and D_3 for the center, LWP, and RWP sensor. Assuming that the pavement surface in the middle has no rutting, the rut depth in the left and right wheel path can be calculated using the distance differences shown in Equations (4-1) and (4-2).

$$RD_L = D_2 - D_1 \tag{4-1}$$

$$RD_R = D_3 - D_1 \tag{4-2}$$

Ideally, the centerline of a lane can be used as the reference when configuring a point-based rut bar system on a transverse profile. However, the location of centerline is often undecided on a transverse profile as the survey vehicle wanders during the survey. On the other hand, lane marking is visible on the 2D intensity data, and, thus, was used as the reference to configure a point-base rut system in this study. The test lane width is 3,353 mm (11 ft) wide, and the lane marking is about 152 mm (6 in.) wide. Thus, a 3-point rut bar system can be configured as shown in Figure 4-23.

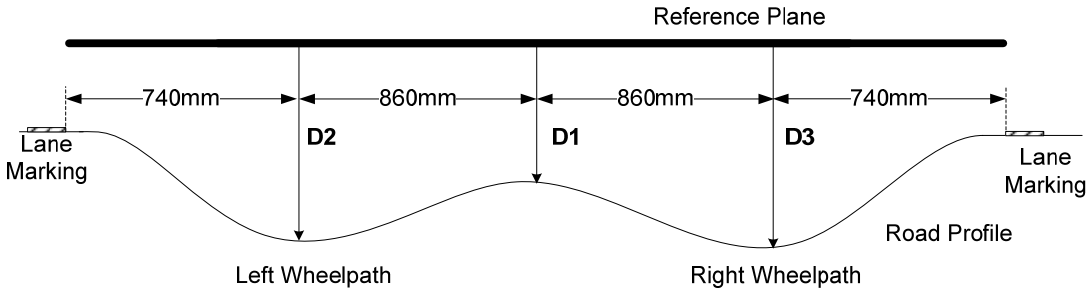

Figure 4-23 Sketch of the 3-point rut bar configuration

For a 5-point rut bar system, the one used by Hossain et al. (2002), which is shown in Figure 4-24, was adopted. The spacing between the sensor on the wheel path and the one on the road centerline is 875 mm. The outer sensor is located 546 mm from the wheel path sensor. Similar to the 3-point system, lane marking was used as the reference when configuring the 5-point system on transverse profiles. The distance between the edge of lane marking and the wheel path sensor is 179 mm. The left and

right rut depth can be computed using the left and right three sensor range data, which are shown in Equations (4-3) and (4-4).

$$R_L = D_4 - (D_3 + D_5)/2 \tag{4-3}$$

$$R_R = D_2 - (D_1 + D_3)/2 \tag{4-4}$$

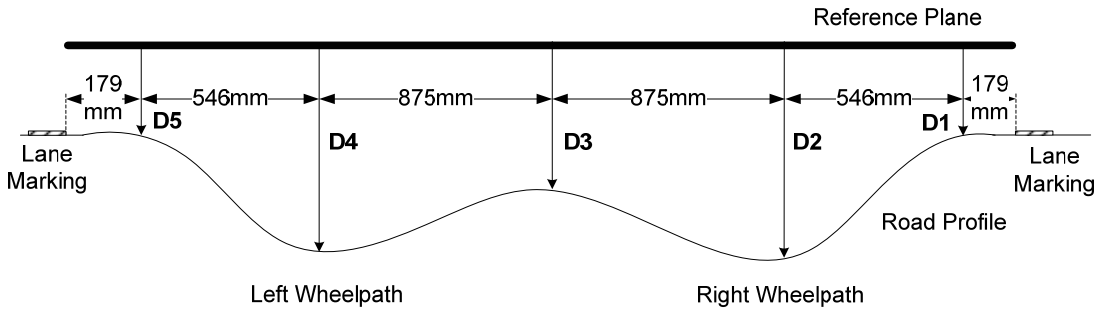

Figure 4-24 Sketch of the 5-point rut bar configuration

For 7- to 31-point systems, it was assumed that such a system can cover the whole lane width. Thus, the distance between the leftmost and rightmost point sensors is 3,200 mm. Also, the spacing between any two neighboring sensors was set to be the same. It is 400 mm for a 9-point rut bar system, as illustrated in Figure 4-25. Based on the down-sampled transverse profiles, the rut depth was calculated using the DCT-based simulated straightedge method presented in Section 4.1.1.2.

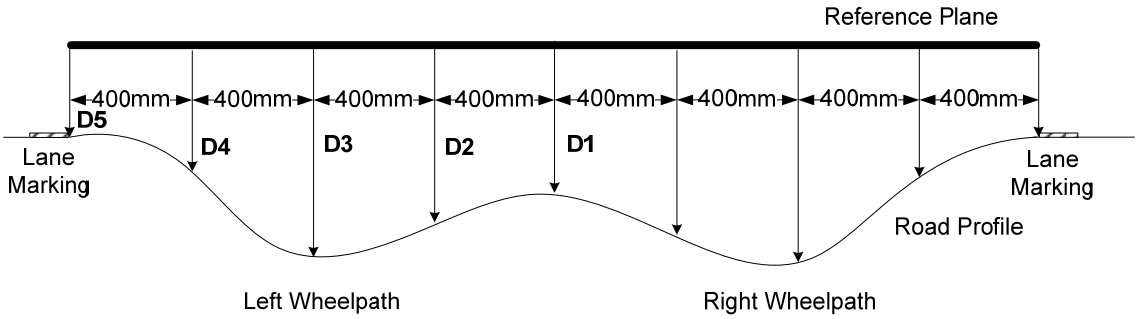

Figure 4-25 Sketch of the 9-point rut bar configuration

4.4.2 Test Data

The test data were collected using the 3D line laser system on four asphalt paved roadway test sections; each was 10 m long. For each test section, a total of 2,000 half-lane transverse profiles were collected and analyzed in this study. The four test sections covered four different severity levels of rutting and two main rut shapes, V-shape and U-shape. Figure 4-26 shows the typical transverse profiles covering half a lane. The portion of transverse profiles outside the lane marking has been removed. As shown in Figure 4-26, the rutting for most transverse profiles is located on wheel paths, except for the profile shown in Figure 4-26(b), which is slightly shifted to the left (i.e., the lane marking side). Figure 4-26(d) and (c) are two typical pavement profiles with a U shape and a V shape. A U-shape rut has less impact on the rut depth measurement error brought by a point-based rut bar system because the valley is relatively flat and wide and the possibility of a sensor located on it is high. In contrast, a V-shape rut has a narrow valley, and it is hard for a sensor to be precisely located on the top of the valley. So, a V-shape rut has greater impact on the measurement error when a point-based rut bar system is used.

The configuration of 3-, 5-, 9-, and 31-point rut bar systems on typical transverse profiles from these four test sections are presented in Figure 4-26. As the number of laser sensor increases, a rut bar system is better at capturing the rut shape. When the number of laser sensor becomes 31 (i.e., when the spacing between two sensors is 105 mm), the rut shape for four transverse profiles can all be captured well. Meanwhile, as the number of laser sensor increases, the rut depth measurement accuracy becomes less sensitive to the spacing configuration of a rut bar system. The sensors in a 31-point system can be set as equally spaced. However, the configuration of a rut bar system with 3, 5, or 9 laser sensors must be designed carefully to assure accurate and repeatable rut depth measurements.

It is also observed in Figure 4-26 that due to the change of rut shape, it is difficult to find an optimal configuration for a rut bar system with fewer sensors. For example, the 3-point and 5-point system configurations shown in Figure 4-26(a) and (d) can capture the maximum rut depth, but they cannot capture it for ruts shown in Figure 4-26(b) and (c), for which the rut depth will be significantly underestimated.

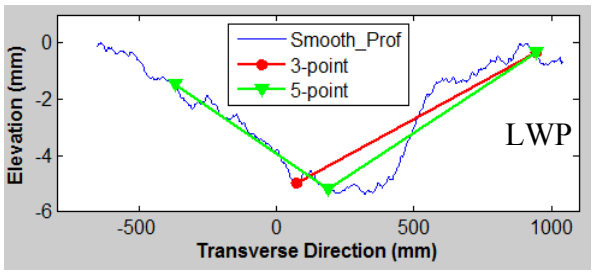

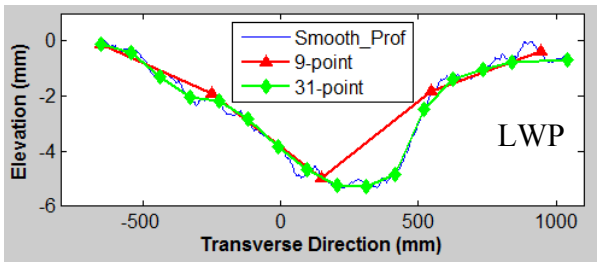

(a) Minor

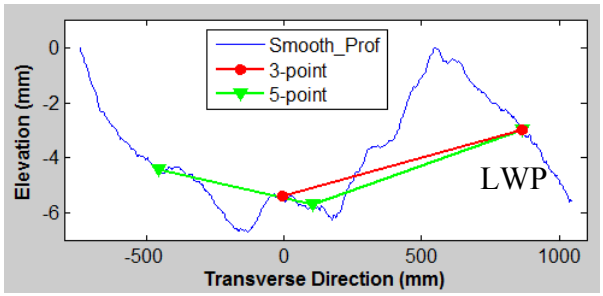

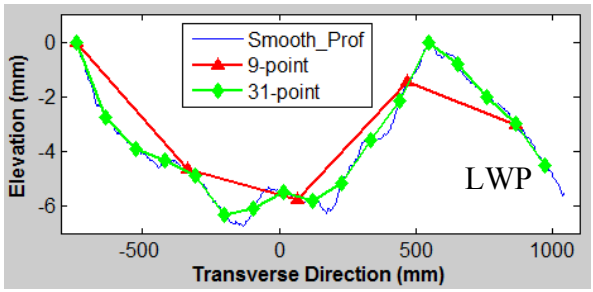

(b) Low

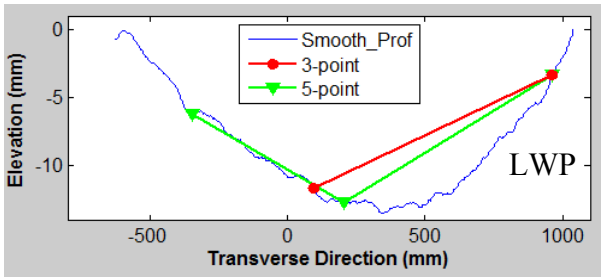

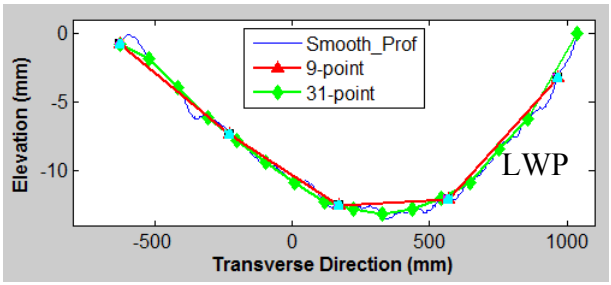

(c) Medium

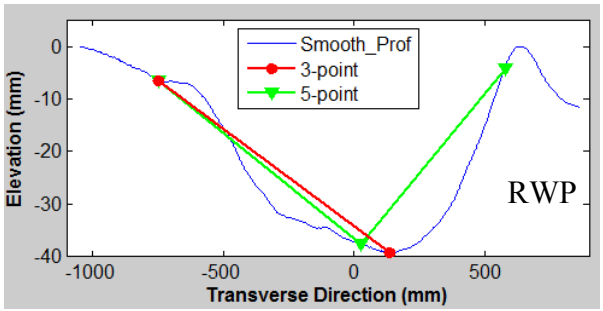

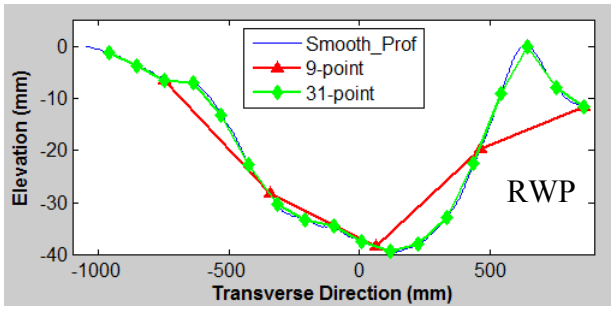

(d) High

Figure 4-26 Road transverse profiles and point-based system configurations

4.4.3 Test Results

Figure 4-27 shows the calculated rut depths in the driving direction. The blue line indicates the distribution of the ground truth rut depths in the driving direction. In comparison, the distributions of rut depths measured by different point-based rut bar systems are also drawn in Figure 4-27 with different colors. For better reading of the chart, only the results from 3-, 5-, 9- and 31-point rut bar systems are presented. Generally, the rut depth measurement accuracy increases with the increasing number of sensors. However, for those rut bar systems with fewer sensors, the rut depth measurement error is largely affected by the rut shape. For example, based on the experimental test results shown in Figure 4-27, it is difficult to tell if the 3- or 5- rut bar system is better. In some cases, for example in Figure 4-27(d), a 3-point rut bar system could outperform a 9-point one.

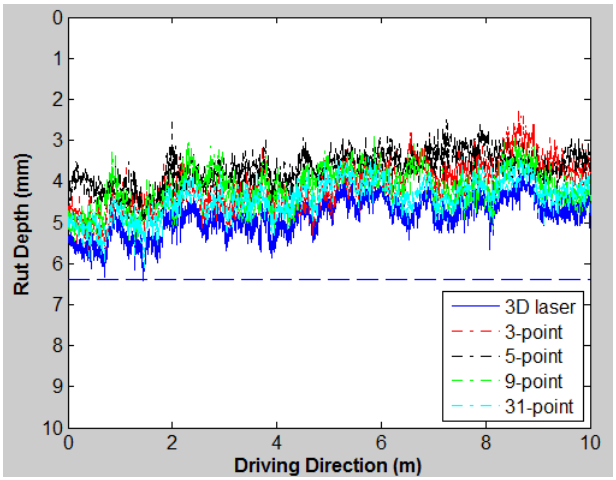

(a) Minor

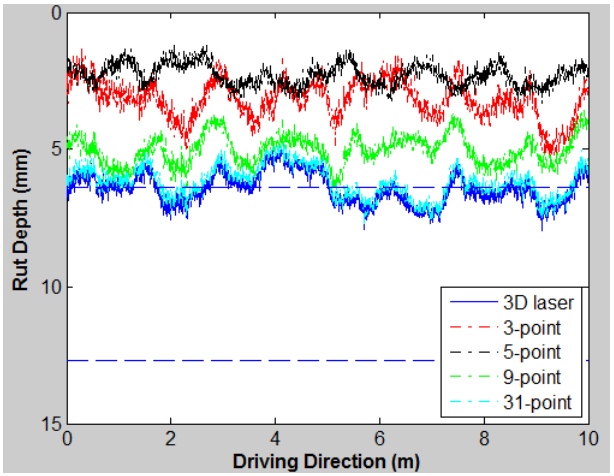

(b) Low

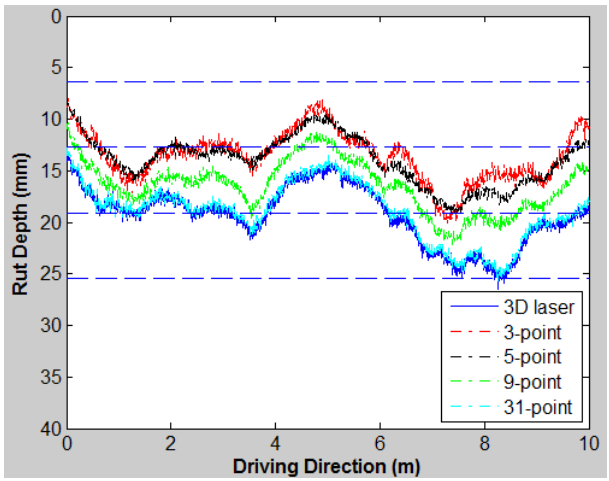

(c) Medium

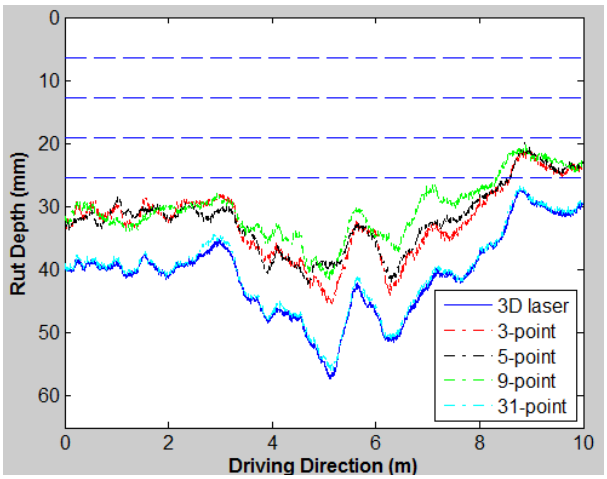

(d) High

Figure 4-27 Measurement errors of point-based rut bar systems in the driving direction

The corresponding means of absolute and relative measurement errors for all point-based rut bar systems are shown in Figure 4-28. As shown in Figure 4-28(a), for those rut bar systems with fewer sensors, the absolute measurement error increases with the increasing rut depth. However, this trend doesn't apply to a rut bar system with more sensors. For the 31-point rut bar system, the mean absolute rut depth measurement error is about 0.4 mm, which is very close to the ground truth. The relative measurement error varies among different ruts and different rut bar systems, as shown in Figure 4-28(b). The relative rut depth measurement errors for a 3-point and a 5-point rut bar systems vary from 16% to 51% and from 22% to 64%, respectively. When the sensor number increases to 9, the mean errors vary from 14% to 25%. If the number of sensors increases to 31, the average measurement errors are lowered to between 1% and 9%. For those rut bar systems with fewer sensors, the rut shape plays an important role in affecting measurement error. For example, when the location of maximum rut depth is close to the lane marking, the side sensor for a 5-point rut bar system often fails to capture the outmost highest point, which will perform worse than a 3-point system. Thus, based on the test results shown in Figure 4-28(b), it is difficult to tell whether a 3-point or a 5-point rut bar system is better. Even a 9-point system could perform worse than a 3-point or 5-

point in some cases. Thus, a rut bar system with fewer sensors performs less consistently among various rut shapes. Nevertheless, the overall trend is clear: the measurement error decreases with the increasing number of sensors. If the number of sensors is greater than 29, the mean error for all four sites drops below 10%. In other words, when the spacing between adjacent sensors is 112 mm or less, the rut depth measurement error becomes 10% or less. This is close to the 100 mm spacing, which gives an average of 5% rut depth measurement error, recommended for use for routine data collection by Chen et al. (2001).

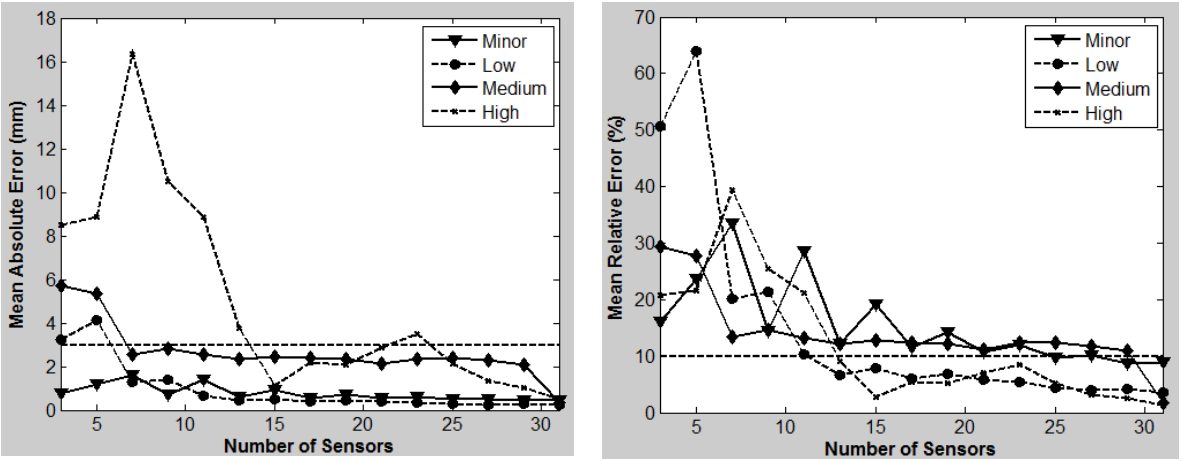

(a) Absolute measurement errors (b) Relative measurement errors

Figure 4-28 Relationship between the number of laser sensors and the measurement error

4.4.4 Summary

The high-resolution 3D continuous transverse profiles acquired by the emerging 3D line laser system were first used in this study to assess the rut depth measurement error of point-based rut bar systems. The 3D line laser system can readily provide a large volume of high-resolution transverse profiles to characterize and quantify the rut depth measurement errors of different point-based rut bar systems. The quantitative assessment results can be used by transportation agencies to determine the potential error of the point-based rut bar systems they are using and to provide a guideline for choosing a rut

bar system that will provide an acceptable accuracy for their network-level rutting survey.

In this study, the commonly used 3-point and 5-point rut bar systems and equally-spaced rut bar systems using 7 to 31 laser sensors were tested using the transverse profiles acquired by a 3D line laser system as ground truth profiles. The test data was collected on four 10-m roadway sections that cover various rut depths and rut shapes. Test results show that the relative rut depth measurement error generally decreases with the increasing number of laser sensors. However, the trend is unclear for rut bar systems with fewer sensors because, in these cases, the rut shape plays an important role in affecting the rut depth measurement accuracy. A 3-point rut bar system could occasionally outperform a 5-point system. The test results also show that the commonly used 3-point and 5-point rut bar systems can underestimate the rut depth significantly. The relative rut depth measurement error for a 3-point and a 5-point rut bar system varies from 16% to 51% and from 22% to 64%, respectively. The relative measurement error consistently drops under 10% only when the number of sensors is greater than 29. In conclusion, to achieve desirable accuracy, the number of sensors on a point-based rut bar system should be sufficient to capture various rut shapes. Besides using the 3D line laser system to establish the reference to assess the rut depth measurement accuracy of point-based rut bar systems, using the 3D line laser system for more accurate and repeatable rut depth measurement is recommended.

4.5 Summary

Experimental tests were conducted in the laboratory and in the field with established ground truths to assess the accuracy and repeatability of 1D rut depth obtained using the 3D line laser imaging system. Experimental tests in the laboratory also validated the accuracy of 3D rut volume measurement. The test results show that the 3D line laser system is promising in delivering accurate and repeatable measurements of the

rut depth, rut length, and rut volume consistently for the majority of a roadway network. The detailed results are summarized as follows:

- Both laboratory and field tests show that the 3D line laser system can provide satisfactorily accurate rut depth measurements. Laboratory test results show that the absolute difference between DCT-method-measured rut depths and the ground truth varies from 0.0 mm to 0.7 mm. Due to the uncontrolled environment, such as vehicle wandering, the results from field tests are inferior to the ones in the laboratory. However, the absolute difference, which ranges from 0.8 mm to 2.1 mm, still satisfies the rut depth measurement requirement, which is +/-3 mm, for multiple transportation agencies (ADOT 2002; McGhee 2004).
- Both laboratory and field tests show that the 3D line laser system can provide rut depth measurements with high repeatability and reproducibility. The laboratory test shows that the standard deviation of rut depths collected repeatedly for 2,000 times is no more than 0.3 mm. According to the field test, the median standard deviation of rut depths collected repeatedly at the same location ranges from 0.1 mm to 0.5 mm. In addition, the 3D line laser system has a high reproducibility across different surveyors. The cross-correlation of rut depth profiles collected by two different surveyors for the same test section is 0.983 and 0.997 for the LWP and RWP, respectively. The tests also reveal that the 3D line laser system may have a better repeatability on interstate highways.
- A laboratory test on a regular bowl shows that the relative rut length and rut volume measurement error is around 3.1% and 3.8%, respectively, which is satisfatory for engineering use.
- The accuracy and repeatability of point-based rut bar systems were quantitatively evaluated by simulating different rut bar systems (with the number of sensors varying from 3 to 31) using transverse profiles acquired by the 3D line laser

system. Test results show that generally the relative rut depth measurement error decreases with the increasing number of laser sensors. However, the trend is unclear for rut bar systems with fewer sensors because, in these cases, the rut shape affects rut depth measurement error more than the number of sensors. Thus, a 3-point rut bar system could outperform a 5-point system occasionally. The test results also show that the commonly used 3-point and 5-point rut bar systems can underestimate the rut depth significantly. The relative rut depth measurement error for a 3-point and a 5-point rut bar system varies from 16% to 51% and from 22% to 64%, respectively. The relative measurement error consistently drops under 10%, only when the number of sensors is greater than 29.

CHAPTER 5 A SENSOR-BASED AND SPATIALLY-ENABLED PAVEMENT RUTTING CONDITION ASSESSMENT METHODOLOGY

To address the research need to improve existing 1D rut depth measurement accuracy and repeatability and to measure additional 2D and 3D rutting characteristics utilizing the emerging 3D line laser imaging technology, a sensor-based and spatially-enabled pavement rutting condition assessment (SS-PRCA) methodology is proposed in this thesis. The methodology takes advantage of the high-resolution 3D line laser imaging technology, location reference technology, optimization programming techniques, statistical analysis methods, and GIS technology to enhance existing pavement rutting condition assessment practices. As shown in Figure 5-1, the proposed methodology consists of six modules. They are (1) data acquisition, (2) data processing, (3) data segmentation, (4) statistical analysis, (5) data visualization, and (6) decision support. More details of these modules, including the data processing module, data segmentation module, and decision support module, are presented in the subsequent chapters in this thesis.

5.1 Data Acquisition

The **data acquisition module (Module 1)** uses a 3D line laser system to acquire high-resolution 3D range data, consisting of 3D continuous transverse profiles, a Global Position System (GPS), an Inertia Measurement Unit (IMU), and a Distance Measurement Instrument (DMI) to provide corresponding location reference, and a camera to take images of the roadway environment. The optimal laser configuration (e.g., the sampling interval between two transverse profiles and the transverse profile tilt angle) needs to be studied to assure the collected 3D range data have the adequate resolution to

assess network-level pavement rutting condition as well as other distresses (e.g., transverse cracks).

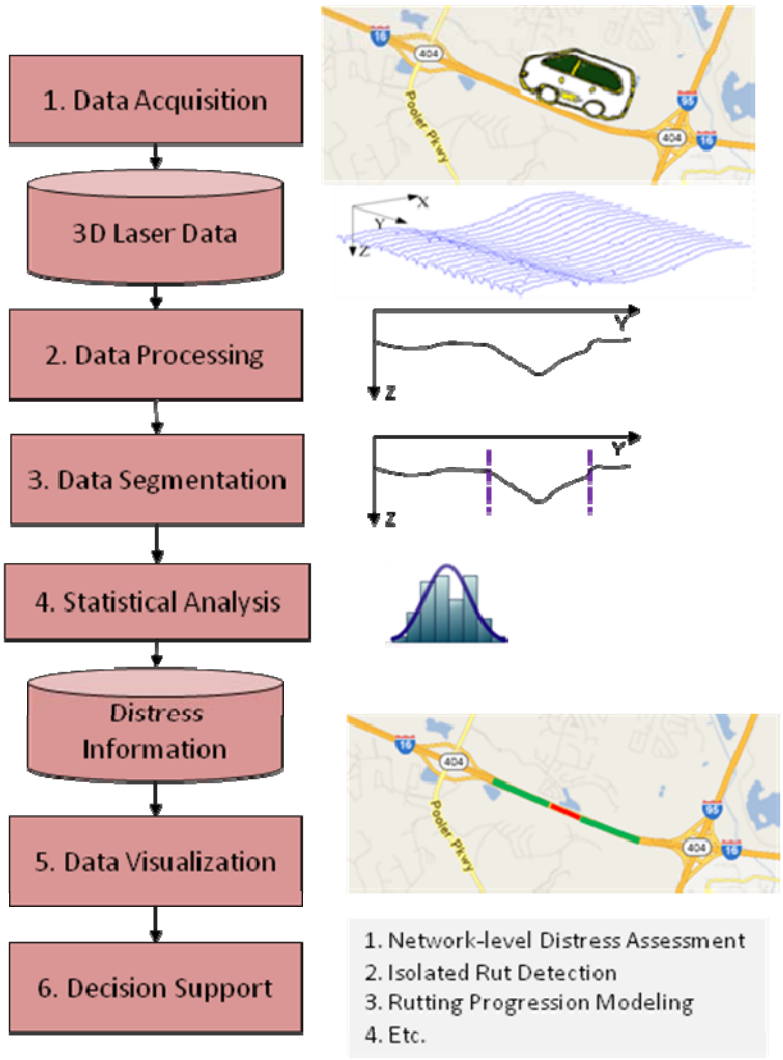

Figure 5-1 A sensor-based and spatially-enabled pavement rutting condition assessment methodology

In the future, a standard data quality assurance (QA) and quality control (QC) procedure, will need to be established when the 3D line laser system is implemented in practices. The QA/QC procedure will include calibration of the equipment and software routines for checking the reasonableness and completeness of the data. Key indicators (e.g., standard deviation and acceptable accuracy) need to be proposed for measuring the

deviations of the collected 3D range data from expected patterns and for determining whether the deviations are caused by actual occurrences or false data. The standard QA/QC procedure is the core of the data acquisition module, and it will be studied in the future.

5.2 Data Processing

The collected 3D range data will be processed in the **data processing module (Module 2)**, and the rutting measurements, such as the 1D rut depth, rut width, and 2D rut cross-sectional area, will be extracted. The noises, irregular data, and non-rutting features, such as cracking and potholes, need to be removed in this module. Due to the enormous amount of data points in the 3D range data, methods are needed to extract pavement rutting measurements automatically in a reasonable time period. Various signal processing algorithms and engineering knowledge will be employed to process the 3D range data and obtain accurate rutting measurements.

5.3 Data Segmentation

In the **Data Segmentation Module (Module 3)**, the continuous pavement rutting measurements obtained from Module 2 need to be partitioned into uniform segments. This module is needed to minimize the data storage requirement and, most importantly, to provide meaningful pavement segments (e.g., a reasonable long segment rather than small 5 mm segments) with uniform rutting condition so that meaningful statistics can be derived for each uniform segment in the next Module. A method to determine optimal and engineering-meaningful pavement segments with uniform rutting condition will be proposed.

5.4 Statistical Analysis

In the **Statistical Analysis Module (Module 4)**, statistics of obtained rutting measurements will be derived in support of network-level pavement management decisions, e.g., statewide pavement rutting condition assessment.

5.5 Data Visualization

In the **Data Visualization Module (Module 5)**, 1D rutting statistical information and 2D roadway images will be integrated and presented on a GIS map. The visualization capability allows both the overall assessment of the pavement rutting condition and other pavement management decisions in an efficient and intuitive way. For instance, the rutting information can be visualized along with additional data (e.g., the traffic volume, deflection data, and coring results) on a GIS map to assist in diagnosing the causes of rutting, identifying logical treatment projects, and determining adequate treatments. This data visualization module's focus will be on registering the 1D rutting statistics to the linear reference system (LRS) commonly used in GDOT's management practices.

5.6 Decision Support

Finally, **in the Decision Support Module (Module 6)**, applications will be developed to report the pavement rutting measurements and the statistical information in support of both network-level and project-level pavement management decisions. For example, the representative rut depth in each management section can be derived and directly stored into a PMS (e.g., GPAM) at the network-level. Integrated with the historical data, road sections with dramatic condition changes will be reported and prioritized for maintenance activities. To support the network-level pavement management decisions, it is important to derive meaningful statistical indicators (e.g., the representative rut depth in one mile) that state DOTs, like GDOT, can integrate them with the legacy data. To be successful, it is crucial for engineers to be involved in choosing

adequate statistical indicators to support existing network-level rutting condition surveys. This network-level rutting condition assessment application's focus will be on gaining involvement from state DOTs and interpreting the derived statistical information, for instance, whether the average rut depth is an adequate indicator to represent the overall pavement rutting condition within a pavement management section and what additional indicators are needed to better support pavement management decisions. In support of the project-level decisions, the rich rutting measurements will be used to identify isolated spots with severe rutting problems to which low-cost, localized treatment could be applied. Ultimately, the high-resolution and high-quality rutting information will help in improving our understanding about the rutting progression behavior and thereby improving the reliability of rutting progression modeling.

CHAPTER 6 METHODS DEVELOPED FOR SUBSTANTIATING THE RUTTING CONDITION ASSESSMENT METHODOLOGY

To substantiate the sensor-based and spatially-enabled pavement rutting condition assessment methodology proposed in Chapter 5, methods and procedures are proposed. In particular, these modules, the data processing module, data segmentation module, and decision support module, are studied and presented in this chapter. First, in the data processing module, a threshold-based outlier removal method employing the multivariate adaptive regression splines (MARS) technique is proposed to remove outliers observed in the rut depth measurements. Then, in the data segmentation module, a modified topological-ordering-based segment clustering (MTOSC) method is proposed to optimally partition the continuous roadway network into segments with uniform rutting condition. Because of computational time concerns, an overlapping-reducing heuristic method is proposed to practically solve large-scale segmentation problems. Third, in the decision support module, a network-level rutting condition assessment application is proposed to support the data items, statistical analyses, and reports needed in GDOT's pavement management system. Also, a project-level isolated rut detection application is proposed in support of project-level pavement management using the 3D line laser system.

6.1 Data Processing - Threshold-based Outlier Removal Method

Outliers, as shown in Figure 6-1, were observed in the rut depth measurements, and they need to be removed. A threshold-based outlier removal method is proposed in the Data Processing Module (Module 2) based on the observation that the slopes of isolated rut are relatively smaller than those of outliers. Table 6-1 summarizes the

characteristics of isolated ruts and five types of outliers identified based on their causes in the longitudinal rut depth profiles. They are outliers caused by transverse cracks, potholes and patches, raised pavement markings, rail tracks, and other objects (e.g., tree branches on the road). Figure 6-2 shows close-ups of each type of outliers. As shown in Figure 6-2, the outliers caused by raised pavement markings are distinct. They are usually 100-125 mm wide and 2.5-4 (of 1/8 of an inch) high. The outliers caused by rail tracks and potholes usually have very sharp edges. However, the slopes of isolated ruts are relatively small, usually smaller than 0.3 in/ft. Thus, a threshold-based method is proposed to remove outliers in the rut depth measurements.

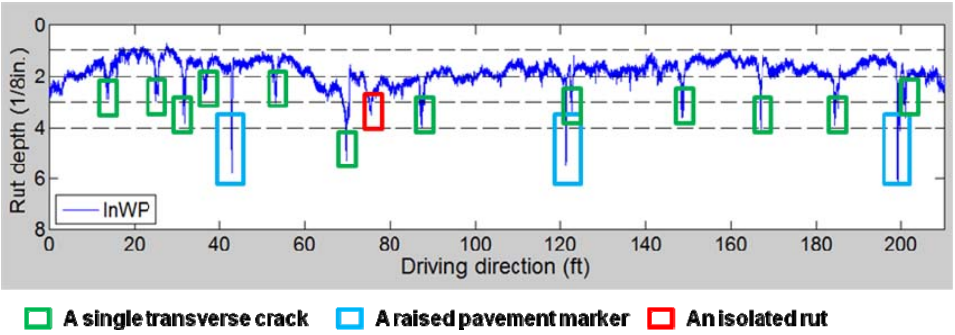

Figure 6-1 Potential outliers and isolated rut

Table 6-1 Characteristics of Outliers and Isolated Ruts

Outliers	Length (mm)	Depth (1/8 in)	Slope (in/ft)
Transverse Cracks	25-500	0.8-3	0.3-6.0
Raised Pavement Marker	100-125	2.5-4	1.8-2.7
Rail Tracks	--	20	≥2.5
A Pothole	60	1.6	2.0
Another Object	400	5	0.9
Isolated Ruts	≥800	≥2	≤0.3

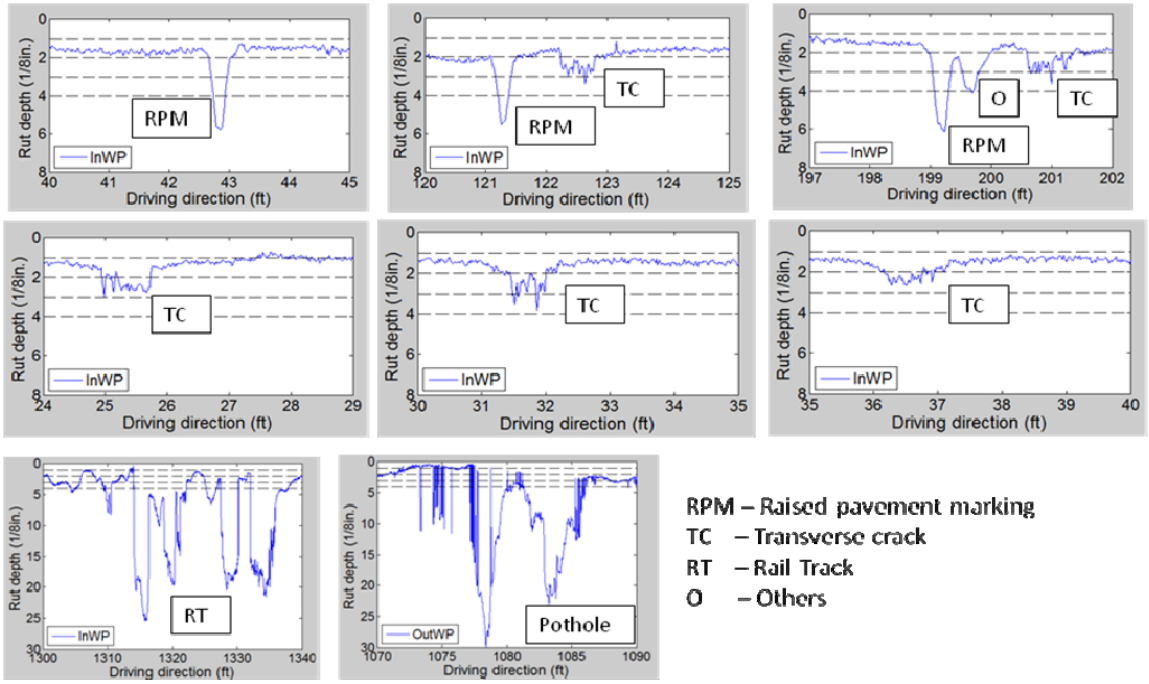

Figure 6-2 Examples of outliers

The key of this threshold-based outlier removal method is to calculate the slope. Typically, the whole profile is partitioned into profile segments, and then linear regression is applied to calculate the slope of each profile segment. However, the calculated slope of each profile segment highly depends on the size of the profile segment, and it is challenging to determine a proper segment size that is suitable for outliers with varying lengths. Therefore, a flexible regression technique is needed to handle various outliers. Through the literature review, it is found that the multivariate adaptive regression splines (MARS) technique, which is a non-parametric regression technique introduced by Friedman (1991), can provide the flexibility. Its concept is to model a given profile with piecewise linear models while maintaining the continuity between these models. More importantly, it can automatically model the profile without prior knowledge of the non-linearity. Hence, in this study, MARS is employed to obtain piecewise linear fitting models of the longitudinal rut depth profile. Based on the linear fitting models, the slopes are calculated.

Usually, the longitudinal rut depth profile can be long, and as the profile gets longer, the processing time required by MARS increases exponentially. Therefore, it is inefficient to process a long rut depth profile at a time. The long rut depth profile is recommended to be partitioned into several profile segments, and MARS can be used to process each of segments. On the other hand, the more segments the profile is partitioned into, the more artificial jumps will exist between segments. After trial and error, a profile segment that covers a 100-ft road section is determined to be able to balance the processing time against the number of artificial jumps.

For illustration purpose, a 5-ft profile segment is given in Figure 6-3 to illustrate the threshold-based outlier removal method. The method includes the following steps:

- **Step 1**. Process the longitudinal rut depth profile segment using MARS. The output of MARS is the blue polyline in Figure 6-3(b). A total of 7 straight lines were determined to be able to fit the rut depth profile satisfactorily (i.e., with least model complexity and satisfactory goodness-of-fit). The slopes of these 7 straight lines were calculated and presented in Figure 6-3(c).
- **Step 2**. Check for any slope whose absolute value is greater than a specified threshold k. After examining various types of outliers, a relatively conservative threshold, k = 1/4 in/ft., was determined to be appropriate. If there is at least one slope that is greater than the threshold, go to Step 3; otherwise, go to the next profile segment. In Figure 6-3(c), it was found that 3 out of 7 slopes were lying outside the dashed lines.
- **Step 3**. Find the straight line with the maximum absolute slope.
- **Step 4**. Locate two ends of the straight line, which has the maximum absolute slope, and then remove the one end that is further away from the median value of this profile segment. In Figure 6-3(d), the point highlighted with a red circle was then removed.

- **Step 5**. Update the slope list, and then go back to Step 2 until all the slopes are smaller than the predefined threshold. The blue line in Figure 6-3(e) is the filtered profile. Compared to the profile before filtering, the outliers were successfully removed.

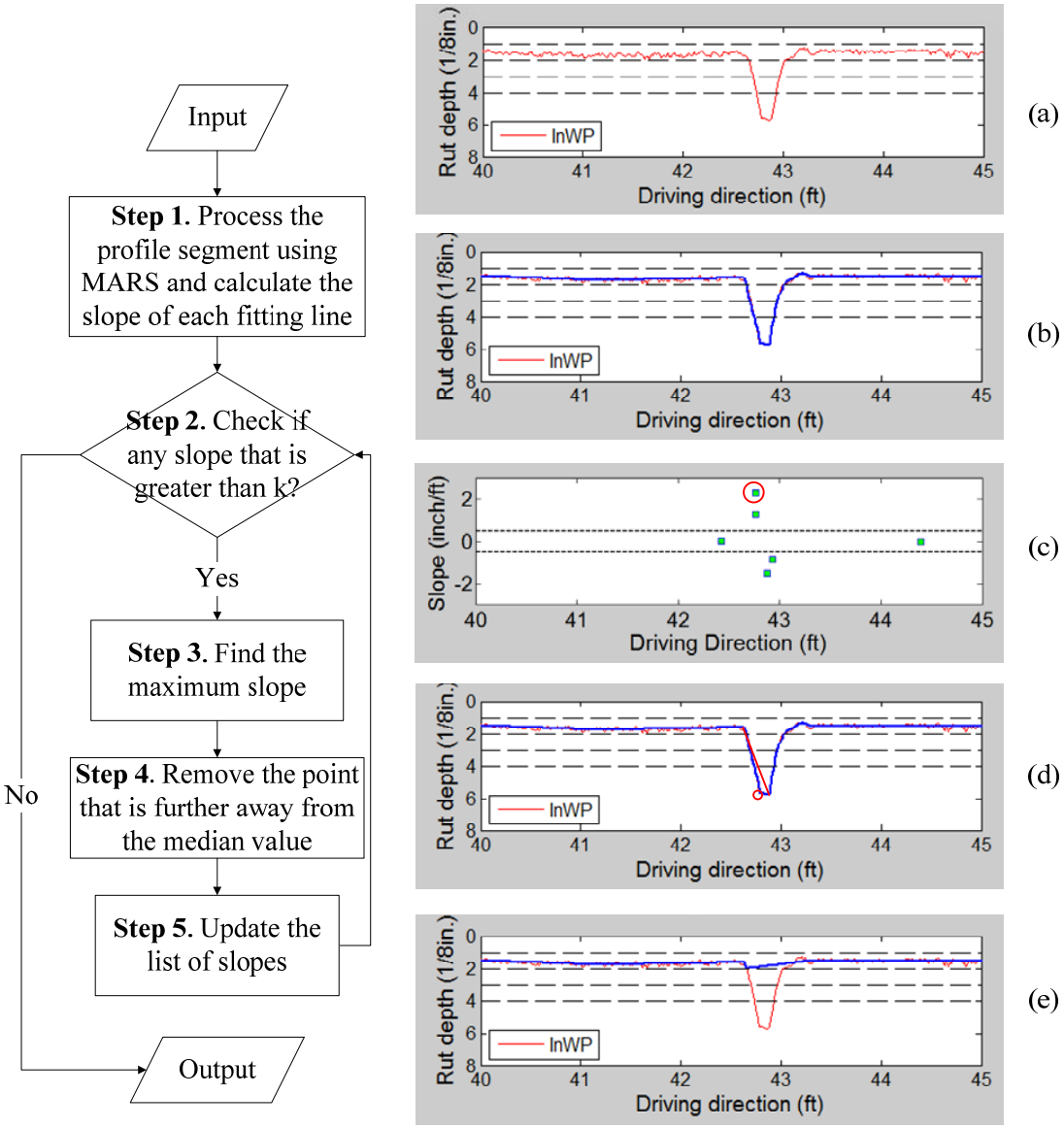

Figure 6-3 Procedures of outlier removal

A sensitivity study was conducted to assess the sensitivity of the outlier removal method to the slope threshold and the window size. A test section with one isolated rut

and two outliers was selected for testing. The isolated rut is around 6 ft long and 1/2 in. deep. One of the outliers is caused by the pothole and is around 1 ft long and 5/8 in. The other one is caused by a longitudinal crack and is roughly 0.5 ft long and 3/4 in. Four slope thresholds, 1/8 in/ft, 1/4 in/ft, 3/8 in/ft, and 1/2 in/ft, and two window sizes, 1 m and 5 m, were tested. These two window sizes were selected because they take similar processing time when the outlier removal method is applied to a fixed-length roadway section (e.g., 1 mile). If the window size is greater than 5 m, much more processing time is needed.

Figures 6-4 and 6-5 summarize the test results. Each figure consists of four subfigures, which show the input rut depth data (the blue profile) and the outlier removal results (the red profile) under different slope thresholds. The sensitivity study results show that the outlier removal method might not be able to preserve the complete shape of isolated ruts as the slope threshold decreases. For example, when the slope threshold decreases from 1/4 in/ft to 1/8 in/ft, the isolated rut was partially removed, as shown in Figure 6-4(a). On the other hand, if the slope threshold increases, some outliers might not be removed. As shown in Figure 6-5, the outlier close to Location 90 ft was not entirely removed when the slope threshold increased from 1/8 in/ft to 1/4 in/ft. Based on the sensitivity study results, a 1/4 in/ft. slope threshold is recommended since it can effectively preserve the complete shape of an isolated rut and remove most outliers.

Additionally, the study results show that by decreasing the window size from 5 m to 1 m, the outliers were better removed, and the shape of the isolated rut was better preserved. As shown in Figure 6-4(a) and Figure 6-5(a), when the window size decreased to 1 m, the outliers at around Location 90 ft were more completely removed. Meanwhile, the complete shape of the isolated rut at around Location 15 ft was well preserved. These trends are reasonable because of the objective of the MARS technique, which is to use piecewise linear models to fit the rut depth profile with the least model complexity and

satisfactory goodness-of-fit. As the window size increases, modeling the outliers within the window would increase the model complexity; however, not modeling some of the outliers has a smaller impact on the overall goodness-of-fit. Therefore, a relatively small window size is recommended because it protects isolated ruts from being removed and ensures the complete removal of outliers.

In the future, the outlier removal method can be improved by 1) incorporating a method to handle outliers consisting of multiple-shaped spikes, as shown in Figure 6-6, and 2), and testing more data with varying shapes of outliers to recommend a more robust slope threshold.

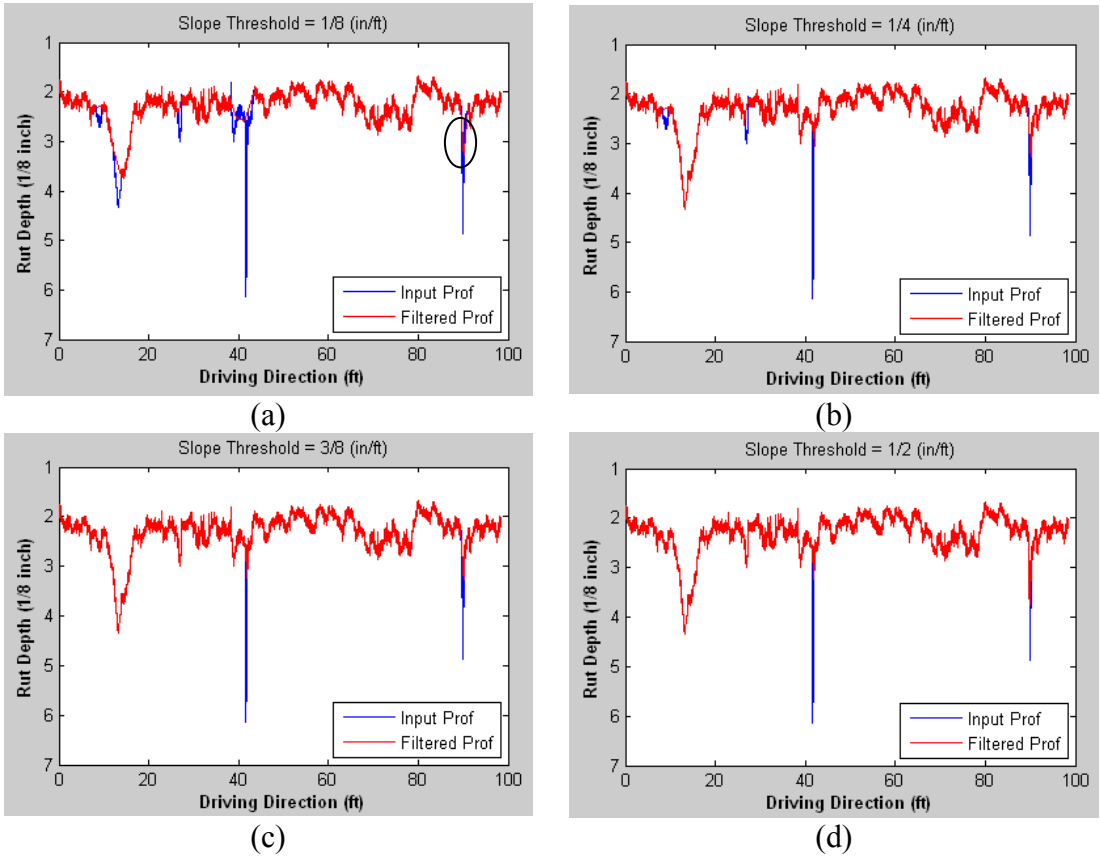

Figure 6-4 outlier removal results (window size =5 m)

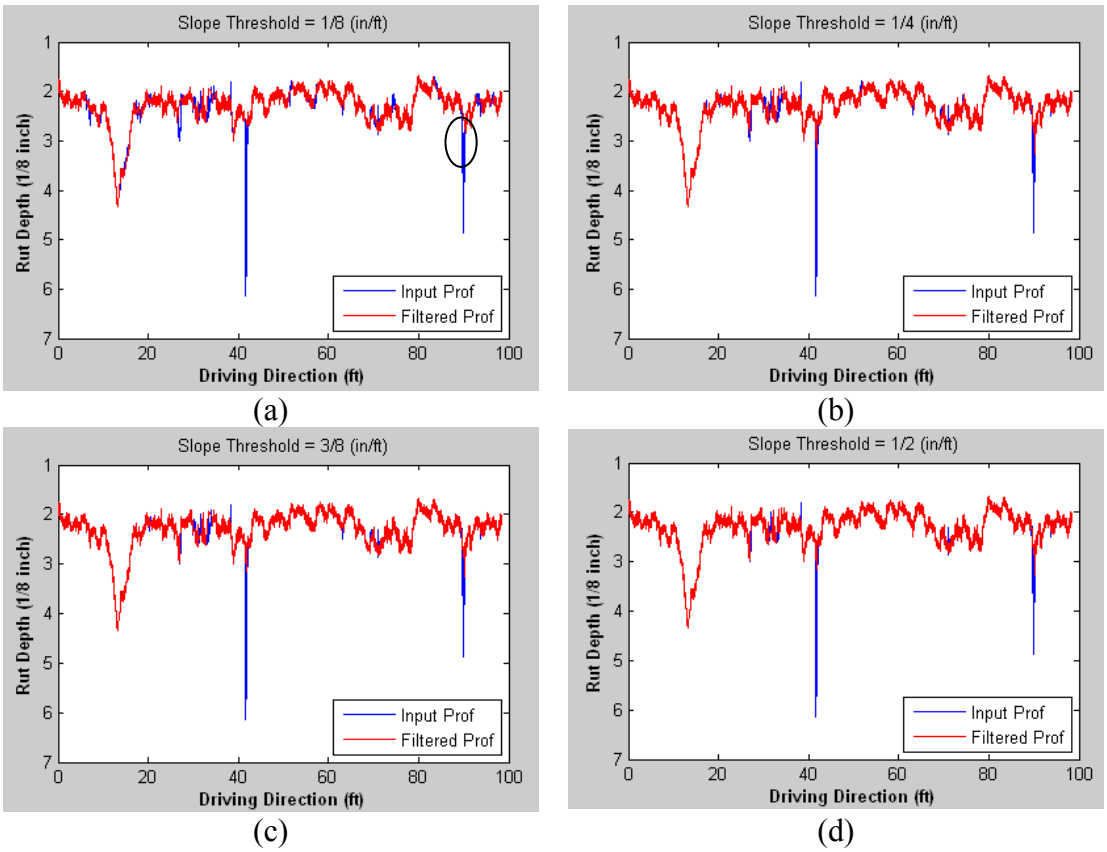

Figure 6-5 outlier removal results (window size =1 m)

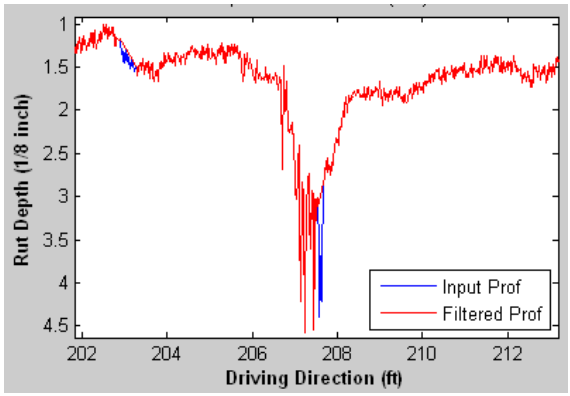

Figure 6-6 Outlier removal results (window size =1 m)

6.2 Data Segmentation - Homogeneous Segmentation Methods

As discussed in the literature review in Chapter 2, the continuous pavement rut depths in the driving direction obtained from the Data Processing Module (Module 2)

need to be partitioned into meaningful pavement segments with uniform rutting condition to apply a cost-effective treatment to each homogeneous segment. The segmentation is conducted in the Data Segmentation Module (Module 3). A homogeneous segmentation method that can generate the optimal homogeneous segmentation solution and incorporate engineering considerations is proposed and presented in this section. The homogeneous segmentation problem is first formulated into a nonlinear integer programming (NLIP) problem. Because the NLIP problem is a 1D clustering problem with string property, it can be converted to an equivalent network flow problem, in which each feasible combinations of pavement segments corresponds to a path in the directed acyclic network model and the optimal homogeneous segment solution corresponds to the shortest path in the network model .

6.2.1 Problem Formulation

As defined previously, the homogeneous segmentation problem is to partition the pavement rut depth measurements in the driving direction into segments wherein the rut depth measurements are similar to each other. Two engineering requirements (Ping et al. 1999) were incorporated as the exogenous restrictions. One is the minimum length requirement that a homogeneous segment is required to be sufficiently long. It is set from a cost-effectiveness consideration, since a short road segment has administrative costs similar to a long road segment. The other requirement is that any neighboring segments should be sufficiently different from each other, which is denoted as the minimum difference requirement. It forces the difference between the mean rut depth measurements of two neighboring segments to be at least a certain value. This constrained segmentation problem is formulated into an NLIP problem as shown in the following paragraphs.

Suppose a set of rut depth measurements includes *m* contiguous measurements, denoted by M , where each measurement $i = 1,...,m$ is a rut depth value r_i. Let

contiguous measurements be partitioned into n segments, denoted by N. This segmentation problem is to assign the measurement *i* into the segment *j* such that the sum of the measurement variances for all segments is minimized.

Let x_{ij} be a binary decision variable that indicates whether the measurement *i* belongs to segment *j* ($x_{ij}=1$) or not ($x_{ij}=0$). Then the average rut depth and the variance of rut depths in each segment *j*, where $j=1,...,n$ can be calculated as the following:

$$\bar{r}_j = \sum_{i=1}^{m} r_i x_{ij} / \sum_{i=1}^{m} x_{ij} \tag{6-1}$$

$$Var_j = \sum_{i=1}^{m} (r_i x_{ij} - \bar{r}_j)^2 \tag{6-2}$$

Further, let y_j be a binary decision variable that represents whether segment *j* is empty (i.e., $y_j=0$) or not (i.e., $y_j=1$). With these notations, the NLIP problem is as follows:

$$\min \quad \sum_{j=1}^{n} \sum_{i=1}^{m} (r_i x_{ij} - \bar{r}_j)^2 \tag{6-3}$$

s.t.

$$\sum_{j=1}^{n} x_{ij} = 1 \qquad ,\forall i \in M \tag{6-4}$$

$$x_{ij} \le y_j \qquad ,\forall i \in M,\ j \in N \tag{6-5}$$

$$y_j \ge y_{j+1} \qquad ,\forall j = 1,...,n-1 \tag{6-6}$$

$$\left.\begin{aligned} -y_j Q \le \bar{r}_j \le y_j Q \qquad & ,\forall j \in N \\ \sum_{i=1}^{m} r_i x_{ij} / \sum_{i=1}^{m} x_{ij} - (1-y_j)Q \le \bar{r}_j \le \sum_{i=1}^{m} r_i x_{ij} / \sum_{i=1}^{m} x_{ij} + (1-y_j)Q, & \forall j \in N \end{aligned}\right\} \tag{6-7}$$

$$\sum_{j' \le j} x_{ij'} + \sum_{j' > j} x_{i'j'} \le 1 \qquad ,\forall i, i' \in M, i' < i;\ j \in N \tag{6-8}$$

$$\sum_{i=1}^{m} x_{ij} \ge L y_j \qquad ,\forall j \in N \tag{6-9}$$

$$\left|\bar{r}_j - \bar{r}_{j+1}\right| \ge D y_j \qquad ,\forall j \in N \tag{6-10}$$

$$x_{ij}, y_j \in \{0,1\}; \qquad ,\forall i \in M,\ j \in N \tag{6-11}$$

In particular, the objective of this NLIP is to minimize the sum of the measurement variances for all segments. Constraints (6-4) are set so that each measurement can only be assigned to a single segment, instead of multiple segments. Constraints (6-5) are to ensure that if $y_j = 0$, then no measurement will belong to that segment. Constraints (6-6) force the non-empty segments to be put ahead of empty segments. Constraints (6-7) model the calculation of the average rut depth for each non-empty segment. They follow these observations that when $y_j = 0$, $\bar{r}_j = 0$ and when $y_j = 1$, $\bar{r}_j = \sum_{i=1}^{m} r_i x_{ij} / \sum_{i=1}^{m} x_{ij}$. Constraints (6-8) are continuity constraints. They set up the restriction that only contiguous measurements can be assigned to the same segment. Constraints (6-9) ensure that each segment contains at least *L* measurements. Constraints (6-10) specify that the average rut depths of adjacent non-empty segments should be sufficiently large, i.e., at least *D*. Finally, constraints (6-11) require that x_{ij} and y_j are 0, 1 binary variables. This NLIP has $O(mn)$ decision variables and $O(m^2 n)$ constraints.

Since the segmentation problem is a one-dimensional clustering problem with string properties, it can be converted to a network flow problem. Each homogeneous segment can be viewed as a node in the network flow model, and each combination of segments corresponds to a path from the dummy source node to the dummy sink node. Figure 6-7 is an example, containing 5 rut depth measurements, to illustrate the conversion of the segmentation problem into a network flow problem. If a partition point is set between the third and forth measurements, these 5 rut depth measurements are clustered into two homogeneous segments. These two segments correspond to two nodes, (1-3) and (4-5), in the network flow model. This combination of segments becomes a path from the dummy source node (0-0) to the dummy sink node (6-6). The variance within each segment is the distance to walk through the corresponding node. Figure 6-7(b) shows another possible combination of segments. It corresponds to another path in

the network flow model. By doing this conversion, the segmentation problem, which is targeted at minimizing the sum of the measurement variances of all segments, is equivalent to a problem that aims at finding the shortest path from the source node to the sink node for the corresponding network flow model.

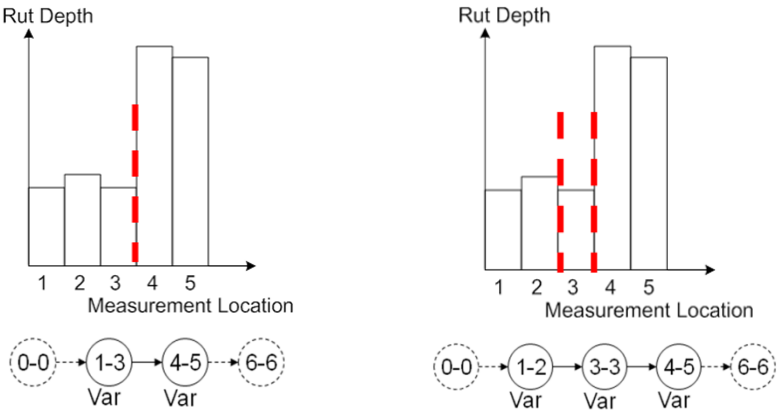

(a) Combination 1 (b) Combination 2

Figure 6-7 Conversion of the segmentation problem into a network flow problem

The one-dimensional clustering problem with string properties has been investigated in previous studies. Vinod (1969) and Rao (1971) proposed several mathematical programming formulations for this type of problem. Jensen (1969) and Bellman (1973) applied the dynamic programming technique to solve clustering problems. Novick (2009) extensively discussed and generalized the string property. Wang et al. (2011) converted the segment clustering problem (SCP) into a network flow problem and proposed a topological-ordering-based segment clustering (TOSC) method to solve the SCP. However, the homogeneous segmentation problem in this dissertation has one extra constraint set, the minimum difference constraints (11). These constraints, although largely reducing the feasible solution space, complicate the problem and make it impossible to directly adopt the TOSC method proposed by Wang et al. (2011). A modified TOSC (MTOSC) method is proposed (Li and Tsai 2012) and presented in the next subsection.

6.2.2 MTOSC Method

To solve the constrained homogeneous segmentation problem, an MTOSC method is proposed. It first conducts an exhaustive search to identify all feasible segmentation combinations and organizes them into a network model in topological ordering. Then, the shortest path from the source node to the sink node of the network model is determined, which corresponds to the optimal segmentation solution.

The network model is denoted as a partition graph (PG). A PG consists of a qualified node set and a qualified arc set. In particular, the node set $V = \{(r_s, r_t) : s, t = 1, ..., m\}$ contains all qualified nodes, e.g., (r_s, r_t), that satisfy the minimum length requirement, where r_s and r_t are the start and end rut depth measurements of this node. The node set also includes a dummy sink node, (r_{m+1}, r_{m+1}), which indicates the end of a segmentation. This representation of segments is because the segmentation problem has the string property, i.e., all measurements inside a segment have to be adjacent. Therefore, a segment can be represented using the start and end rut depth measurements; the measurements in between are also assigned to the same segment. In other words, the node (r_s, r_t) consists of rut depths r_i, where $1 \le s \le i \le t \le m+1$. In total, there are at most $m(m+1)/2$ nodes. It requires $O(m^2)$ time to construct those nodes and $O(m^2)$ storage space. The number of nodes can be further reduced if considering the minimum length requirement.

The next step is to identify the qualified arc set. Each arc in the qualified arc set $E = \{(r_s, r_t, r_{t'}) : s, t, t' = 1, 2, ..., m+1\}$ connects two nodes that satisfy the minimum difference requirement. In other words, the difference between the average rut depth of node (r_s, r_t) and that of its neighboring node $(r_{t+1}, r_{t'})$ is at least *D*. It costs $O(m^3)$ processing time to construct E, and, conceptually, E has $O(m^3)$ arcs. However, the

actual number of arcs in E highly depends on the input data and the preset external constraints. For example, if the minimum difference *D* is set to be 10 mm instead of 5 mm, the number of qualified arcs may be reduced significantly.

After having the qualified node set and qualified arc set ready, a PG is constructed and organized in topological ordering. It contains all feasible segmentation solutions. The construction of the PG costs $O(m^3)$ processing time and $O(m^2)$ storage space. Then, the PG is searched for the shortest path from r_1 to r_{m+1}, which corresponds to the optimal segmentation. The detailed method is presented below:

Step 1. Create qualified node set and update the accumulative variance labels for each node

For $t = L$ to m do

For $s = 1$ to s-L+1 do

Step 1.1. Calculate the average rut depth and variance for each node (r_s, r_t) by

$$\overline{r}_{s,t} = \sum_{i=s}^{t} r_i / (t - s + 1);$$

$$Var_{s,t} = \sum_{i=s}^{t} (r_i - \overline{r}_{s,t})^2;$$

Step 1.2. Initialize the accumulative variance label for each node (r_s, r_t) by

$C(r_s, r_t) = \infty$; set $C(r_s, r_t) = 0$, where $s = 1$;

Step 1.3. Initialize the label for predecessor node by

$P(r_s, r_t) = NULL$;

Step 1.4. Update the accumulative variance label by scanning all arcs that direct to each node (r_s, r_t)

For s' = 1 to s-L do

If $\left|\overline{r}_{s',s-1} - \overline{r}_{s,t}\right| \geq D$, then

If $C(r_s, r_t) > C(r_{s'}, r_{s-1}) + Var_{s',s-1}$ then

$$C(r_s, r_t) = C(r_{s'}, r_{s-1}) + Var_{s',s-1};\ P(r_s, r_t) = s';$$

Step 2. Create the sink node and update its accumulative variance label

Step 2.1. Initialize the label of accumulative variance and the label for predecessor node

$$C(r_{m+1}, r_{m+1}) = \infty;\ P(r_{m+1}, r_{m+1}) = NULL;$$

Step 2.2. Update the accumulative variance label by scanning all arcs that direct to the sink node

For s' = 1 to m-L+1 do

If $C(r_{m+1}, r_{m+1}) > C(r_{s'}, r_m) + Var_{s',m}$ then

$C(r_{m+1}, r_{m+1}) = C(r_{s'}, r_m) + Var_{s',m}$; $P(r_{m+1}, r_{m+1}) = s'$;

Step 3. Trace the shortest path from r_{m+1} back to r_1

If $C(r_{m+1}, r_{m+1}) = \infty$ then

No feasible segmentation exists, STOP.

Else

The optimal segmentation is available and can be outputted by tracing from r_{m+1} back to r_1 based on predecessors. The total variance equals to $C(r_{m+1}, r_{m+1})$.

In this MTOSC, Step 2 is the most time-consuming one. It takes $O(m^3)$ time to construct the qualified node set and scan over all potential arcs. Hence, the MTOSC can solve the homogeneous segmentation problem within polynomial time to the number of measurements, i.e., $O(m^3)$ time.

Figure 6-8 illustrates how the PG is constructed and how the MTOSC works. First, the qualified node set, consisting of 10 nodes, is identified. Those 10 nodes satisfy the minimum length requirement. They are organized in topological ordering. Then, all potential arcs that direct to each node are determined and drawn in Figure 6-8, but not all of them are qualified. The dashed lines are potential arcs but not qualified arcs. Only the solid lines are qualified arcs; they connect nodes that satisfy the minimum difference requirement. The third step is to scan over qualified arcs that direct to each node and update the accumulative variance of each node. For example, the initial accumulative variance for the nodes (r_1, r_3) and (r_4, r_6) are 0 and ∞, respectively. Because of the existence of the qualified arc (r_1, r_4, r_6), the latter is updated to $C(r_4, r_6) = C(r_1, r_3) + Var_{1,3} = 600$. Finally, it is traced back from r_7 to r_1, and it is

determined that the shortest path consists of nodes (r_1, r_3), (r_4, r_6), and (r_7, r_7) with the accumulative variance $Var_{1,3} + Var_{4,6} = 600 + 600 = 1200$.

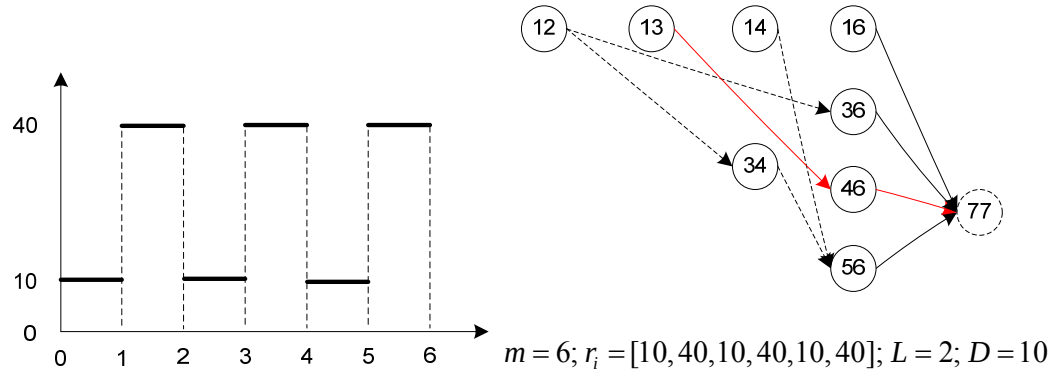

(a) Rut depth measurements (b) Partition graph

Figure 6-8 Illustration of the homogeneous segmentation method

6.2.3 Overlapping-Reducing Heuristic Method

Although the MTOSC method provides the optimal solution and can be used as a benchmarking standard to evaluate heuristic segmentation methods, it costs a significant amount of computational time, which makes it impractical to use the MTOSC to solve large-scale problems. To solve large-scale segmentation problems, an overlapping-reducing heuristic method is further proposed and presented in this subsection.

The heuristic method is based on the observation that the previous method of constructing the PG allows a high overlap between two successive nodes, e.g., (r_s, r_t) and $(r_{s+1}, r_{t'})$, which is not necessarily needed. For instance, when constructing the qualified node set for the PG, after having one node (r_s, r_t), one of its successive node will be (r_{s+1}, r_{t+1}), as shown in Figure 6-9. There is only one measurement difference between these two nodes, which does not bring too much additional statistical information into the second node. Therefore, in the heuristic method, a smaller overlap between two

successive nodes is allowed. For instance, s' could be equal to $(s+t)/2$ when $s+t$ is even. There is only approximately 50% overlap between two nodes under this case.

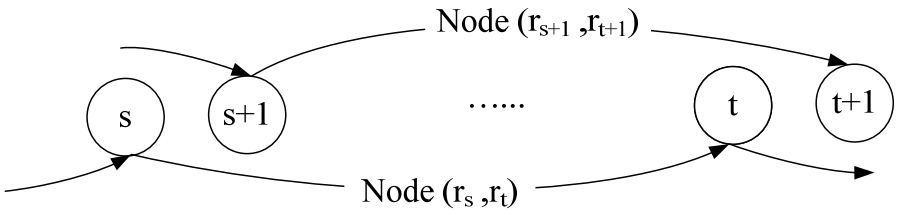

Figure 6-9 Illustration of successive nodes

By reducing the overlap, the number of feasible nodes and arcs is reduced and the computational time is shortened. Assume there is a gap, denoted as g, between s and s'. Then, there will be, conceptually, at most $O(m^2/g)$ nodes, and it requires $O(m^2/g)$ time to construct those nodes and $O(m^2/g)$ storage space. Because the number of nodes is reduced, the maximum number of arcs is also reduced to $O(m^3/g^2)$, and the processing time of constructing E becomes $O(m^3/g^2)$. In summary, the construction of the PG costs $O(m^3/g^2)$ processing time and $O(m^2/g)$ storage space. Therefore, compared with the MTOSC, the heuristic method can reduce the processing time and is more capable of solving large-scale homogeneous segmentation problems. Experimental tests are presented in Appendix A to assess how much overlap is optimal, which can, on one hand, significantly reduce the processing time and, on the other hand, won't compromise much of the segmentation optimality.

6.3 Decision Support - Network-level Rutting Condition Assessment Procedure

A procedure is needed in the Decision Support Module (Module 6) to report the pavement rutting condition and the statistical information in support of network-level pavement management decisions. In this section, such a network-level rutting condition assessment procedure is proposed. A proper statistical indicator is recommended to

represent the condition of each pavement segment. Several case studies on interstate highways, state routes, and county roads are presented in Chapter 7 to demonstrate the feasibility of this procedure.

6.3.1 Network-level Rutting Condition Assessment Procedure using a 3D Line Laser System

The proposed network-level rutting condition assessment procedure using a 3D line laser system includes the following steps:

- **Step 1**. Collect 3D range data for each project from the start milepost (MP) to the end MP.
- **Step 2**. Process the 3D range data to obtain rutting measurements for individual transverse profiles. A rut depth computation method is employed in this step. The obtained rutting measurements are then aligned to form longitudinal rut depth profiles for both wheel paths in the driving direction. One example profile is given in Figure 6-1.
- **Step 3**. Use the threshold-based outlier removal method proposed in Section 6.1 to filter the longitudinal rut depth profiles and remove outliers caused by wide transverse cracks and raised pavement markings based on the assumption that the rut depth would not suddenly change.
- **Step 4**. Establish the milepost-based linear referencing, which is used in GDOT's network-level survey practices, in the 3D range data. The DMI-measured location reference is translated into the milepost-based linear referencing. The longitudinal rut depth profiles are then divided into segments (typically 1 mile long) according to the milepost-based linear referencing.
- **Step 5**. Analyze each 1-mile segment and report the representative rut depths for both wheel paths and both driving directions using different statistical factors,

such as 60th percentile, average, standard deviation, and linear percentages of different severity levels of rutting.

6.3.2 Step 4 - Establishment of Milepost-based Linear Referencing

Because the survey vehicle cannot maintain a perfectly straight driving line, the DMI-recorded distance that the vehicle actually traveled is usually longer than the length of the survey project. The longitudinal rut depth profiles are found to be longer than the project, e.g., perhaps, 10.5 miles instead of 10.3 miles of the actual project length. Therefore, the DMI-measured location reference needs to be translated into the milepost-based linear referencing used in GDOT's network-level survey practices, so that the longitudinal rut depth profiles of a project can be divided into segments accordingly. Each segment is typically 1 mile long. Sometimes, the first segment or the last segment of a project may be less than 1 mile.

To translate the DMI-measured location reference into the milepost-based referencing, an assumption is made that the vehicle wandering occurs uniformly throughout the entire project. Under this assumption, a practical method is proposed to divide the longitudinal rut depth profile data into segments proportional to the segment length. In the future, the Geo3D sign detection results can be used as a medium to mapping of the referencing systems from the DMI-based into the milepost-based, since the Geo3D system and the 3D line laser system are synchronized using the same DMI. This method is a more accurate method.

6.3.3 Step 5 - Statistical Analyses

With the filtered rut depth profiles, statistical analyses are conducted. Commonly used statistical indicators, including mean, median, 60th percentile, minimum, maximum, skewness, standard deviation, linear percentages of minor, low, medium, and severe rutting, are calculated. In addition, the maximum rut depth density, which is more

intuitive to engineers, is used to show the homogeneity of rutting condition within a 1-mile segment. The rut depth density at each point is estimated using the percentage of rut depths that fall in a fixed interval around the point. The maximum rut depth density is the maximum of rut depth densities for the 1-mile segment. For the example shown in Figure 6-10, the maximum rut depth density equals $\frac{\max(Area_i)}{Total\ Area} * 100\%$, where the total area is the whole area under the curve. In this study, Δ is set to be 1/16 in.

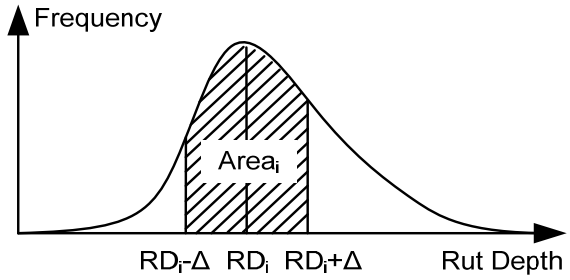

Figure 6-10 Illustration of the rut depth density

6.4 Decision Support - Project-level Isolated Rut Detection Method

As identified in Chapter 2, there is a need to develop a method to automatically detect isolated ruts in support of project-level pavement management decisions, e.g., low-cost, localized maintenance planning. An automated isolated rut detection method is proposed in the Decision Support Module (Module 6) to identify isolated ruts using the 3D range data collected by the 3D line laser system. Pavement engineering knowledge is extensively incorporated to establish the criteria for identifying isolated ruts.

The isolated rut detection method, as illustrated in Figure 6-11, uses the filtered longitudinal rut depth profile as input and includes two steps: (1) determination of rut termini in the driving direction and (2) computation of rut volume. An example of the longitudinal rut depth profile is given in Figure 6-11(c). Based on the longitudinal rut depth profiles, the automated method first determine the termini of isolated ruts, which

are marked with a green square (the start point) and a yellow circle (the end point) shown in Figure 6-11(d). Then, the rut rut volume is calculated for each isolated rut.

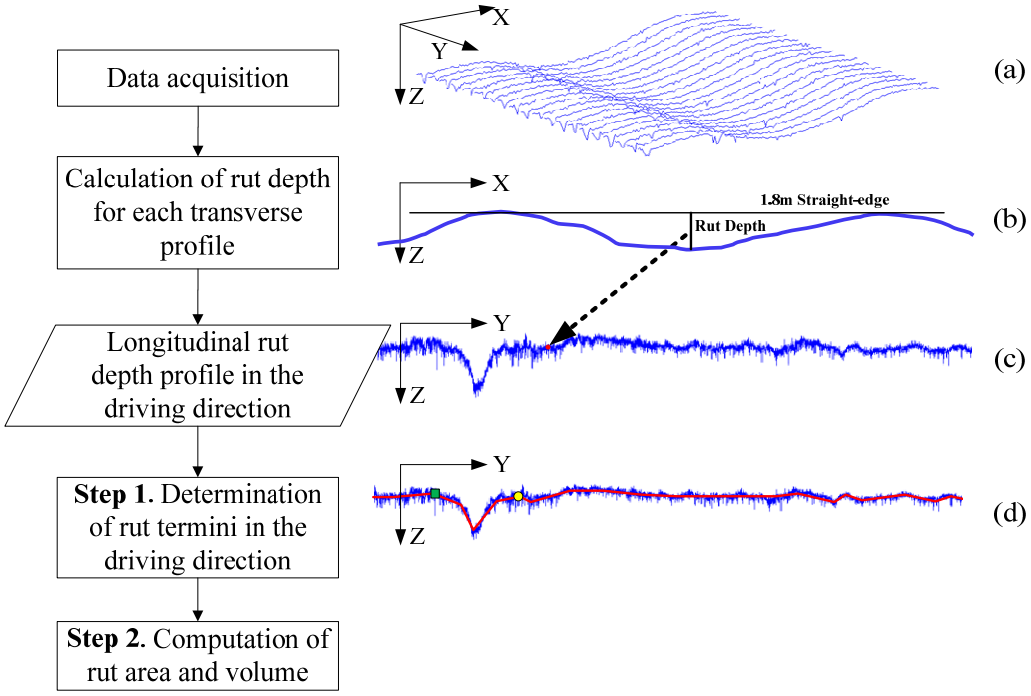

Figure 6-11 Isolated rut detection method

Step 1. Determination of Rut Termini in the Driving Direction

This step is to determine the termini of each isolated rut in the driving direction. It includes two sub-steps: (1) determine homogeneous segments and (2) determine the termini of each isolated rut.

Step 1.1 Determine homogeneous segments

With the filtered longitudinal rut depth profile, the homogeneous segmentation method proposed in Section 6.2 is used to determine the homogeneous segments, wherein the pavement rutting condition is relatively uniform. This step further reduces data and preserves only the necessary details. The homogeneous segmentation results can be saved into a Pavement Maintenance Management System and can be used to support isolated distress detection and maintenance operation design.

Step 1.2 Determine the termini of isolated ruts

After consulting GDOT pavement engineers, rules have been proposed to represent an isolated rut and determine its termini. Items used in the rules are shown in Figure 6-12. The rules are the following:

- Rut depth requirement. The rut needs to be deeper than 1/4 in. to be considered as an isolated rut. Thus, 1/4 in. depth is set as a threshold, although it can be changed.
- Rut length requirement. The portion of the rut that is greater than the threshold (e.g., 1/4 in.) needs to be sufficiently long (i.e., the length > RutLen shown in Figure 6-12) so that the rut can become an isolated rut. The AASHTO provisional standard PP69 defines a rut as at least 100 ft long (AASHTO 2010). The GDOT manual defines a rut as at least 20 ft long (GDOT 2007). It is suggested setting RutLen as 10 ft, since deep-base patching, a localized treatment, can be applied to a 10-ft section if it exhibits local base failure.
- Rut division criterion. If the two isolated ruts are close to each other (i.e., the distance < RutDist shown in Figure 6-12), they should be counted as a single one. The suggested RutDist is 20 ft.
- Rut termini determination rule. The termini of an isolated rut are the points that enclose it. However, if the surrounding pavement shows continuous shallow rutting (e.g., 1/8 in.), engineers suggest using the points where the longitudinal rut depth profile crosses the threshold line as the termini of an isolated rut. This is because, in practice, only the worst spots that show rutting deeper than 1/4 in. need to be treated.

Based on the inputs from GDOT pavement engineers, the isolated ruts are identified by (1) thresholding the filtered longitudinal rut depth profile, (2) identifying spots with rutting deeper than the predefined threshold 1/4 in. and creating the first list of

isolated ruts, (3) removing ruts that are shorter than RutLen (10 ft), (4) merging ruts that are close to each other (i.e., their distance is smaller than RutDist (20 ft)), and (5) removing the rut within which the majority (e.g., 70%) of rut depths is shallower than 3/8 in. The final list of isolated ruts is then obtained. The termini of isolated ruts are marked by the solid short lines in Figure 6-12, which are the spots where the rut depth starts to be shallower than the threshold (e.g., 1/4 in.).

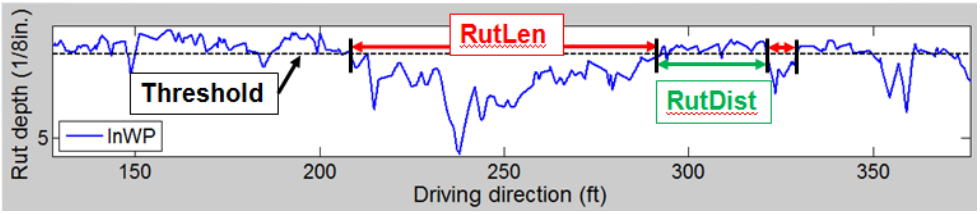

Figure 6-12 Criteria for representing an isolated rut

Step 2. Computation of Rut Volume

This step computes additional information about isolated ruts, including maximum rut depth, rut length, and rut volume. Rut volume is the sum of all cross-sectional areas multiplied by the interval between two successive measurements in the driving direction.

CHAPTER 7 CASE STUDY FOR DECISION SUPPORT

1D rut depth can be measured reliably and accurately using the 3D line laser system as presented in Chapter 4. A methodology for utilizing the 3D line laser system to support informed, data-driven pavement management decision making is outlined in Chapter 5 and substantiated with methods and decision support applications, including network-level rutting condition assessment and project-level isolated rut detection in Chapter 6. The network-level pavement rutting condition assessment is to report the representative 1D rut depth and additional statistical information in support of network-level decision making; and project-level isolated rut detection is to detect isolated road sections with severe rutting problems for project-level low-cost, localized treatments. To demonstrate the applicability of the substantiated methodology and developed applications, case studies were carried out on the actual roadways, including one interstate highway, two state routes, and one city road. The case study results are presented in this chapter. In addition, case studies were also performed to explore the potential benefits of using the 3D line laser system in improving pavement rutting progression modeling.

7.1 Network-level Rutting Condition Assessment

A network-level rutting condition assessment procedure was proposed in Chapter 6 to support network-level pavement management decisions. Case studies were carried out to evaluate the applicability of the proposed procedure. The test site selection, data collection, and case study results are presented in this section. Additionally, the determination of an adequate sampling interval and the performance (i.e., processing speed and data storage need) of the proposed procedure were assessed. The potential issues of the proposed procedure were finally discussed.

7.1.1 Test Site Selection

In the process of test site selection, an effort was made to cover interstate highways and non-interstate highways, while targeting pavement sections that had rutting of different severity levels. After reviewing the treatment criteria in GDOT, four groups of rut depths were identified for investigation. They are minor (rut depth shallower than 1/4 in.), low (rut depth between 1/4 in. and 1/2 in.), medium (rut depth between 1/2 in. and 1 in.), and severe (rut depth greater than 1 in.). Also, the selected test site was required to have varying surface conditions (e.g., few cracks, severe cracking, or potholes) and other conditions (e.g., integrity of pavement marking and presence of railroad crossings). These two factors are considered because they may impact the rut depth measurement accuracy.

To locate possible test sites, the annual survey results from GDOT were reviewed. A list of routes was identified based on the fact that the routes exhibited a variety of rut depths and surface conditions. This list was then narrowed down by performing a preliminary visual investigation and considering the factors mentioned above. Finally, I-95, SR 275, SR 67, and Benton Blvd. were selected as test sites. Table 7-1 shows the detailed information about these test sites.

SR 275 and SR 67 are two-lane rural roads. SR 275 has a dead end, serves only a small amount of traffic, and has low to medium severity levels of rutting and few cracks. SR 67 experienced a much higher traffic volume and exhibited medium to severe cracking. I-95 is an interstate highway that connects Florida and Washington, D.C. The short section from MP 101 to MP 100 was selected as a test site. It is paved with SMA plus OGFC. The annual average daily traffic (AADT) is more than 50,000. This section is still in good condition and exhibits little rutting or cracking. It has a low severity level of raveling. The last test site is Benton Blvd., which is a county road. It was selected as a test site because it exhibits severe rutting (as deep as 2 in.), severe cracking, and potholes.

Table 7-1 Selected Test Sites

Case #	Test Site	Section (MP)	AADT	Rut Depth (in)	Surface Condition
1	SR 275	0-5	1,890	1/8 – 3/4	Few cracks
2	SR 67	9-15	7,570	0-1/8	Medium to severe cracking
3	I-95	101-100	>50,000	1/8 – 1/4	Few cracks; low severity level raveling
4	Benton	--	--	1/4 - 2	Severe cracking and potholes

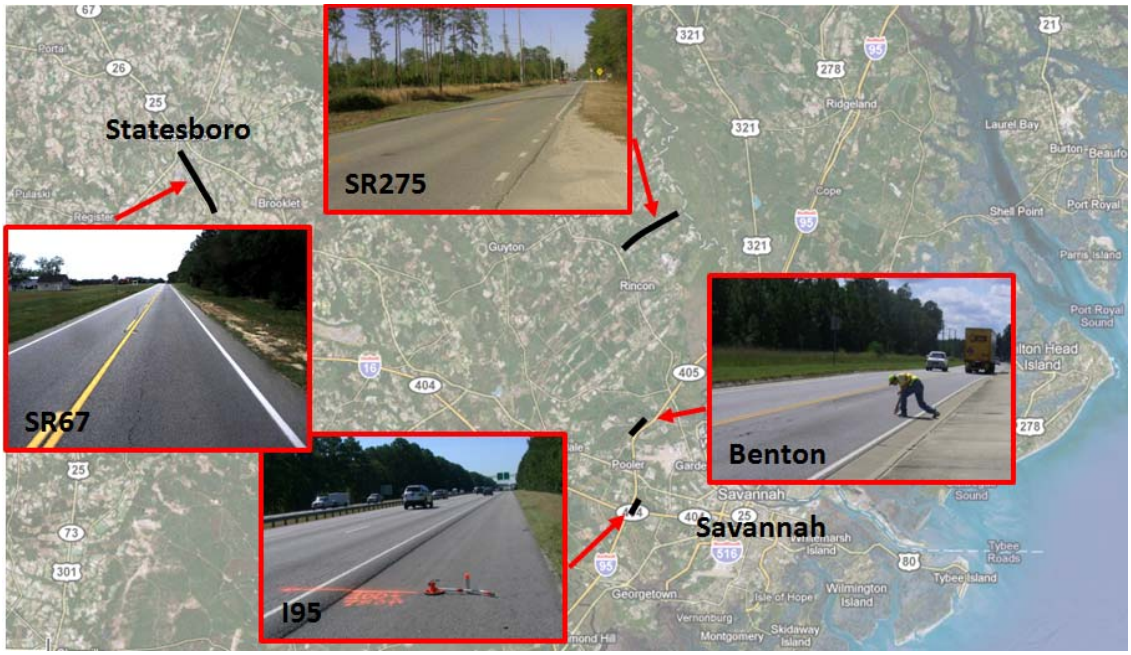

Figure 7-1 Test site locations

7.1.2 Data Collection

Once the test sites were finalized, a manual rutting survey was conducted on SR 275 and SR 67 by GDOT liaison engineers in accordance with GDOT's protocol. A manual survey was not conducted on I-95 due to the high traffic volume. Then, 3D range data was collected using the 3D line laser system at 5 mm intervals in the driving direction. Data was collected on SR 275 three times so that the repeatability of the 3D line laser system could be evaluated. For other test sites, only one run of data was collected.

7.1.3 Case Study Results – SR 275

The collected 3D range data was analyzed using the procedure proposed in Section 6.3. Only the case study results for SR 275 are reported in this subsection. Figure 7-2 shows the roadway environment on the SR 275 test site.

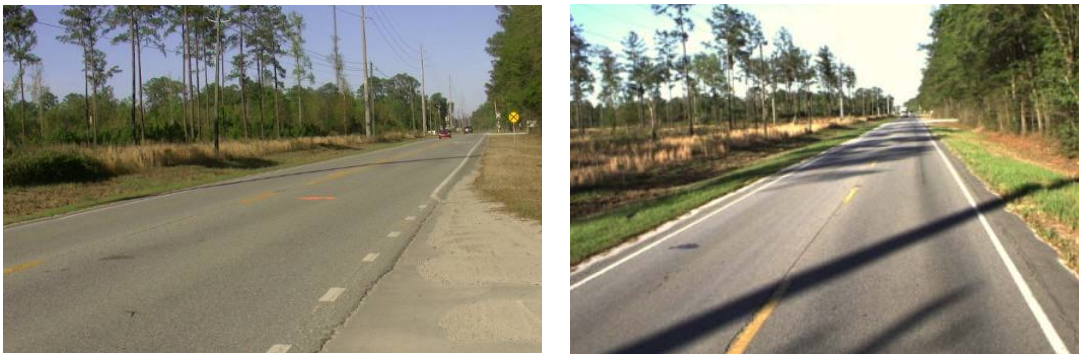

(a) Roadway environment (b) Rutting

Figure 7-2 Field test on SR 275

The longitudinal rut depth profiles were first obtained. The longitudinal rut depth profiles shown in Figure 7-3 for the outside lane of SR 275, southbound (SB) from MP 0.8 to MP 0, is given as an example. As shown in Figure 7-3, the rutting condition within this mile is relatively uniform. The maximum rut depth on this route is close to 1/2 in. The 100-ft representative sample section identified by GDOT pavement liaisons during the manual survey is highlighted with the green rectangles. For the LWP, the rutting condition in the selected 100-ft representative section can represent the majority of the rutting condition within this mile, whereas a relatively worse 100 ft was selected for the RWP. Several factors have prevented manual surveys from capturing the representative rut depth. First, it is not easy to observe the rutting from a windshield survey. Therefore, the selection of a 100-ft representative section is mainly based on the cracking. Second, the selection of a 100-ft representative section is subjective. Finally, even if a 100-ft representative section was located correctly, only a limited number of straightedge measurements were manually taken in the field.

In the next step, the longitudinal rut depth profiles (shown in Figure 7-3) are filtered using the outlier removal method presented in Section 6.1. The red profiles shown in Figure 7-4 are the filtered data. With the filtered data, statistical analyses were conducted. Figure 7-5 shows the histogram of the filtered rutting data. Obviously, the data has some positive skew and does not follow a normal distribution. Statistical indicators, including mean, median, 60th percentile, minimum, maximum, skewness, standard deviation, maximum density, linear percentages of minor, low, medium, and severe rutting, are calculated and presented in Table 7-2.

As shown in Table 7-2, the proposed procedure shows high repeatability among three runs when reporting most statistics. For instance, the maximum absolute difference among mean rut depths collected from three runs is close to 0. The maximum absolute difference among the linear percentages of different severity levels of rutting is 2%.

In addition, as shown in Table 7-2, the candidates of representative rut depth, including mean, median, and 60th percentile of rut depth, are very close to each other. The 60th percentile is the indicator recommended by GDOT pavement engineers to be used as the representative pavement condition in one mile.

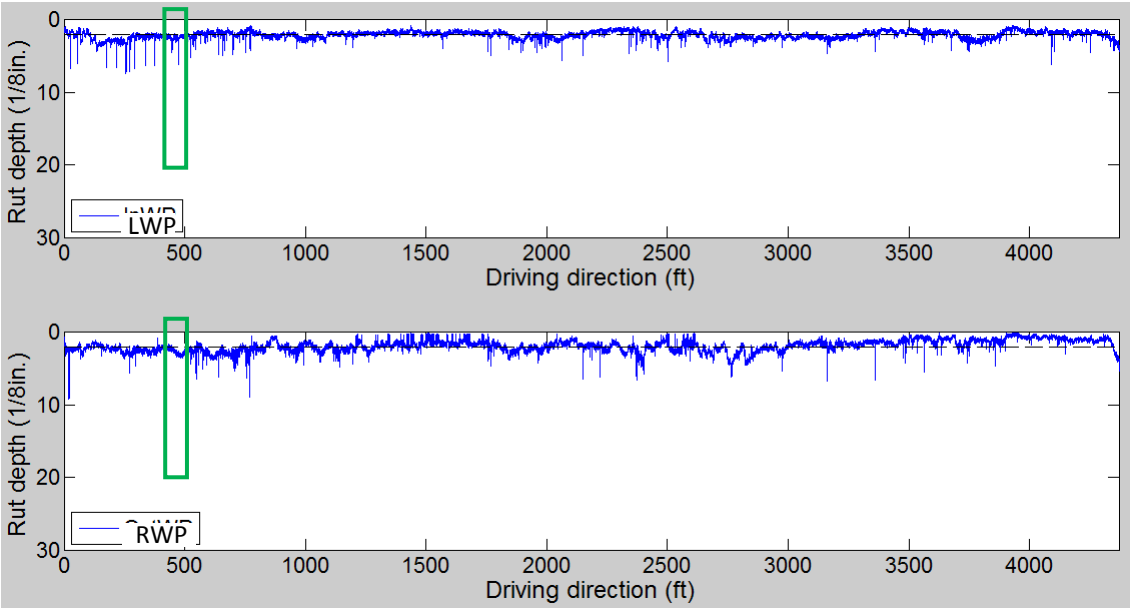

Figure 7-3 Raw data (SR 275 SB from MP 0.8 to MP 0)

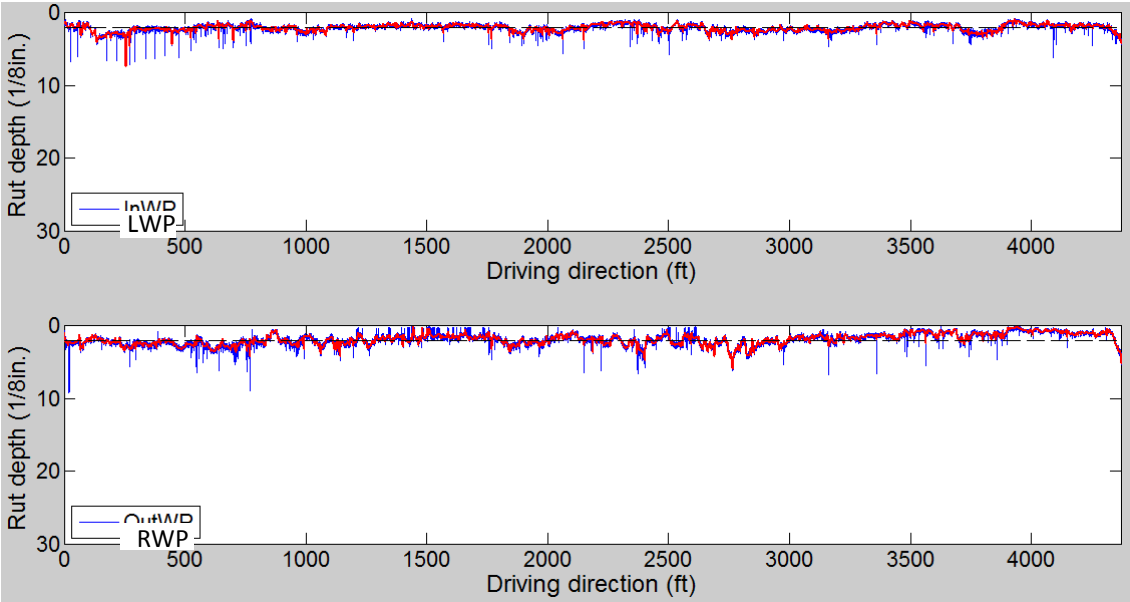

Figure 7-4 Raw (blue) and filtered data (red) (SR275 SB from MP 0.8 to MP 0)

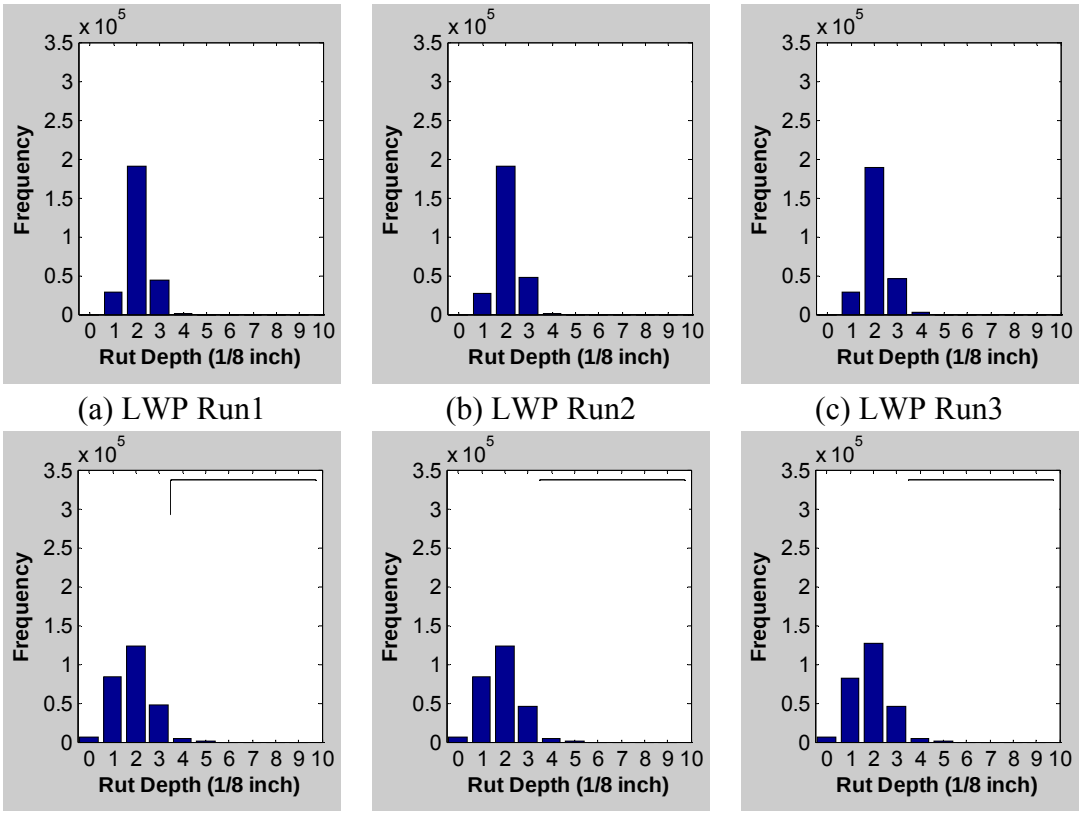

(a) LWP Run1 (b) LWP Run2 (c) LWP Run3

(d) RWP Run1 (e) RWP Run2 (f) RWP Run3

Figure 7-5 Histogram of filtered data (SR 275 SB from MP 0.8 to MP 0)

Table 7-2 Reported Indicators (SR 275)

Indicators	LWP Rut Depth (1/8 in)					RWP Rut Depth (1/8 in)				
	Run1	Run2	Run3	Avg	Diff	Run1	Run2	Run3	Avg	Diff
Mean	2.0	2.1	2.1	2.1	0.1	1.8	1.9	1.9	1.9	0.1
Median	2.0	2.0	2.0	2.0	0.0	1.8	1.8	1.8	1.8	0.0
60^{th} Prct	2.1	2.2	2.1	2.1	0.1	2.0	2.0	2.1	2.0	0.1
Min	0.3	0.8	0.4	0.5	0.5	0.2	0.1	0.2	0.2	0.1
Max	7.2	7.4	7.3	7.3	0.2	6.1	6.0	6.0	6.0	0.1
Skewness	0.9	0.9	0.8	0.9	0.1	0.3	0.4	0.4	0.4	0.1
Std	0.5	0.5	0.5	0.5	0.0	0.8	0.8	0.8	0.8	0.0
Max Density	72%	72%	71%	72%	1%	49%	48%	48%	48%	1%
Minor	51%	49%	50%	50%	2%	59%	59%	57%	58%	2%
Low	49%	50%	50%	50%	1%	41%	40%	42%	41%	2%
Medium	0%	0%	0%	0%	0%	1%	1%	1%	1%	0%
Severe	0%	0%	0%	0%	0%	0%	0%	0%	0%	0%

Besides the section from MP 0.8 to MP 0, other sections on SR275 were analyzed similarly, and the analysis results are listed in Tables 7-3,7-4, and 7-5. As shown in Table 7-3, the statistical indicators, mean, median, and 60th percentile of rut depths, provide similar rut depth for all road segments. These statistical indicators were also compared with manual survey results. For half of the road segments in Table 7-3, the manual survey results are not available, since only the lane in the worst condition on two lane roads was rated according to the GDOT's survey manual. The comparison shows that for road segments with small standard deviation (e.g., smaller than 1/8 in.), the pavement rutting condition within the road segment is relatively uniform so that the manual survey can provide results similar to the automated survey results; however, as the standard deviation increases, the manual survey has a greater opportunity to underestimate or overestimate the representative rutting condition. Additional tests are needed to further confirm this observation.

Table 7-3 Results for SR 275

	MP	LWP Rut Depth (1/8 in)				RWP Rut Depth (1/8 in)			
		Mean	Median	60^{th} Prct	Manual	Mean	Median	60th Prct	Manual
SB	5-4	1.1	1.0	1.1	1	0.9	0.8	0.9	1
	4-3	0.8	0.8	0.8	N/A	0.8	0.7	0.8	N/A
	3-2	1.1	0.8	0.9	N/A	0.9	0.8	0.9	N/A
	2-1	1.6	1.6	1.8	2	1.6	1.4	1.6	4
	1-0	2.4	2.2	2.4	3	2.1	2.0	2.2	3
NB	0-1	2.6	2.6	2.8	N/A	1.4	1.3	1.4	N/A
	1-2	1.8	1.7	2.0	N/A	2.3	1.9	2.1	N/A
	2-3	1.1	0.9	1.0	0	1.4	0.9	1.1	1
	3-4	0.8	0.8	0.8	1	0.7	0.6	0.7	1
	4-5	1.0	1.0	1.1	N/A	0.9	0.8	0.9	N/A

It is also observed in Table 7-4 that as the standard deviation increases, the maximum density generally decreases. This is understandable since as the standard deviation increases, more dispersion exists from the average, and the maximum density is expected to be smaller. An exception is the RWP of road segment from MP 2 to MP 3, which has the highest standard deviation among all segments, which is 1.5 of 1/8 in., and, a relatively high maximum density, 67%, in the meanwhile. This exception was analyzed by examining the longitudinal rut depth profile. As shown in Figure 7-6, the majority of this segment has minor, uniform rutting, and only the first 700 ft exhibits severe rutting. The maximum rut depth for the 700 ft section is as high as 1 in. This isolated severe rutting is resulted from a longitudinal construction joint, which is in the middle of the lane after a new right-turn lane was added and the lane lines were repainted. The isolated severe rutting has results in the high standard deviation value and the rest minor and uniform rutting has caused the relatively high maximum density value. Hence, the combination of a high standard deviation and a relatively high maximum density could be an indication of the presence of isolated severe rutting. Further tests are needed to verify this finding.

Table 7-4 Results for SR 275 (Continued)

	MP	LWP Rut Depth (1/8 in)					RWP Rut Depth (1/8 in)				
		Min	Max	Skewness	Std	Max Density	Min	Max	Skewness	Std	Max Density
SB	5-4	0.3	2.8	0.4	0.3	94%	0.2	3.9	1.5	0.4	85%
	4-3	0.3	2.4	0.8	0.2	99%	0.2	6.5	3.5	0.4	94%
	3-2	0.1	4.2	1.7	0.7	79%	0.2	5.1	2.6	0.6	82%
	2-1	0.3	5.8	0.4	0.8	42%	0.0	7.4	1.5	1.0	58%
	1-0	0.0	9.8	2.4	0.9	60%	0.2	13.8	2.6	1.1	48%
NB	0-1	0.0	4.7	-0.2	0.7	50%	0.2	4.7	1.2	0.5	75%
	1-2	0.3	8.5	0.7	0.9	45%	0.2	8.6	1.1	1.4	39%
	2-3	0.1	4.5	1.7	0.7	72%	0.1	9.3	2.6	1.5	67%
	3-4	0.3	2.5	1.4	0.2	99%	0.2	4.1	2.0	0.3	97%
	4-5	0.4	3.5	2.1	0.3	94%	0.2	3.3	1.1	0.4	84%

The case study results on the four selected road sections show the following:

- The proposed network-level rutting survey procedure has good repeatability.
- The proposed procedure can report the representative rut depth, i.e., the 60th percentile, as suggested by engineers from GDOT. The representative rut depth can be directly fed into COPACES, the pavement condition database managed by GDOT, to support pavement management and maintenance.
- The proposed procedure can also report additional statistical indicators, e.g., mean, maximum, standard deviation, maximum density, and linear percentage of minor, low, medium, and severe rutting, which are useful in support of the network-level pavement management decision making.

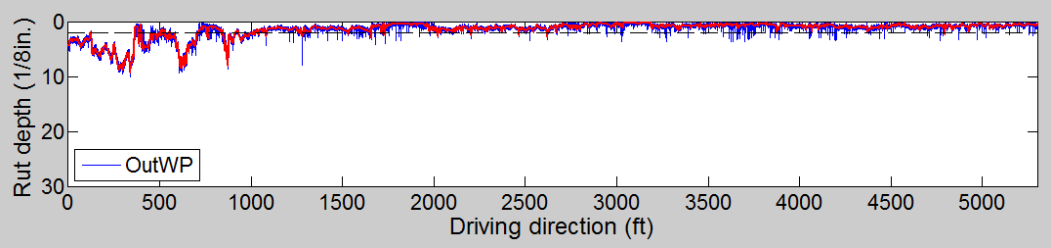

Figure 7-6 Raw data and cleaned data (SR275 NB MP2-3, RWP)

Table 7-5 Results for SR 275 (Continued)

	MP	LWP Rut Depth (1/8 in)				RWP Rut Depth (1/8 in)			
		Minor	Low	Medium	Severe	Minor	Low	Medium	Severe
SB	5-4	100%	0%	0%	0%	98%	2%	0%	0%
	4-3	100%	0%	0%	0%	99%	1%	0%	0%
	3-2	85%	15%	0%	0%	95%	5%	0%	0%
	2-1	70%	30%	0%	0%	76%	20%	4%	0%
	1-0	36%	59%	5%	0%	50%	47%	3%	0%
NB	0-1	19%	79%	2%	0%	90%	10%	0%	0%
	1-2	63%	36%	1%	0%	55%	30%	15%	0%
	2-3	87%	12%	1%	0%	84%	9%	7%	0%
	3-4	100%	0%	0%	0%	100%	0%	0%	0%
	4-5	98%	2%	0%	0%	99%	1%	0%	0%

7.1.4 Computational Consideration

This subsection discusses the determination of an adequate sampling interval for the proposed procedure. According to a review of available literature, there is little consistency on the sampling interval used by different state transportation agencies. Usually, there is a balance between the sampling interval and the processing time. The smaller the interval, the more accurate the network-level survey results, but the processing time is longer. To determine an adequate sampling interval, this subsection evaluates the impact of the sampling interval on the accuracy of network-level rutting surveys and the data processing time. The second part of this subsection assesses the data storage need when using the proposed procedure for network-level rutting condition assessment accuracy. The potential means to reduce the data storage needs are also recommended.

7.1.4.1 Sampling Interval and Network-level Rutting Condition Assessment Accuracy

To determine an adequate sampling interval that will not compromise the network-level rutting condition assessment accuracy, experimental tests were conducted

by comparing statistical indicators reported at other six sampling intervals, including 6 in., 1 ft, 3 ft, and 10 ft, 20 ft, and 100 ft, with those reported at 5 mm intervals. The statistical indicators, including mean, 60th percentile, standard deviation, and linear percentages of minor, low, medium, and severe rutting (as defined by PennDOT), were used as measures of network-level rutting condition. A 1-mile 3D range data collected from Benton Blvd. were selected for test because there were diverse rutting conditions available. The LWP rutting was relatively uniform and the RWP rutting was less uniform. The test results are shown in Table 7-6. As shown in the results, the statistical indicators, including mean, 60th percentile, and standard deviation, are insensitive to the sampling interval. Notable changes were only observed on linear percentages of minor and low severity levels of rutting when the sampling interval increased to 100 ft. More road sections need to be tested to obtain more conclusive results.

Table 7-6 Impact of Sampling Interval on Network-level Rutting Condition Assessment Accuracy

	Sampling Interval	5 mm	6 in	1 ft	3 ft	10 ft	20 ft	100 ft
Benton (LWP)	Mean (1/8 in)	1.7	1.7	1.7	1.7	1.7	1.7	1.7
	60th Prct (1/8 in)	1.8	1.8	1.8	1.8	1.8	1.8	1.9
	Std (1/8 in)	0.9	0.9	0.9	0.8	0.9	0.9	0.9
	Minor	68%	68%	68%	68%	67%	68%	64%
	Low	31%	31%	31%	31%	33%	31%	36%
	Medium	1%	1%	1%	1%	1%	1%	0%
	Severe	0%	0%	0%	0%	0%	0%	0%
Benton (RWP)	Mean (1/8 in)	2.1	2.1	2.1	2.1	2.1	2.1	2.1
	60th Prct (1/8 in)	2.0	2.0	2.0	2.0	2.0	2.1	2.0
	Std (1/8 in)	1.4	1.4	1.4	1.4	1.4	1.4	1.5
	Minor	60%	60%	60%	59%	60%	59%	60%
	Low	29%	28%	29%	28%	29%	30%	28%
	Medium	12%	12%	12%	12%	12%	11%	12%
	Severe	0%	0%	0%	0%	0%	0%	0%

7.1.4.2 Sampling Interval and Processing Time

To estimate the relationship between the sampling interval and the processing time (per mile), experimental tests were conducted on a computer with a Windows 7, 64-bit operating system that has i7 CPU @ 2.67 GHz and 12 GB RAM. Both road sections on SR 275 and Benton Blvd. were analyzed. For each case, 200 data files were tested. Each data file contained 1,000 transverse profiles collected from a 4-m wide and 5-m long road section at 5 mm intervals. Six sampling intervals, i.e., 5 mm, 50 mm (2 in.), 100 mm (4 in.), 150 mm (6 in.), 300 mm (1 ft), and 2.5 m, were analyzed. Two of those intervals, i.e., 150 mm and 300 mm, have been used by state transportation agencies, including ODOT and KDOT.

The test results, as shown in Table 7-7 and Figure 7-7, indicate that the processing times for data from either SR 275 or Benton Blvd. are similar. This means that the processing time is not impacted by the amount of cracking on the pavement surface. Additionally, the processing time per mile decreases significantly when the sampling interval increases from 5 mm to 50 mm, and, then, go flat gradually when the sampling interval increases from 50 mm to 2.5 m. The time needed to process 1-mile data becomes less than 0.1 hour if the sampling interval is 100 mm or greater. There may be some I/O processes, e.g., reading the input and writing the output, which cannot be saved by increasing the sampling interval. If the sampling interval is 1 ft, within one hour, 13 miles of data can be processed and rut depth values can be obtained.

Table 7-7 Sampling Interval versus Processing Time

Sampling Interval (mm)		5	50	100	150	300	2500
Processing Time per Mile (hour)	SR 275	0.65	0.12	0.1	0.09	0.08	0.07
	Benton	0.65	0.13	0.1	0.09	0.08	0.07
Processed Data per Hour (mile)	SR 275	1.5	8.4	10.5	11.4	12.9	14.7
	Benton	1.5	7.8	10.2	11.4	13.1	14.8

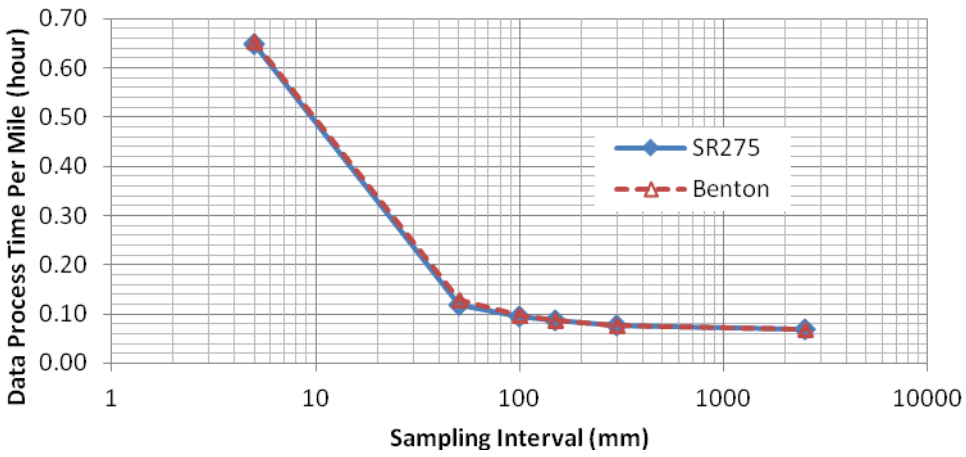

Figure 7-7 Sampling interval versus data processing speed (mile/hour)

7.1.4.3 Aggregation Interval and Network-level Survey Accuracy

According to a literature review of state DOTs' survey practices, most state DOTs use 0.1 mile as the aggregation interval when processing the automatically collected rutting data. This subsection estimates the relationship between the aggregation interval and the network-level rutting survey accuracy. Experimental tests were conducted using the data collected from SR 275 and Benton Blvd. The rutting data was aggregated into 0.1 mile and 1 mile, respectively. The results indicate that there is significant variation within the 0.1 mile for data collected from Benton Blvd., as shown in Figure 7-8; the rutting condition on SR 275, shown in Figure 7-9, is relatively uniform. It is suggested that when the standard deviation is high, e.g., greater than 2 (of 1/8 in.), the aggregation into 1 mile will lose significant details. A smaller aggregation interval is more appropriate for road sections with large variation. Ultimately, segments with uniform rutting condition will be identified and aggregating to the homogeneous segments is a meaningful and effective way to store rutting information.

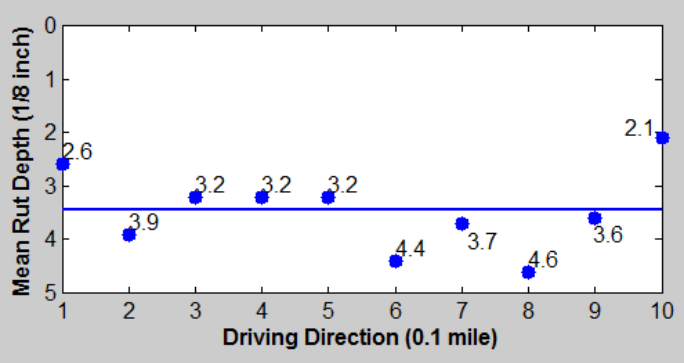

Figure 7-8 Aggregated rut depths at 0.1 mile intervals (Benton Blvd. LWP, std = 1.6 of 1/8 in.)

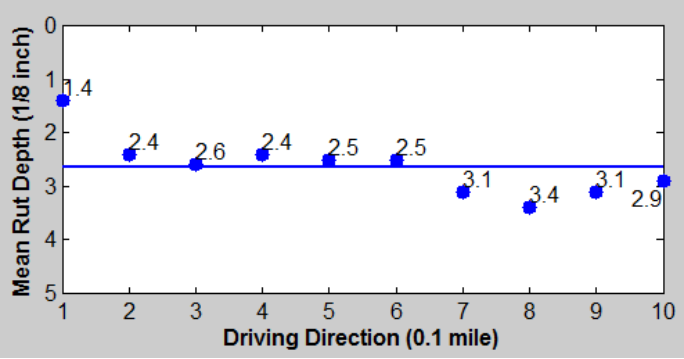

Figure 7-9 Aggregated rut depths at 0.1 mile intervals (SR 275 MP0-1 RWP, std = 0.5 of 1/8 in.)

7.1.4.4 Data Storage Need

According to Table 7-8, a significant amount of hard disk space is required to store the raw data, i.e., 3D continuous transverse profiles. If surveying the 18,000 centerline miles of highway maintained by GDOT, at least 33.0 TB (=18000 miles / 100 miles * 94 GB * 2 lanes) hard disk storage per year is needed. Thus, storing the raw data will demand tremendous hard disk storage. Besides, an extra effort will be required to manage and maintain the huge amount of data. Therefore, storing all the raw data is not recommended; instead, it is recommended to store the processed results.

The processed results, including the rutting measurements such as rut depth and width at a specified interval, from the raw data are stored in XML files. The storage need

for XML files is 4.2 TB for 18,000 lane miles of highway when the sampling interval is 5 mm. The data storage need is 13% of the need to store all the 3D raw data. The XML files can be read to obtain longitudinal rut depth profiles. Thereby, the storage need for longitudinal rut depth profiles is further reduced. It is assumed that each rut depth value requires 4 bytes of storage space. A total of 85.8 GB (=18000 miles * 1600 m/miles * 1000 mm/m / 5 mm * 2 WP * 2 lanes * 4 bytes) disk storage is needed per year. Up to this point, the data storage need has been reduced by around 99.7%. In the future, this storage need can be further reduced by aggregating and reporting rut depth into bigger intervals.

Table 7-8 Data Storage Need per Inspection for Every 100-Lanemile of the Highway Network

Sampling interval	Raw data	XML files	Longitudinal rut depth profiles
5 mm	94 GB (3 MB / 5 m)	11.9 GB (390 KB / 5 m)	250 MB (8 KB / 5 m)

7.1.5 Discussions

Several issues have been identified during the tests. They are listed as follows:

- Issue of half-lane rut depth calculation

Currently, rut depths were calculated for half-lane transverse profiles. An assumption is made that the rut shape is symmetrical to the center line. However, this assumption may not hold, and the rut depth for some cases may be underestimated. Figure 7-10 shows such an example. Figure 7-10(a) is the half-lane profile collected by the left sensor and Figure 7-10(b) is the one by the right sensor. As shown in Figure 7-10, the hump in the middle was captured by the left sensor and not the right sensor. Therefore, the rut depth for the RWP can be underestimated if it is calculated using the right half-lane profile only. There is a need to combine the left and right half-lane profiles to obtain full-lane profiles for rutting condition assessment.

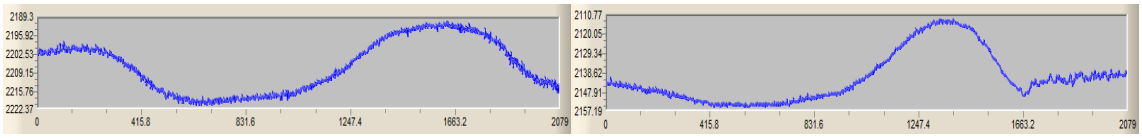

(a) Left profile (b) Right profile

Figure 7-10 Issue of half-lane rut depth calculation

- Issue of lane marking detection

In the 3D line laser system, the lane marking detection is performed on fixed-length road sections. Each of such road section is 5m long for this study, and only the portion of transverse profile between the lane markings is used for rut depth calculation. Thus, it is crucial to accurately detect lane markings. However, current software provided by the 3D line laser system manufacture is not robust enough to correctly detect lane markings for all road sections. An example is given in Figure 7-11, which shows the lane marking detection results for three adjacent road sections, S1, S2, and S3. The purple straight lines in Figure 7-11 are the detected lane markings. Compared to S1 and S3, S2's detected lane markings shift upward significantly. This shift causes abrupt changes of rut depth and rut width at boundaries between adjacent sections, as shown in Figure 7-12. This may potentially impact the accuracy of rut depth and width measurements. The lane marking detection method can be enhanced by using neighboring road sections' lane marking detection results to make a more accurate estimation of the lane making locations in current road section.

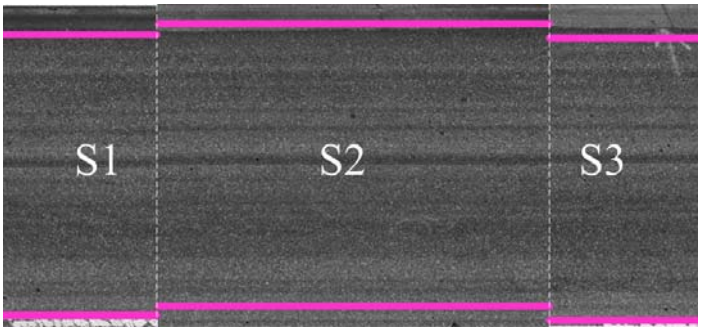

Figure 7-11 Lane marking detection results

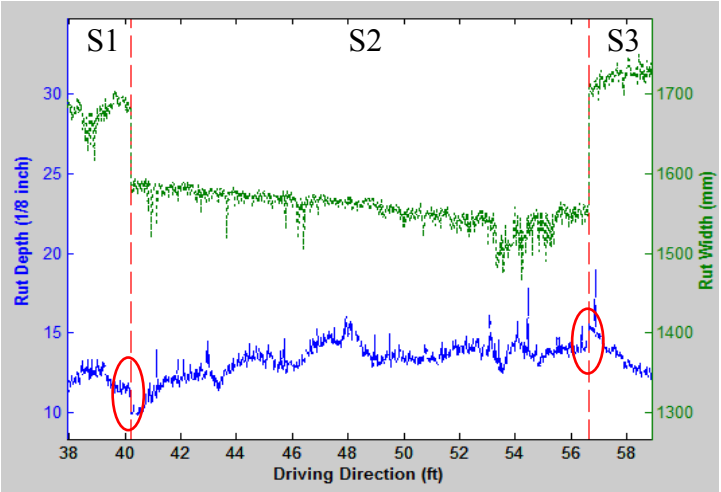

Figure 7-12 Issue of lane marking detection

- Issue of rut depth calculation in the presence of other distresses (e.g., cracking) or other objects

A detailed examination of this issue has been presented in Section 6.1. It is concluded that the current 3D line laser system software provided by the manufacture could not provide accurate rut depth calculation when rutting is accompanied with non-rutting features, such as transverse cracks, potholes and patches, raised pavement markers, rail tracks, and other objects (e.g., tree branches on the road). This is because of the lack of robust and efficient methods to detect and remove these non-rutting features.

7.2 Project-level Isolated Rut Detection

This section presents a case study on I-95 near Savannah, Georgia, to demonstrate the feasibility of the automated isolated rut detection method proposed in Chapter 6. The southbound lane of I-95 from MP 101 to MP 100 was selected as a test section. Figure 7-13 shows the location of the test section.

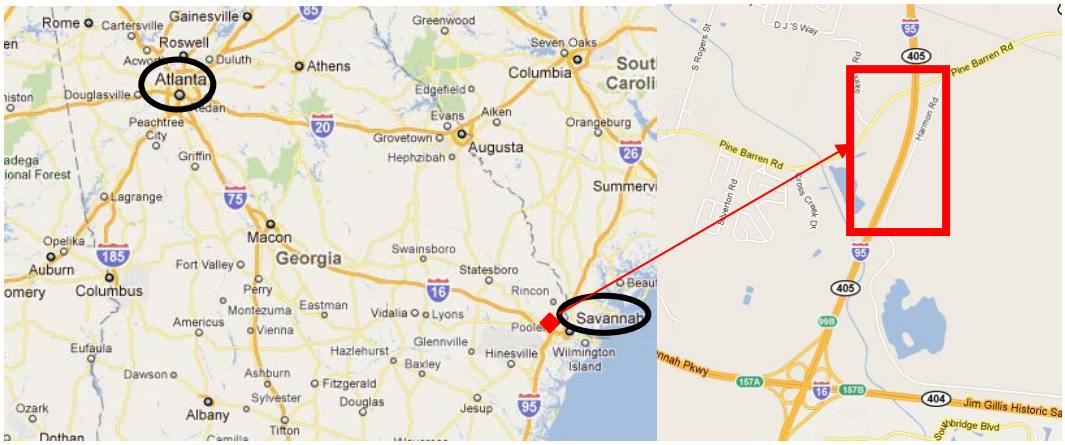

Figure 7-13 Location of the test section on I-95

7.2.1 Test Results

The longitudinal rut depth profile, i.e., the distribution of rut depths in the driving direction, for the LWP is the blue line shown in Figure 7-14. The total length of this profile is 5,350 ft, slightly longer than 5,280 ft (1 mile). This results from the difference between the DMI reading and the actual roadway section length. The threshold-based outlier removal method was used to remove outliers (i.e., abnormally higher and lower values) in the longitudinal rut depth profile. A zoom-in view of outliers between 1410 ft and 1420 ft is shown in Figure 7-15. The red profile is the filtered longitudinal rut depth profile. As shown in Figure 7-14, the outliers in the blue profile were successfully filtered out.

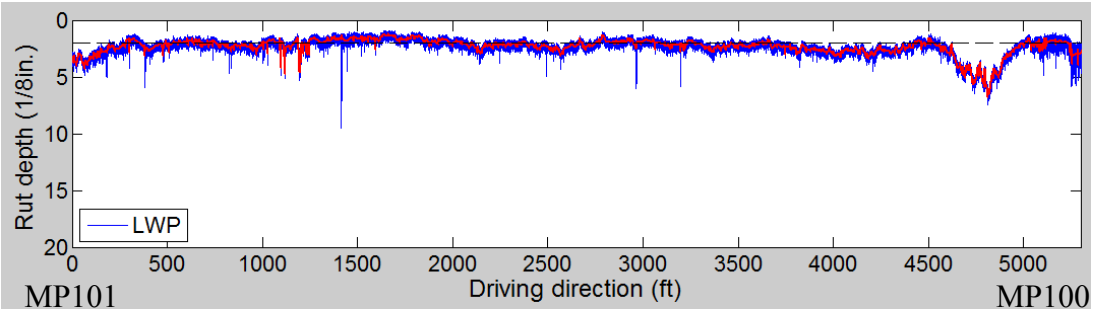

Figure 7-14 Raw longitudinal rut depth profile (blue) and filtered profile (red)

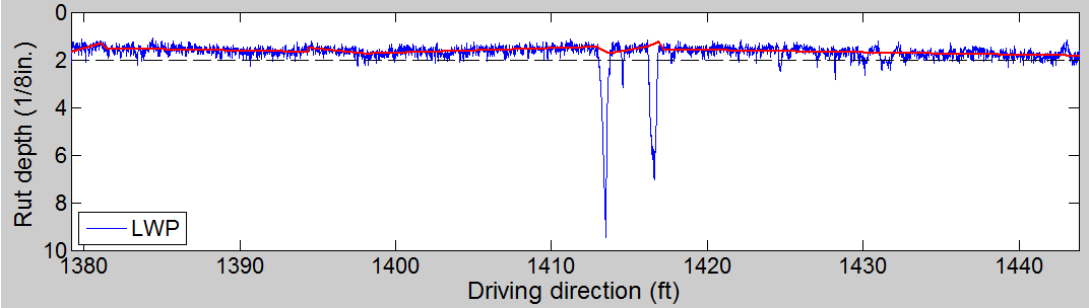

Figure 7-15 Raw longitudinal rut depth profile (blue) and filtered profile (red)

Figure 7-16 and Table 7-9 summarizes the homogeneous segmentation results, obtained when setting the minimum segment length, i.e., MinLen, as 10 ft, and the minimum mean rut depth difference, MinDiff, as 1/8 in. Each break point on the red profile corresponds to the bound between two adjacent homogeneous segments. The values of those red line segments are the mean rut depth for each homogeneous segment. As shown in Figure 7-16, the homogeneous segmentation method has successfully captured every point at which the pavement rutting condition changes significantly. Table 7-9 tabulates the first 10 homogeneous segments, including the MP, start DMI, end DMI, length, mean rut depth, and standard deviation. This table can be saved into databases and used to support project-level pavement management.

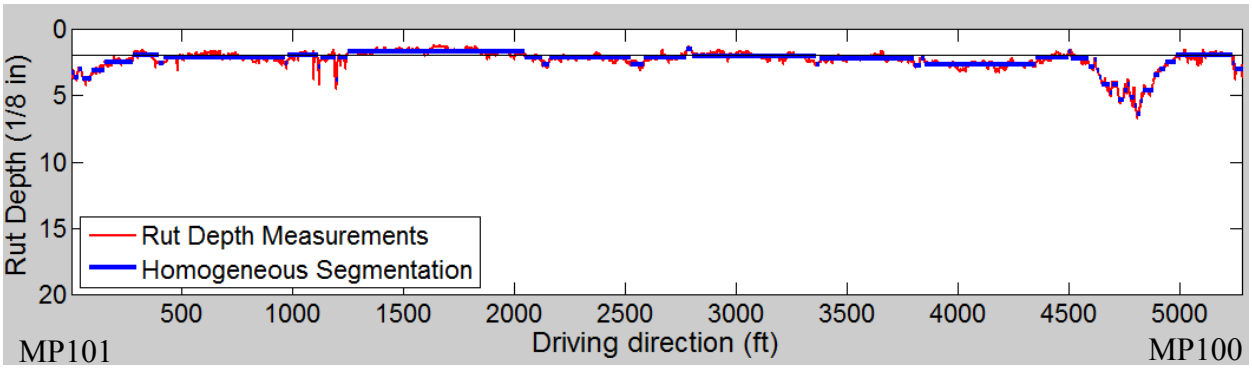

Figure 7-16 Homogeneous segmentation results (MinLen = 10 ft and MinDiff = 1/8 in)

Figure 7-17 and Table 7-10 show the isolated rut detection results. Two isolated ruts are detected (labeled as 1 and 2 in Figure 7-17). One is 282 ft long (from 1 ft to 283 ft) and the other one is 481 feet long (from 4,501 ft to 4,982 ft). The maximum rut depth

is greater than 1/4 in. for both of them. The rut volume for these isolated ruts is 24 ft^3 and 51 ft^3, respectively.

Table 7-9 Homogeneous Segmentation Results (I-95)

Record #	Start MP (mile)	Start DMI (ft)	End DMI (ft)	Length (ft)	Mean Rut Depth (1/8 in)	Std (1/8 in)
1	101.0	1	16	15	3.3	0.2
2	101.0	16	33	17	3.6	0.2
3	101.0	33	53	20	3.0	0.2
4	101.0	53	95	42	3.7	0.2
5	101.0	95	153	58	3.1	0.2
6	101.0	153	283	130	2.5	0.2
7	100.9	283	398	115	2.0	0.3
8	100.9	398	418	20	2.6	0.1
9	100.9	418	965	547	2.1	0.2
10	100.8	965	980	15	2.6	0.2

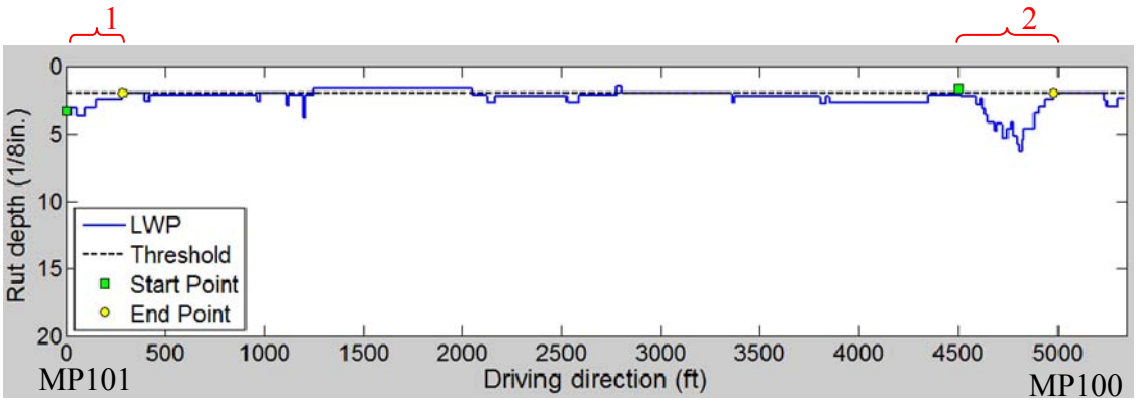

Figure 7-17 Detected isolated ruts using the homogeneous segments

Table 7-10 Isolated Rut Detection Results (I-95)

Record #	Start MP (mile)	Start DMI (ft)	End DMI (ft)	Rut Length (ft)	Max Rut Depth (1/8 in)	Rut Volume (ft^3)
1	101.0	1	283	282	3.7	24
2	100.2	4501	4982	481	6.4	51

7.2.2 Field Verification

A site visit was conducted to confirm that the majority of this road section exhibits no major rutting problem, and there were only two isolated ruts, one of which is shown in Figure 7-18(b). During the site visit, it was found that the isolated ruts are difficult to locate through the manual survey. In contrast, the proposed isolated rut detection method is capable of automatically locating spots with major rutting problems that could potentially lead to hydroplaning problems for the whole roadway network. Therefore, it is very valuable and may substantially improve existing survey and pavement maintenance practices.

(a) Roadway environment (b) Isolated rut

Figure 7-18 Isolated rut verification in the field (I-95)

7.2.3 Summary

This section has presented another application: detection of isolated ruts. A method was proposed to automatically determine the termini of isolated ruts using the 3D line laser system. In addition, the proposed method can also compute the rut length, maximum rut depth, and rut volume. A road section from MP 101 to MP 100 on southbound lanes of I-95 was selected for case study. The case study results show that two isolated ruts on the test section were detected successfully, which demonstrates the feasibility of the proposed method. In the future, more data need to be collected to validate the performance of the proposed method in a network-wide survey.

7.3 Observation of Rutting Progression Behavior

The advanced sensing technology can provide rich high-quality measurements of pavement rutting distress and, therefore, can potentially be used to improve pavement rutting progression modeling. The objective of this section is to assess the feasibility of improving pavement rutting progression modeling using the 3D line laser system. Since the time duration was short, a roadway section with alligator cracking was purposely selected as case study to evaluate whether the 3D line laser system can capture the accelerated rutting progression behavior. Case study results are presented in this section.

7.3.1 Case Study – SR 26

The data collected from SR 26 on November 10, 2010, and March 21, 2012, was analyzed as a case study. The distributions of derived RWP rut depths in the driving direction are plotted in Figure 7-19. As shown in Figure 7-19, the pavement rutting within this 1200-ft road section propagated differently. For the majority of this section, the rut depth remains unchanged. However, the mean rut depth increased by 1.5 and 1.1 (1/8 in.) per year, i.e., 4.8 mm and 3.6 mm per year, respectively, for two isolated sections, one is from 280 ft to 540 ft and the other one is from 700 ft to 800 ft.

It is highly possible that this high rutting propagation rate results from base layer failure. As shown in the 2D intensity data in Figure 7-20 (a), white stains, which are fine aggregates coming from the graded aggregate base (GAB) layer through cracks, were present on the pavement surface. The presence of white stains is a strong indication that the upper asphalt layer had been cracked and the base layer had been damaged by November 2010. Because of the damaged base layer, the rut depth propagated at a high rate from November 2010 to March 2012. A second review of the 3D range data collected from this 1200-ft roadway section verifies that only the two short sections with white stains are exhibiting accelerated rutting.

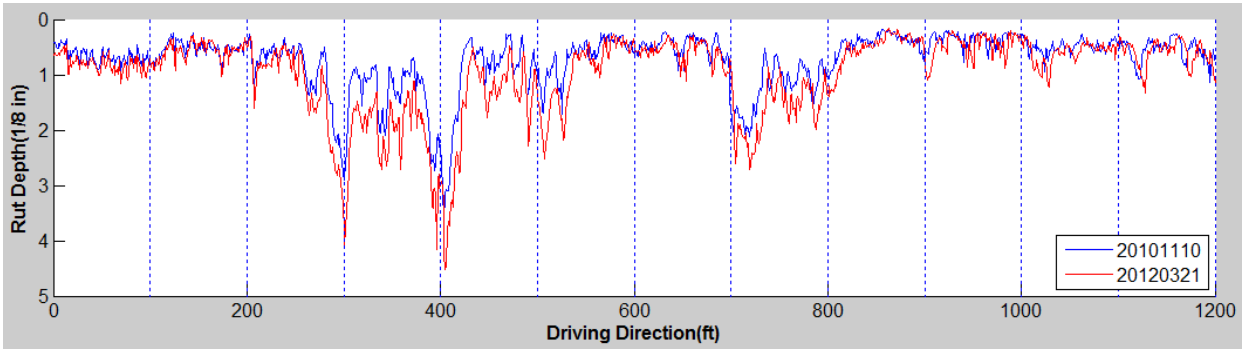

Figure 7-19 Rut depth distribution on SR 26 for RWP

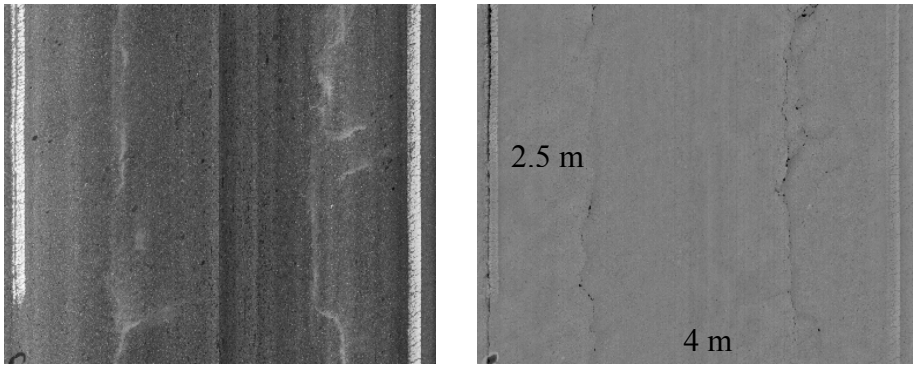

(a) Intensity data (b) Range data

Figure 7-20 Rut depth distribution on SR 26 for RWP (November 2010)

Table 7-11 Rut Depth Measurements for Two Isolated Sections

Section (ft)		Mean (1/8 in)	60th Prct (1/8 in)	99th Prct (1/8 in)
280-540	20101110	3.9	3.6	10.3
	20120321	5.9	6.0	13.6
	Increment (per year)	1.5	1.8	2.5
700-800	20101110	3.6	3.7	6.8
	20120321	5.1	5.3	8.7
	Increment (per year)	1.1	1.2	1.4

7.3.3 Summary

This section presents an assessment of the feasibility of modeling pavement rutting progression using the emerging 3D line laser imaging technology. A short road

sections on SR 26 was selected for case study. The case study shows the following results:

- The rich 3D data enables researchers to study the detailed behavior of rutting progression. Because of its high-resolution, the 3D line laser system can potentially be used to more accurately identify 1D rut depth and 2D rut shape change and to more reliably model the rutting progression behavior. There is a good potential to establish a reliable sensor-based rut progression model.
- It is observed clearly that the rutting progression does not occur uniformly across the test sections. Rutting on two isolated sections with potential base layer failure was propagating at a much higher rate. There is a need to consider the inherent heterogeneity that can be readily observed using sensing technology to support the development of a sensor-based and more reliable rut progression model.

7.4 Summary

This chapter presents case studies on an interstate highway (I-95), state routes (SR 275 and SR 67), and a city road (Benton Blvd.) to demonstrate the applicability of using the 3D line laser system for network-level rutting condition survey and isolated rut detection as proposed in Chapter 6. Additionally, a case study was carried out on SR 26 to observe the rutting progression behavior captured using the 3D line laser system and explore the potential benefits of using the 3D line laser system to improve rutting progression modeling. The following are the major findings:

- Case studies on one interstate highway (I-95), two state routes (SR 275 and SR 67), and one city road (Benton Blvd.) show that the detailed rutting information (e.g., minimum, maximum, standard deviation in one mile), in addition to the mean rut depth, can be derived utilizing the 3D range data collected using the 3D line laser system. This information can better support maintenance decision making at the network-level. The 60th percentile rut depth is recommended by

GDOT pavement engineers as an indicator of the representative rut depth measurement in one mile.

- The case study on I-95 demonstrates that the proposed method can feasibly be used to process 3D range data and detect isolated ruts in support of low-cost, localized treatment. In addition, the method can also compute the rut length, maximum rut depth, and rut volume.
- Case studies on SR 26 disclose the potential benefits of utilizing the 3D line laser system in improving pavement rutting progression modeling. The benefits are two-fold: (1) the rich 3D data enables researchers to study the detailed rutting progression behavior; (2) the heterogeneity of rutting progression, which needs to be considered when modeling the rutting progression, can be captured using the 3D line laser system. Because of these benefits, there is a good potential to establish a reliable sensor-based rutting progression model in the future.

CHAPTER 8 CONCLUSIONS AND RECOMMENDATIONS

Pavement rutting is one of the major asphalt pavement surface distresses affecting pavement structure integrity and driving safety and is also a required performance measure specified in the Highway Performance Monitoring System (HPMS). Manual rutting measurement method is still used by many state Departments of Transportation (DOTs), like Georgia DOT; however, it is time-consuming, labor-intensive, and dangerous. Although point-based rut bar systems have been developed and utilized by state DOTs to measure rutting conditions, they often underestimate rut depth measurements. There is an urgent need to develop an automated method to accurately and reliably measure rutting conditions. With the advance of sensing technology, emerging 3D line laser imaging technology is capable of collecting high-resolution 3D range data at highway speed (e.g., 100 km/h). Research is needed to develop methodologies using this advanced sensing technology to 1) process 3D range data, 2) automatically extract 1D rut depth measurements and 2D/3D rutting characteristics, 3) assess the accuracy and repeatability of rutting measurements, 4) explore more detailed information to support current and future pavement management decisions, e.g., network-level condition assessment and project-level isolated rut detection. This chapter summarizes the major contributions, findings, and recommendations for future research.

8.1 Contributions

The contributions of this research are the following:

- A methodology was, for the first time, proposed to use the high-resolution 3D line laser imaging technology, location reference technology, optimization programming techniques, statistical analyses methods, and GIS technology, to support both current and future network-level and project-level pavement rutting

condition assessment practices. The proposed methodology consists of six modules: data acquisition, data processing, data segmentation, statistical analysis, data visualization, and decision support. The proposed methodology is substantiated with a series of new methods and procedures.

- A threshold-based outlier removal method employing the multivariate adaptive regression splines (MARS) technique was proposed to remove outliers in the rut depth measurements based on the observation that the slopes of isolated ruts are relatively smaller than those of outliers caused by non-rutting features, such as transverse cracks, potholes, raised pavement markers, and rail tracks.
- A modified topological-ordering-based segment clustering (MTOSC) method was proposed to optimally partition the continuous roadway network into segments with uniform rutting condition to enable pavement engineers to apply a cost-effective treatment to each uniform segment. The proposed method also provides the flexibility to incorporate engineering considerations, including the minimum segment length and minimum mean difference between neighboring segments.
- An overlapping-reducing heuristic method was proposed to solve large-scale segmentation problems by reducing the overlap between two successive segments.
- A network-level rutting condition assessment procedure was proposed to report the pavement rutting condition and the statistical information in support of network-level pavement management decisions. Besides removing outliers, this procedure includes these two crucial steps. First, a practical method is proposed to translate the DMI-measured location reference into the milepost-based linear referencing used in GDOT's network-level survey practices. Second, a representative rutting condition (60^{th} percentile of rut depths as recommended by GODT pavement engineers) for each 1-mile segment is reported and additional

statistical indicators, including maximum rut depth, standard deviation, and maximum rut density, are also provided to enable GDOT engineers to better assess rutting condition and make more informed decisions at the network-level.

- An automated isolated rut detection method was proposed to determine the termini of isolated ruts using the 3D range data collected by the 3D line laser system. The proposed method incorporates pavement engineers' knowledge, including adequate length and depth of an isolated rut, for establishing meaningful criteria for isolated rut detection.
- Comprehensive laboratory and field tests were conducted to validate the accuracy and repeatability of 1D rut depth obtained using the 3D line laser system. Experimental tests were also conducted in the laboratory to validate the accuracy of 3D rut volume measurement.
- Case studies on one interstate highway (I-95), two state routes (SR 275 and SR 67), and one city road (Benton Blvd.) were conducted to demonstrate the capability of the proposed methods and procedures, including the outlier removal method, the homogeneous segmentation method, the overlapping-reducing heuristic method, the network-level rutting condition assessment procedure, and isolated rut detection method.
- The rut depth measurement errors of the commonly used point-based rut bar systems were quantitatively assessed by down-sampling the reference transverse profiles acquired using a 3D line laser system.

8.2 Findings

A methodology was for the first time proposed in this research using the emerging 3D line laser imaging technology to improve existing 1D rut depth measurement accuracy and repeatability and to measure additional 2D and 3D characteristics.

Experimental tests were carried out to validate the accuracy and repeatability of rutting measurements, including rut depth, rut length, and rut volume, using the 3D line laser system. Methods and procedures were proposed to utilize the rutting measurements in support of both network-level and project-level pavement management decisions. Here is a summary of findings.

- **The 3D line laser system is capable of providing quality 3D range data consistently for the majority of pavement surfaces.**

  Experimental tests in the laboratory show that the standard deviation of range measurement uncertainties (also known as 3D noises) in the 3D range data is around 0.43 mm for objects with uniform intensity. This is consistent with the specification of the 3D line laser system that the depth measurement accuracy is 0.5 mm.

  Irregular data, including missing points and unseemly points, were observed in the 3D range data. Missing points occur when the pavement surface gets out of the measurement range of the 3D line laser system, when the pavement surface is occluded, or when the laser line on the CCD sensor is dim. Unseemly points are possibly caused by reflective components present on asphalt pavement surfaces. Nevertheless, they are only a small group of data and, consequently, have minimal impact on the quality of the 3D range data.

- **The 3D line laser system is promising in delivering accurate and repeatable measurements of the rut depth, rut length, and rut volume for the majority of a roadway network.**

  Both laboratory and field tests show that the 3D line laser system can provide satisfactorily accurate rut depth measurements. The absolute difference between DCT-method-measured rut depths and the ground truth varies from 0.0

mm to 2.1 mm, which meets the rut depth measurement requirement (i.e., +/-3 mm) for multiple transportation agencies (ADOT 2002, McGhee 2004).

Laboratory and field tests also show that the 3D line laser system can provide rut depth measurements with high repeatability and reproducibility for roadways with both lane markings in fine condition. According to the laboratory test, the standard deviation of rut depths collected repeatedly for 2,000 times is no more than 0.3 mm. According to the field test, the median of standard deviations of rut depths collected repeatedly at the same location ranges from 0.1 mm to 0.5 mm. In addition, the 3D line laser system has a high reproducibility across different surveyors. The cross-correlation of rut depth profiles collected by two different surveyors for the test section is 0.983 and 0.997 for the LWP and RWP, respectively. The tests also reveal that the 3D line laser system has a better repeatability on interstate highways.

A laboratory test on a regular bowl shows that the relative rut length and rut volume measurement error is around 3.1% and 3.8%, respectively, which is satisfatory for engineering use.

- **The commonly used 3-point and 5-point rut bar systems can underestimate the rut depth as much as 51% and 64%.**

The high-resolution 3D range data acquired using the emerging 3D line laser system was first used to assess the rut depth measurement error of point-based rut bar systems. The quantitative assessment results show that for point-based rut bar systems (with the number of sensors varying from 3 to 31), the relative rut depth measurement error generally decreases with the increasing number of laser sensors. However, the trend is unclear for rut bar systems with fewer sensors because in these cases the rut shape affects rut depth measurement error more than the number of sensors. Thus, a 3-point rut bar system could

outperform a 5-point system occasionally. The test results also show that the commonly used 3-point and 5-point rut bar systems can underestimate the rut depth significantly. The relative rut depth measurement error for a 3-point and a 5-point rut bar system varies from 16% to 51% and from 22% to 64%, respectively. The relative measurement error consistently drops under 10%, only when the number of sensors is greater than 29.

- **The proposed homogeneous segmentation method can provide the optimal homogeneous rutting segments. The overlapping-reducing heuristic method can be used to effectively solve large-scale problems.**

  Experimental tests show that the homogeneous segmentation method, MTOSC, provides the optimal homogeneous segmentations successfully for all 200 synthetic datasets. It is promising to be used as a benchmarking standard for quantitatively assessing the accuracy of heuristic or approximation methods. In addition, the proposed MTOSC method has the following advantages. First, the method provides the flexibility of adjusting the minimum difference and minimum section length constraints to take into account the important engineering considerations. Second, it does not make any assumption on the distribution of the input data, such as the Cox distribution (Mishalani and Koutsopoulos 2002) or normal distribution (Thomas 2005). The method can also be applied to the determination of homogeneous pavement condition segments of other distress types or an overall rating.

  The overlapping-reducing method, which allows less overlap between two successive segments, is tested using both small-scale and large-scale synthetic datasets, as well as a real dataset from I-95. Test results show that as the overlap between two successive segments decreases, the processing time decreases exponentially at a cost of increasing accumulative segmentation error. Sensitivity

study shows that when the overlap between two successive segments is 90%, the method can significantly shorten the processing time and do not compromise much of the segmentation accuracy. The test results on a real dataset are intuitively reasonable which demonstrates the applicability of the MTOSC and heuristic method in real-world problems.

In addition, the proposed segmentation methods can be used to effectively store only meaningful rutting information, e.g., the beginning and ending of homogeneous segments. Thus, it can reduce the data storage need.

- **The proposed network-level rutting condition assessment procedure utilizing a 3D line laser system can be feasibly used to support network-level pavement rutting condition survey.**

  Case studies on one interstate highway (I-95), two state routes (SR 275 and SR 67), and one city road (Benton Blvd.) show that the detailed rutting information (e.g., minimum, maximum, standard deviation in one mile), in addition to the mean rut depth, can be derived from the 3D range data collected using the 3D line laser system. This information can better support maintenance decision making at the network-level. The 60th percentile rut depth is recommended by GDOT pavement engineers as an indicator of the representative rut depth measurement in one mile for the network-level survey.

- **The proposed isolated rut detection method utilizing a 3D line laser system can be feasibly used to detect isolated ruts in support of low-cost, localized treatment.**

  A case study on I-95 demonstrates that the proposed method using a 3D line laser system can be feasibly used to determine the termini of isolated ruts. Besides, the method can also compute additional rutting information, including maximum rut depth, rut length, and rut volume.

- **The 3D line laser system can potentially be used to develop a reliable sensor-based rutting progression model.**

  Case studies on SR 26 disclose the potential benefits of utilizing the 3D line laser system in improving pavement rutting progression modeling. The benefits are two folds: (1) the rich 3D data enables researchers to study the detailed rutting progression behavior; (2) the heterogeneity of rutting progression, which needs to be considered when modeling the rutting progression, can be captured using the 3D line laser system. Because of these benefits, there is a good potential to establish a reliable sensor-based rutting progression model in the future.

8.3 Recommendations for Future Work

In the future, the following studies are recommended:

- More thorough experimental tests and studies are recommended to improve the understanding about the noises in the 3D range data and to propose methods to effectively remove these noises.
- Although the transverse-profile-level rut depth calculation works well for the majority of a roadway network, it may not work well when there are wide transverse cracks and potholes. There is a need to develop methods to remove these non-rutting features for deriving accurate rut depth measurements.
- An enhanced lane marking detection method is needed to handle road sections with lane marking in poor condition or partially missing. For example, the lane marking detection method can be enhanced by using neighboring road sections' lane marking detection results to make a more accurate estimation of the lane making locations in current road section.

- A method is needed to combine two 2-m half-lane transverse profiles from the left and right profiling sensors to obtain a 4-m full-lane transverse profile to improve rut depth measurement accuracy, especially when the rut shapes are not symmetrical.
- Methods are needed to speed up current rut depth computation method, especially when processing network-level overwhelmed 3D range data. It is estimated that current method can process approximately 13 miles of data collected at 1-ft sampling interval every hour, and would require 1,385 hours to process the whole network, e.g. 18,000 center-line miles maintained by GDOT. Parallel processing is a promising method that may be applied to improve the processing speed, since the roadway network can be broken down into smaller segments that can be processed independently.
- Besides 1D rut depth measurements, the 2D and 3D measurements of rutting, e.g., rut shape, can be explored in the future to take advantage of the granularity of the 3D range data. The relationships between 2D or 3D rutting characteristics and the occurrence of accidents can be studied. For example, the transition areas (e.g., from minor to severe rutting) could be the areas with potential safety concern, especially in rainy season, and they can be quantitatively studied with the high-resolution 3D range data. The study will suggest what type of transition areas are potential black spots.
- The proposed MTOSC homogeneous segmentation method does not handle the case shown in Figure 8-1 with an extremely high rut depth measurement. In the future, the proposed MTOSC method can be enhanced by incorporating an additional constraint, such as setting a limit on the change of rut depths within a homogeneous segment or setting a limit on the variation of rut depths within a homogeneous segment.

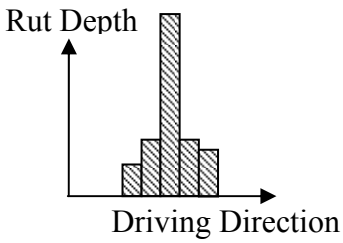

Figure 8-1 A Segment with an extremely high rut depth measurement

- Further study is recommended to spatially integrate the detected rutting on the left and right wheel paths to determine meaningful units for various maintenance activities, such as deep patching, milling, and leveling. Proper criteria considering spatial characteristics, such as gap and overlap between detected rutting, as shown in Figure 8-2, need to be studied. For example, in Figure 8-2(a), the isolated ruts A and B may be combined into a single one that lies between the two dashed lines, since they are partially overlapped with each other. In Figure 8-2(b), although the isolated rut A on the left wheel path is not overlapped with the isolated rut B on the right wheel path, they may be combined into a single isolated rut if the "gap" between these two isolated ruts is relatively small. A proper "gap" needs to be determined based on state DOTs' operations.

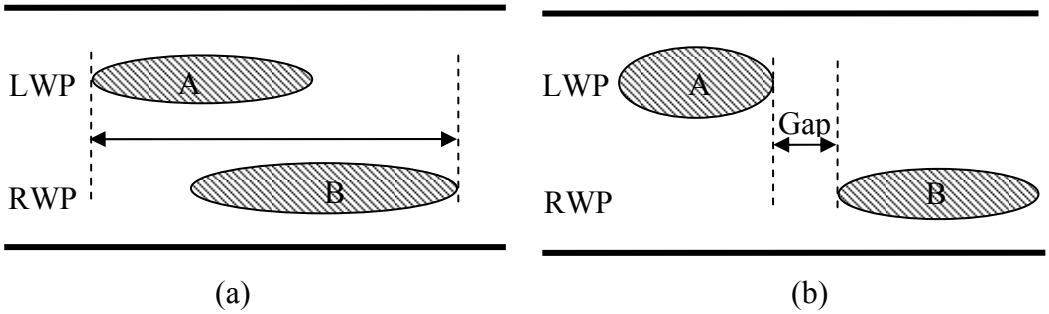

Figure 8-2 Spatial characteristics of isolated ruts

- Current rut volume calculation method, as shown in Figure 8-3(a), only considered the rut volume between the ridges of a rut. However, in practice, to estimate the quantity of materials that need to be removed and filled is complex

and not straightforward. For example, the moderate or severe ruts may be pre-leveled as shown in Figure 8-3(b) in advance of the overlay. Under this case, the shadowed area "V2" needs to be used to estimate the rut filling material needs. Asphalt pavements with severe rutting may need to be milled to certain depth as shown in Figure 8-3(c) before overlay. Methods can be developed in the future to use the 3D contour of pavement surface to more accurately estimate the resurfacing quantities based on actual milling and overlay practices.

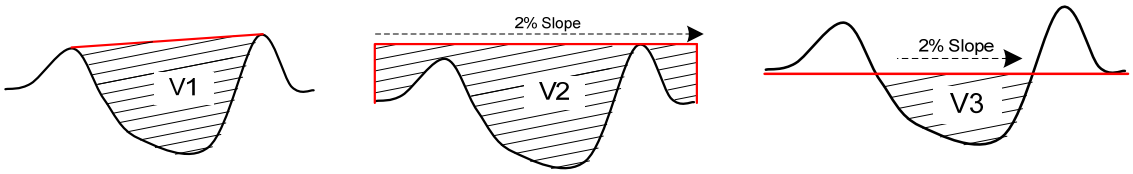

(a) Current rut volume calculation

(b) Estimation of rut filling material needs

(c) Estimation of mill-and-inlay material quantities

Figure 8-3 Rut volume calculation

- An intelligent, sensor-based distress causal factor diagnosis and treatment determination system can be developed by spatially integrating derived rutting measurements with other pavement surface distresses (e.g., alligator cracking). For example, an isolated severe rutting accompanied with severe alligator cracking may be a strong indication of base failure and a deep base patching is needed.
- An effort is needed to integrate the 3D line laser system and an IMU, so that the position change of the 3D line laser system can be detected; the increase in the 3D range data because of lifted profilers will not be "wrongly" recognized as a depression in the road surface; and true 3D pavement surface can be established in the presence of speeding bumps.
- Although this research focuses on rutting, the proposed sensor-based and spatial-enabled methodology using the 3D sensing technology and GIS technology can

be extended to measure, characterize, and integrate other types of pavement surface distresses. For example, the proposed methodology can be extended to cracking. In the data processing module, cracking will be measured using the high-resolution 3D pavement surface data collected using the 3D sensing technology. The crack measurements, as well as rutting measurements, can be registered into the same location referencing system. In the data segmentation module, the rutting and cracking measurements can be partitioned into segments with relatively uniform rutting and cracking conditions, as shown in Figure 8-4, to support cause diagnosis and project-level maintenance operations. The clustered measurements can also be analyzed in the statistical analysis module to assess the network-level pavement rutting and cracking conditions. Both the project-level and network-level pavement rutting and cracking conditions can be visualized on GIS maps in support of an intuitive and efficient way for pavement management decision making. Finally, applications will be developed in the decision support module to support pavement management decisions, e.g., detection of isolated spots with severe rutting and cracking problems.

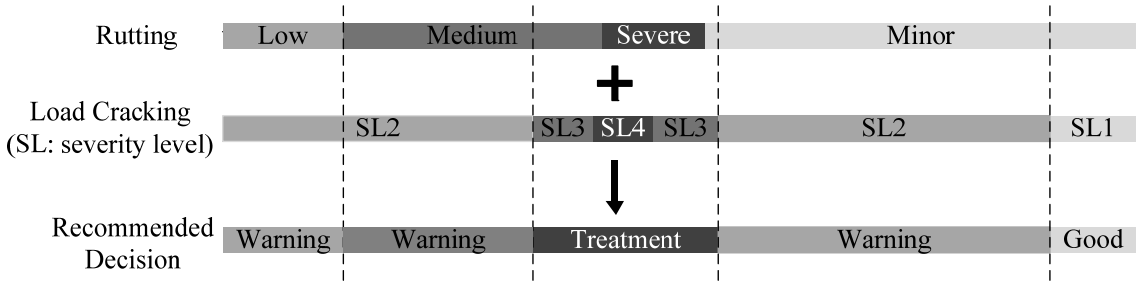

Figure 8-4 Diagnosis of causal factors and treatment determination at project level

APPENDIX A: EXPERIMENTAL TESTS ON HOMOGENEOUS SEGMENTATION METHODS

To assess the validity of the proposed homogenous segmentation method, MTOSC, and the overlapping-reducing heuristic method, experimental tests were conducted and are presented in this appendix.

A.1 Experimental Tests on MTOSC

In this section, the MTOSC was tested using synthetic datasets. Two categories (large-variance and small-variance) of synthetic datasets with known optimal segmentation solutions were generated to validate the accuracy and robustness of the MTOSC. An indicator, the length-weighted sum of squared errors (SSE_p) suggested by Tejeda et al. (2008), was used as a quantitative measurement of the segmentation accuracy. It is a quantitative assessment of how much information is preserved after segmentation. The more information preserved, the smaller the SSE_p is. Its definition is shown in Equation (A-1):

$$SSE_p = \sum_{i=1}^{n} \frac{n_i \sum_{j=1}^{n_i} (r_j - \overline{r}_i)^2}{m} \tag{A-1}$$

where r_j is the rut depth measurement j in the segment i; $\overline{r}_i$ is the mean rut depth data for the homogeneous segment i; n_i is the number of rut depths within the segment i; and n is the total number of homogeneous segments.

The MTOSC was implemented in C language and compiled by Visual C++ 2008. All tests were run on a personal computer with Windows 7 Professional OS, 8.0G RAM, and an Intel Core i7 CPU with 2.13 GHz.

A.1.1 Tests on Synthetic Datasets

To validate the accuracy and robustness of the MTOSC, two categories (small and large data variances) of synthetic datasets, each with 100 random datasets, thus a total of 200 synthetic datasets, were generated and tested. The standard deviation of data within each homogeneous segment was set to be 0.1 mm and 0.5 mm for those two categories, respectively. Each dataset contained 600 rut depth measurements (m = 600). The optimal number of homogeneous segments was known, which was six (n = 6). The length of each of those six homogeneous segments was set to be 100 m, and their mean rut depths were 3, 4, 5, 7, 10, and 5 mm, respectively. Figure 3 shows one example dataset when the standard deviation is 0.5 mm. This level of data variance has blurred the boundary between homogeneous segments. The minimum segment length was set to be 50 m, and the minimum difference was 0.5 mm.

The test results show that the MTOSC solves all 200 synthetic datasets optimally. It also performs consistently across different levels of data variance. For cases with large data variance, such as the case shown in Figure A-5, it is challenging for human eyes to see the partition points correctly. However, the MTOSC succeeded in partitioning it into 6 homogeneous segments.

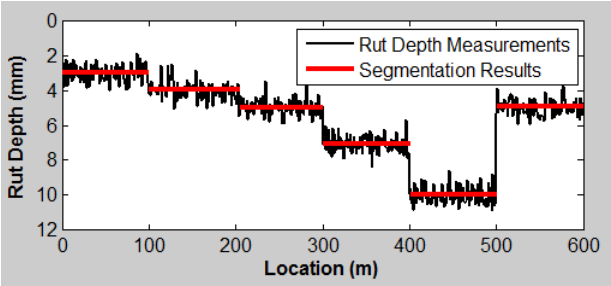

Figure A-5 Segmentation results for a large-variance dataset

A.1.2 Processing Time of MTOSC

The MTOSC was tested using synthetic datasets containing rut depth measurements varying from 500 to 5,000. The test results are summarized in Figure A-6.

As the problem size (i.e., the total number of rut depth measurements within the dataset) increases, the processing time increases exponentially. Therefore, there is a need for an approximation method or heuristic method to solve large-scale segmentation problems.

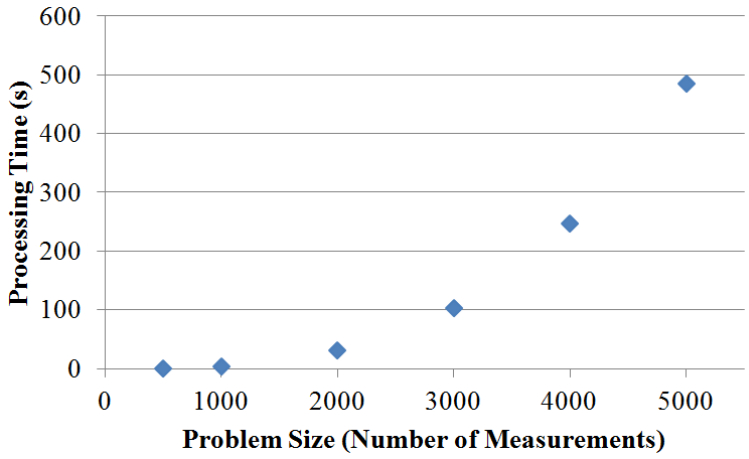

Figure A-6 Processing time versus problem size

A.2 Experimental Tests on the Overlapping-Reducing Heuristic Method

In this section, the overlapping-reducing heuristic method was tested using two synthetic datasets (large-scale and small-scale) and one real dataset. The small-scale synthetic datasets with known optimal segmentation solutions used to test the MTOSC was also used to test the accuracy and robustness of the heuristic method. Additionally, large-scale synthetic datasets were generated for test purposes. A real dataset from I-95 was tested to show the applicability of the heuristic method when it is used to solve real-world problems. The MTOSC was used as the benchmarking standard to evaluate the segmentation accuracy and robustness of the heuristic method.

Typically, the optimality gap was used to indicate how close a heuristic solution is to the optimal solution. It is defined as

$$Optimality\ Gap = \frac{\left|SSE_p - SSE_p^*\right|}{SSE_p^*}\text{, where } SSE_p^* \text{ is the optimal solution} \qquad \text{(A-2)}$$

In addition to the optimality gap, a new indicator, the accumulative segmentation error is proposed. The accumulative segmentation error is defined as the accumulative absolute distance between pairs of partition points, one from the optimal solution and the other one from a heuristic solution. Figure A-7 shows the two-step procedure to compute the accumulative segmentation error, which is described as follows:

- **Step 1**. For each partition point in a heuristic segmentation solution, find the nearest partition point in the optimal solution. The absolute distance between this pair of points (i.e., the number of measurements away from each other) is a portion of the accumulative segmentation error.
- **Step 2**. For each partition point in the optimal solution that has not been paired with any point in the heuristic solution, find the nearest partition point in the heuristic solution. The absolute distance between this pair of points is also counted as a portion of the segmentation error.

The accumulative segmentation error equals the sum of absolute distances between pairs of partition points. It is the sum of distances from Δ_1 to Δ_5 for the example shown in Figure A-7. Compared to the optimality gap, this accumulative segmentation error is more intuitively and directly related to the engineering meaning of segmentation accuracy.

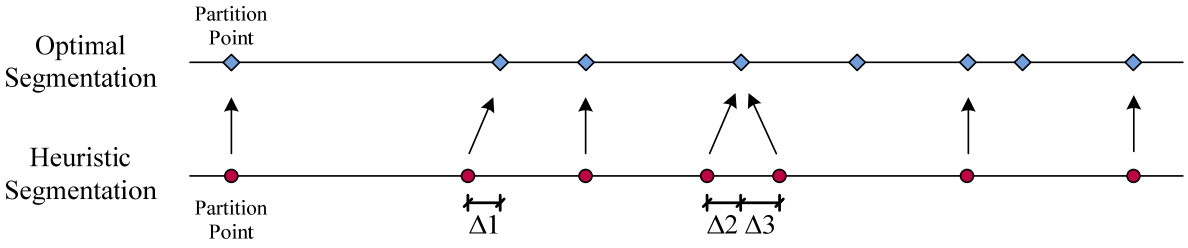

(a) Step 1

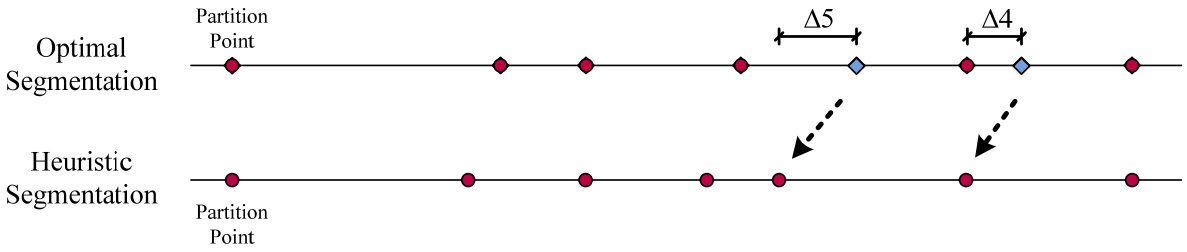

(b) Step 2

Figure A-7 Illustration of the accumulative segmentation error

Both the heuristic method and the MTOSC were implemented in C language and compiled by Visual C++ 2008. All tests were run on a personal computer with Windows XP Professional, 1.0 G RAM, and an Intel Core2 CPU with 1.86 GHz.

A.2.1 Tests on Small-scale Synthetic Datasets

This section presents tests on the small-scale synthetic datasets (i.e., the ones generated in the previous section) to quantitatively assess the accuracy and robustness of the heuristic method. Two hundred small-scale datasets, each of which consisted of 600 rut depth measurements (m=600), were tested. The minimum segment length was set to be 50 m and the minimum difference was 0.5 mm. Different levels of overlap between two successive segments, including 90%, 80%, 70%, 60%, 50%, 40% 30%, and 20%, were tested to suggest an appropriate overlap level that leads to significant reduction of processing time without compromising much of the segmentation accuracy and robustness. The overlap level was defined as the following:

$$Overlap = \frac{L-g}{L} * 100\% \tag{A-3}$$

where L is the minimum segment length and g is the shift between two successive segments.

Table A-1 and Figure A-8 summarize the test results. The test results show that as the overlap level decreases from 98% to 90% (i.e., from a 1-measurement shift to a 5-measurement shift), the mean processing time is reduced by more than 10 times, but the

mean optimality gap and mean accumulative segmentation error does not increase much. If the overlap level keeps decreasing, the mean processing time gradually becomes stable. The mean optimality gap and accumulative segmentation error increases significantly when the overlap level is 70% or drops to 40% or lower. This is because the length of homogeneous segments in these datasets is fixed, and the shifts, e.g., a 5-measurement shift and a 10-measurement shift, are all factors of the fixed segment length.

Table A-1 Test Results on Small-scale Synthetic Datasets

	Overlap (%)		98	90	80	70	60	50	40	30	20
Small-Variance Datasets	Optimality Gap	Mean	0.0	0.9	0.9	3.1	0.9	0.9	7.2	8.8	12.3
		Std	0.0	0.0	0.0	0.1	0.0	0.0	0.3	0.3	0.4
	Accumulative Segmentation Error	Mean	0	5	5	21	5	5	41	54	60
		Std	0	0	0	0	0	0	0	0	1
	Processing Time (s)	Mean	1.6	0.2	0.1	0.1	0.0	0.0	0.0	0.0	0.0
		Std	2.3	0.1	0.1	0.0	0.0	0.0	0.0	0.0	0.0
Large-Variance Datasets	Optimality Gap	Mean	0.0	0.2	0.2	0.7	0.2	0.2	1.8	2.0	3.0
		Std	0.0	0.0	0.0	0.1	0.0	0.0	0.2	0.2	0.2
	Accumulative Segmentation Error	Mean	0	5	5	22	5	5	47	76	62
		Std	0	1	1	6	1	1	16	29	11
	Processing Time (s)	Mean	1.4	0.2	0.1	0.1	0.1	0.0	0.0	0.0	0.0
		Std	1.1	0.4	0.2	0.2	0.1	0.1	0.1	0.1	0.0

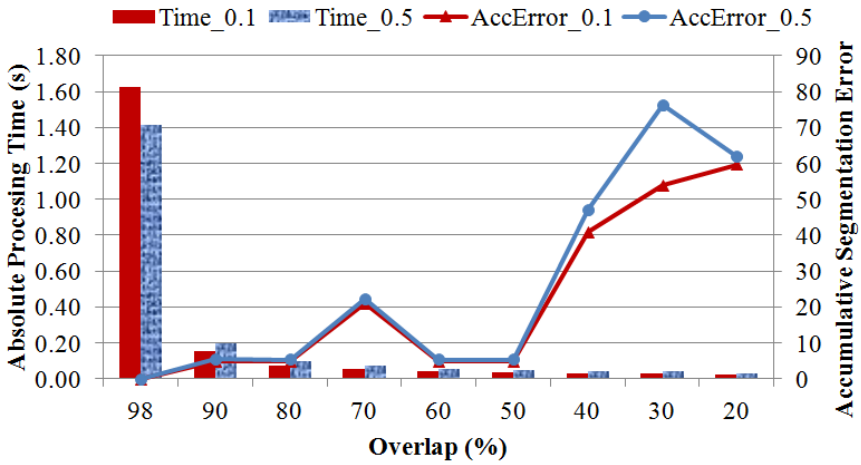

Figure A-8 Test results on synthetic datasets

Figure A-9 shows the 25th, 50th, and 75th percentiles of accumulative segmentation error and optimality gap for small-variance datasets and Figure A-10 shows percentiles for large-variance datasets. As shown in the figures, the differences between the 25th and 75th percentiles are very small. This is understandable, since the lengths and means of homogeneous segments are fixed and datasets with the same variance are highly similar to each other.

One extraordinarily big difference between the 25th and 50th percentiles of the accumulative segmentation error is observed in Figure A-9(b) for the large-variance datasets when the overlap is 30%. The histogram of accumulative segmentation error is shown in Figure A-11. It is found that the segmentation errors are split into two extremes: one is around 55 and the other one is around 155. Figure A-12 shows examples of these two extremes. Figure A-12(a) shows the optimal solution and the heuristic solution when the overlap is 30% for the 11th of the 100 large-variance datasets, and Figure A-12(b) shows the segmentation solutions when the overlap is 30% for the 19th dataset. By comparing Figure A-12(a) and (b), it is found that the heuristic method is sensitive to the variance of rut depth measurements when the overlap level is 30%. When the overlap level decreases to 20%, there might be limited feasible segmentation solutions, so the heuristic method is not sensitive to the variance.

Moreover, although there is a significant difference between the 25th and 50th percentiles of the accumulative segmentation error when the overlap level is 30%; there is no such big difference for the optimality gap shown in Figure A-10(b). In Figure A-12, two datasets with a similar optimality gap but highly different accumulative segmentation errors are visually inspected. It is observed that the heuristic segmentation solution in the 11th dataset is closer to the optimal solution than in the 19th dataset. This indicates that

the accumulative segmentation error is a potentially better measurement of the closeness of a heuristic solution to the optimal solution.

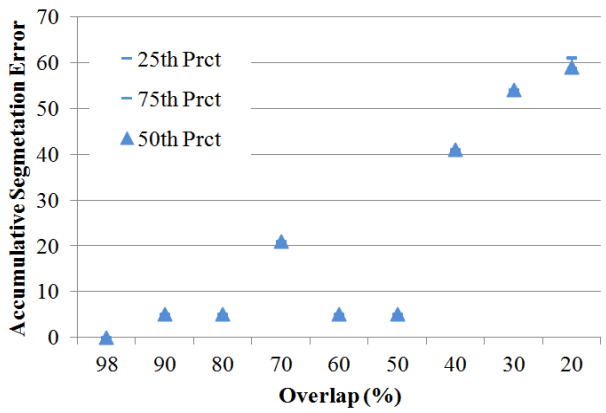

(a) Small-variance datasets

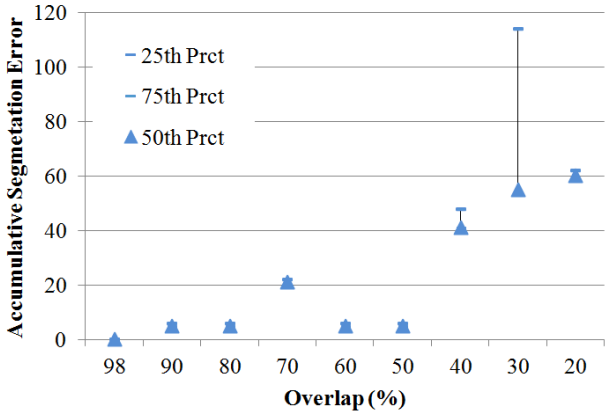

(b) Large-variance datasets

Figure A-9 Test results on synthetic datasets (Continued)

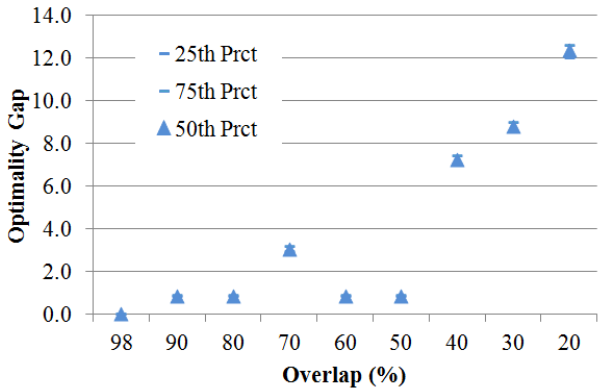

(a) Small-variance datasets

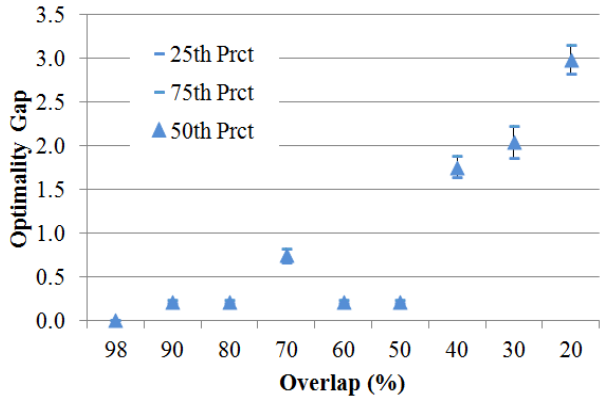

(b) Large-variance datasets

Figure A-10 Test results on synthetic datasets (Continued)

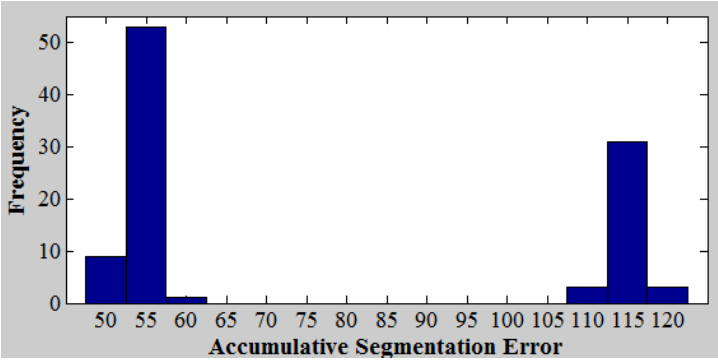

Figure A-11 Histogram of accumulative segmentation error when the overlap is 30%

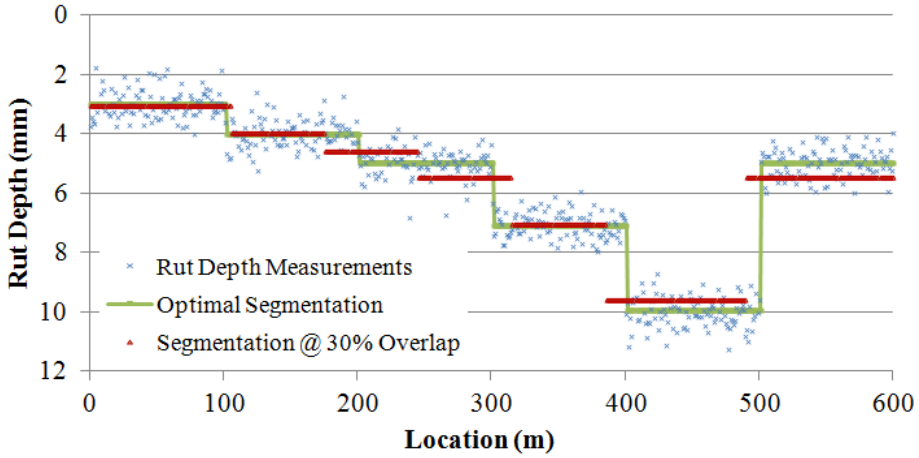

(a) 11th dataset (optimality gap = 2.1 and accumulative segmentation error = 114)

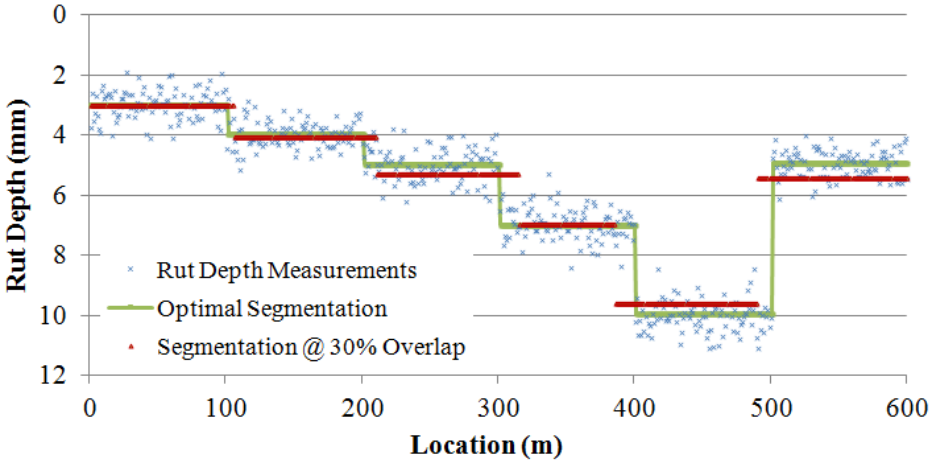

(b) 19th dataset (optimality gap = 2.1 and accumulative segmentation error = 54)

Figure A-12 Comparison of optimality gap and accumulative segmentation error

A.2.2 Tests on Large-scale Synthetic Datasets

This subsection presents tests on large-scale synthetic datasets to quantitatively assess the heuristic method. Each large-scale synthetic dataset consisted of 5,000 rut depth measurements (m = 5000). One hundred large-scale datasets were generated by fixing the overall length of each dataset and drew pseudorandom values from the standard uniform distribution on the open intervals (0, 5000) and (0, 50) as the lengths and means of homogeneous segments, respectively, for each large-scale dataset. The standard deviation within each homogeneous segment was set as 1 mm. The minimum segment length was set to 50 m and the minimum difference was 10 mm. Different levels of overlap between two successive segments, including 90%, 80%, 70%, 60%, 50%, 40% 30%, and 20%, were tested.

Table A-2 and Figures A-9 and A-10 summarize the test results on large-scale synthetic datasets. The test results show a trend that when the overlap level decreases from 98% to 90% (i.e., from a 1-measurement shift to a 5-measurement shift), the mean processing time is reduced by almost 10 times. Processing a dataset with 5,000 measurements originally took close to 10 minutes, but now takes approximately 1 minute. Meanwhile, the mean optimality gap and mean accumulative difference did not increase much. As the overlap level keeps decreasing, the mean processing time gradually goes flat, and the optimality gap and the accumulative difference keep increasing almost linearly. The standard deviation also increases almost linearly. The test results indicate that the reduction of processing time gradually becomes marginal at a cost of constantly-increasing segmentation error. Therefore, setting a 90% overlap between two successive segments may achieve an acceptable balance of benefit and cost.

Table A-2 Test Results on Large-scale Synthetic Datasets

Overlap (%)		98	90	80	70	60	50	40	30	20
Optimality Gap	Mean	0.0	0.2	0.5	0.9	1.2	1.4	1.9	2.4	3.0
	Std	0.0	0.2	0.3	0.5	0.6	0.8	1.1	1.3	1.6
Accumulative	Mean	0	105	192	344	412	430	591	732	856

Segmentation Error	Std	0	125	142	196	195	183	263	336	417
Processing Time (s)	Mean	487	58	26	16	12	9	7	6	5
	Std	9	1	0	0	0	0	0	0	0

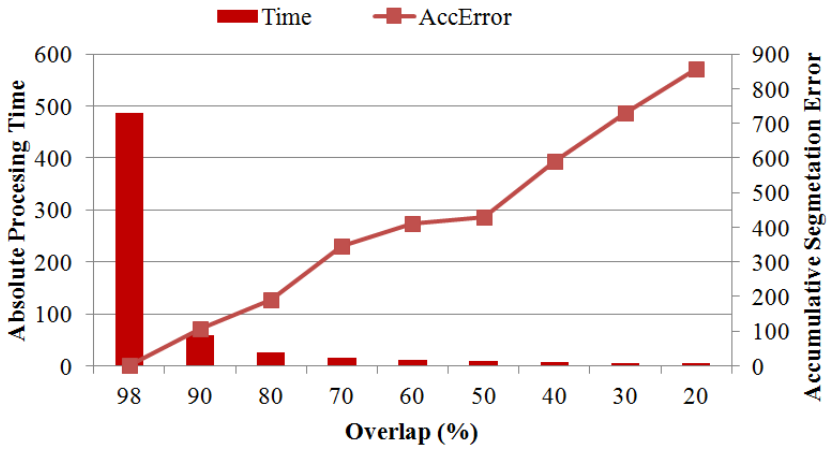

Figure A-13 Test results on large-scale synthetic datasets

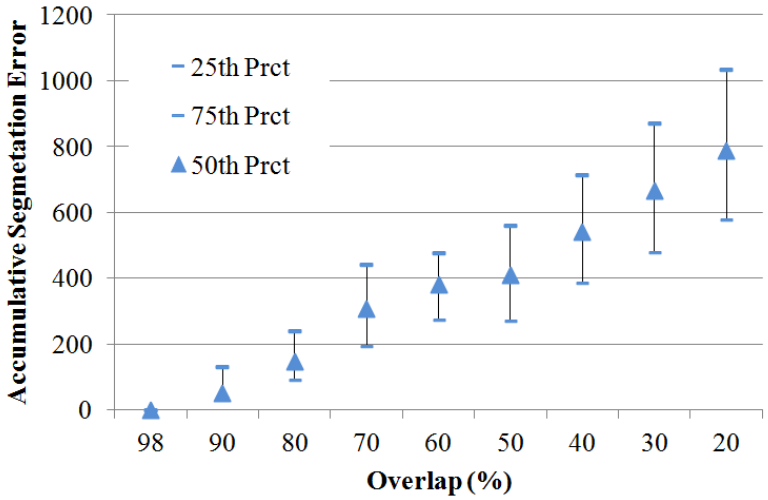

Figure A-14 Test results on large-scale synthetic datasets (Continued)

A.2.3 Tests on a Real Dataset

To assess the applicability of the heuristic method in real-world problems, actual rut data collected by the 3D line laser system from I-95 (from Milepost 101 to Milepost 100) near Savannah, Georgia, were tested. The raw rut depth data were collected at 5 mm intervals along the driving direction, and the mean rut depth for every 1-ft long section

was reported. This dataset contained 5,350 measurements (m = 5350). The optimal number of homogeneous sections was unknown. Four sets of the minimum segment length and minimum difference between the means of adjacent segments were tested: 100 ft and 1.53 mm; 50 ft and 1.53 mm; 10 ft and 1.53 mm; and 10 ft and 3.17 mm.

The test results, when D is fixed to be 1.53 mm, are summarized in Figure A-15. As shown in Figure A-15, the majority of the processing time reduction occurs when the overlap drops from 98% to 90%. The relationship between the overlap and accumulative segmentation error is not fixed. The accumulative segmentation error increases almost linearly as the overlap increases linearly when L is 50 ft; it is not a linear relationship when L is 100 ft. Figure A-16 shows the test results when L is fixed to be 10 ft and D changes from 1.53 mm to 3.17 mm. The test results show that as the minimum difference increases, the number of feasible segmentation solutions is significantly reduced, and, therefore, the accumulative segmentation error becomes insensitive to the overlap level.

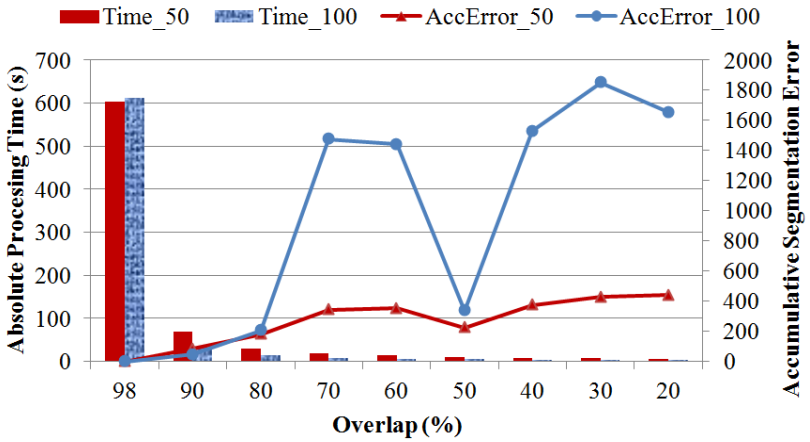

Figure A-15 Test results for the real dataset (D = 1.53 mm)

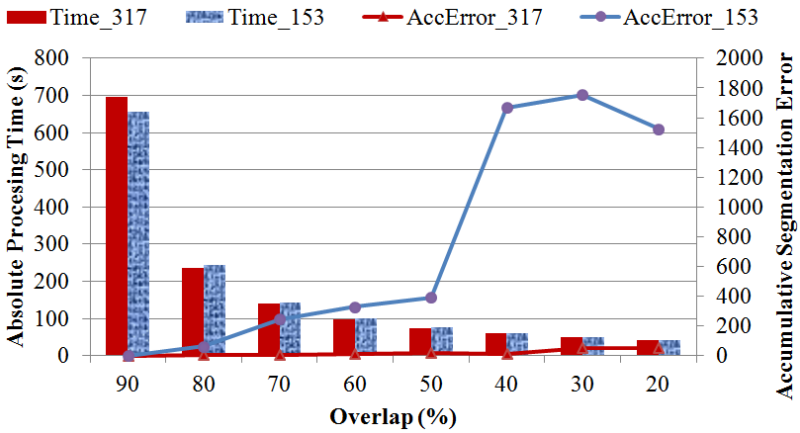

Figure A-16 Test results for the real dataset (L = 10 ft)

Figures from A-13 to A-17 visualize the segmentation results. The red curve is the rut depth measurements reported at 1-ft intervals, and each blue line is the mean rut depth for the corresponding homogeneous segment. It is noted that the MTOSC provides an intuitively reasonable segmentation solution. It captures the ups and downs in the real dataset and preserves as many details as possible. The heuristic method can provide a highly similar segmentation solution when the overlap is 90%.

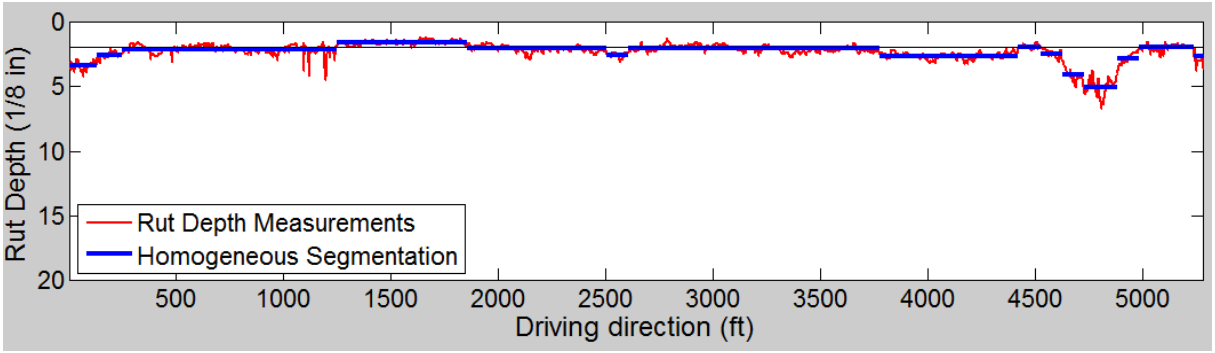

Figure A-17 Segmentation results for a real dataset (L = 100 ft, D = 1.53 mm, and *overlap* = 99%)

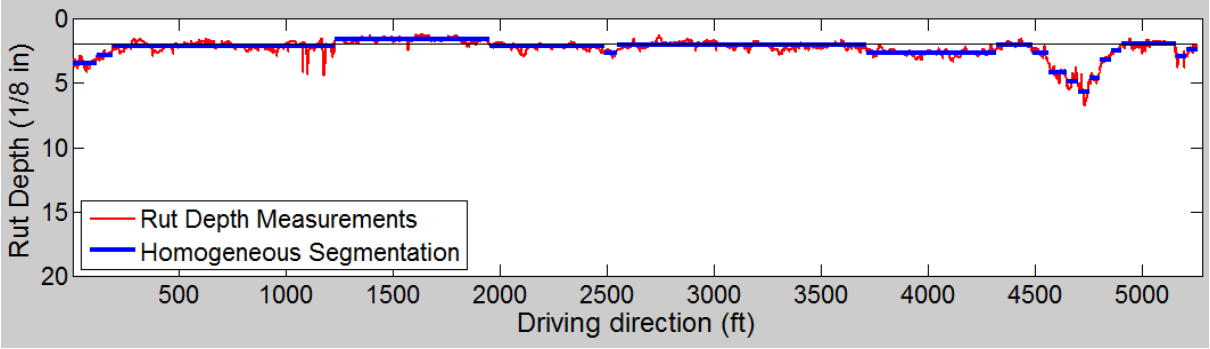

Figure A-18 Segmentation results for a real dataset (L = 50 ft, D = 1.53 mm, and *overlap* = 98%)

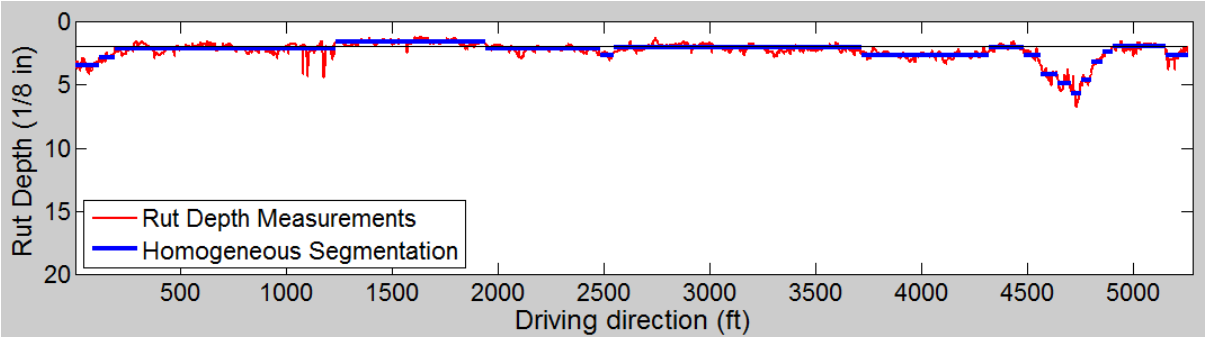

Figure A-19 Segmentation results for a real dataset (L = 50 ft, D = 1.53 mm, and *overlap* = 90%)

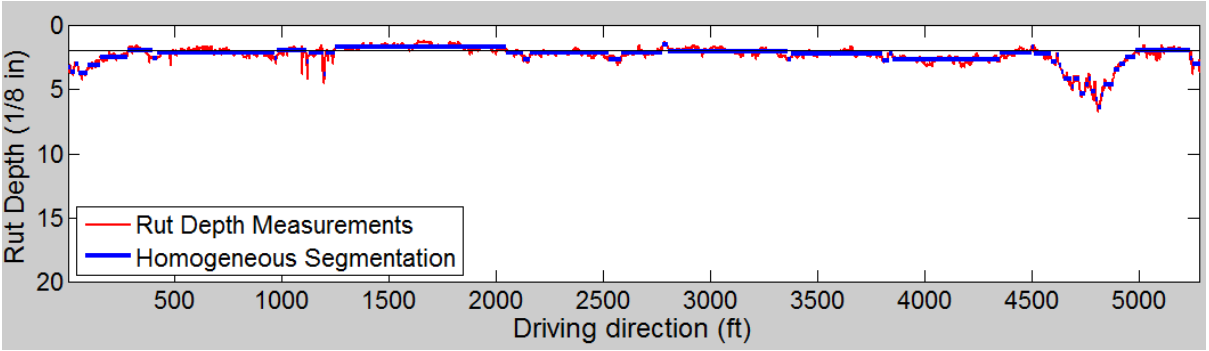

Figure A-20 Segmentation results for a real dataset (L = 10 ft, D = 1.53 mm, and *overlap* = 90%)

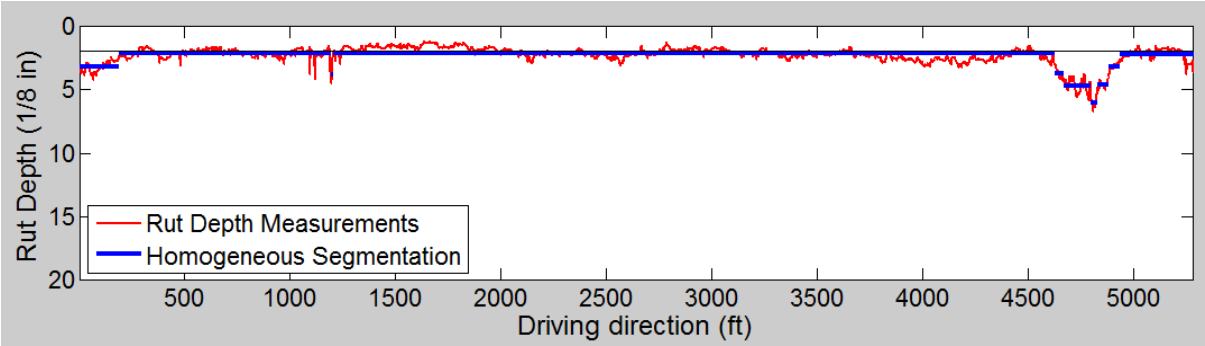

Figure A-21 Segmentation results for a real dataset (L = 10 ft, D = 3.17 mm, and *overlap* = 90%)

Engineers' inputs are very important for determining a sensible segmentation of the pavement rutting data. The system allows engineers to flexibly provide the desirable minimal segment length based on their specific pavement management practices.

A.3 Summary

This appendix presents experimental tests on the MTOSC and the overlapping-reducing heuristic method proposed in Chapter 6. Both synthetic datasets with known optimal segmentation solution and real datasets are used to test the methods. The findings are summarized as follows:

MTOSC can provide the optimal segmentation solution even in the presence of data noise. Test results show that the MTOSC provides the optimal homogeneous segmentation successfully for 200 small-scale synthetic datasets. The test results demonstrate that the MTOSC can provide the optimal solution and is promising as a benchmarking standard with which to evaluate the accuracy of heuristic or approximation methods. In addition, the MTOSC method has the following advantages. First, the method provides the flexibility of adjusting the minimum difference and minimum segment length constraints to take into account important engineering considerations. Second, it does not make any assumption on the distribution of the input data, such as the

Cox distribution (Mishalani and Koutsopoulos 2002) or normal distribution (Thomas 2005).

Although the MTOSC can provide the optimal segmentation solution, it takes exponentially-increasing processing time as the problem size (i.e., the total number of rut depth measurements within the dataset) increases. To solve large-scale segmentation problems, an overlapping-reducing method is proposed in Chapter 6. This heuristic method was tested using small-scale and large-scale synthetic datasets, as well as a real dataset from I-95. The MTOSC is used as the benchmarking standard. Besides the traditionally-used optimality gap, a new indicator, the accumulative segmentation error, is proposed and was utilized to quantitatively assess the segmentation accuracy and robustness of the heuristic method. Test results show that the heuristic method can shorten the processing time by reducing the overlap between two successive segments at a cost of increasing accumulative segmentation error. When the overlap between two successive segments is reduced from 98% to 90%, the heuristic method can shorten the processing time by approximately 10 times without compromise of much segmentation accuracy. The test results on a real dataset are intuitively reasonable, which demonstrates the applicability of the MTOSC and the heuristic method in real-world problems. Moreover, it is found that compared with the optimality gap, the accumulative segmentation error is a potentially better measurement of the closeness of a heuristic solution to the optimal solution.

It is recommended that future studies (1) compare the proposed overlapping-reducing heuristic method with other heuristic methods, such as CDA, and (2) extend the MTOSC and the heuristic method to analyze other roadway condition measurements, such as skid resistance.

REFERENCES

AASHTO. (1986). *Guide for Design of Pavement Structures*, Washington, DC, pp III-17–III-20 and Appendix J.

AASHTO. (1993). *Guide for Design of Pavement Structures*, Washington, DC, pp III-19–III-24 and Appendix J.

AASHTO. (2001). *Pavement Management Guide,* American Association of State Highway and Transportation Officials (AASHTO), Washington, D.C.

AASHTO. (2010). "Standard Practice for Determining Pavement Deformation Parameters and Cross Slope from Collected Transverse Profiles." *AASHTO PP69-10,* American Association of State Highway and Transportation Officials (AASHTO), Washington, D.C.

ADOT (2002). *Terms of Reference, Pavement Rut Depth, Roughness,GPS, Calibration, and Verification Sites*. Alberta Department of Transportation (ADOT), Edmonton, Alberta, Canada.

Ali, H., and Tayabji, S. (1998). "Evaluation of Mechanistic-Empirical Performance Prediction Models for Flexible Pavements." *Transportation Research Record: Journal of the Transportation Research Board*, 1629(-1), 169-180.

Aoki, K., Hamabe, T., Satoh, S., and Akatu, Y. (1998). "Active vibration control apparatus for vehicle." Patent Number 5792948, Nissan Motor Co. Ltd. (Yokohama, Japan), United States.

Archilla, A., and Madanat, S. (2000). "Development of a Pavement Rutting Model from Experimental Data." *Journal of Transportation Engineering*, 126(4), 291-299.

Archilla, A. R. (2000). "Development of Rutting progression Models by Combining Data from Multiple Sources." Ph.D. Dissertation, Department of Civil and Environmental Engineering, University of California, Berkeley, San Francisco, CA.

ASTM. (2005). "Standard Test Method for Measuring Road Roughness by Static Level Method." *ASTM E1364 - 95(2005)*, American Society for Testing and Materials (ASTM), West Conshohocken, PA.

ASTM. (2010). "Standard Test Method for Measuring Rut-Depth of Pavement Surfaces Using a Straightedge." *ASTM E1703/E1703M*, American Society for Testing and Materials (ASTM), West Conshohocken, PA.

ASTM. (2010). "Standard Practice for Preparing Precision and Bias Statements for Test Methods for Construction Materials." *ASTM C670-10*, American Society for Testing and Materials (ASTM), West Conshohocken, PA.

Austroads. (2007). *AG:AM/T010: Validation of a Multi-Laser Profilometer for Measuring Pavement Rutting (Reference Device Method)*. Austroads, Sydney, Australia.

Bellman, R. (1973). “A note on cluster analysis and dynamic programming.” *Mathematical Biosciences*, 18(3–4), 311–312.

Bennett, C. (2004). “Sectioning of road data for pavement management.” *Proceedings of 6th International Conference on Managing Pavements: "the Lessons, the Challenges, the Way Ahead"*, October 19-24, 2004, Brisbane, Queensland, Australia, (CD-Rom), <http://www.lpcb.org/lpcb-downloads/papers/2004_pms.pdf>.

Byrne, M., Albrecht, D., Sanjayan, J., and Kodikara, J. (2009). “Recognizing Patterns in Seasonal Variation of Pavement Roughness Using Minimum Message Length Inference.” *Computer-Aided Civil and Infrastructure Engineering*, 24(2), 120-129.

Cenek, P., Patrick, J., McGuire, J., and Robertson, D. (1994). “New Zealand Experience in Comparing Manual and Automatic Pavement Condition Rating Systems.” *Proceedings of Third International Conference on Managing Pavements,* May 22-26, 1994, San Antonio, TX, Transportation Research Board.

Chen, D. H., Bilyeu, J., Walker, D., and Murphy, M. (2001). "Study of Rut-Depth Measurements." *Transportation Research Record: Journal of the Transportation Research Board*, 1764(-1), 78-88.

Chellappan, K. V., Erden, E., and Urey, H. (2010). "Laser-based displays: a review." *Applied Optics*, 49(25), F79-F98.

Chu, C. Y., and Durango-Cohen, P. L. (2008). "Empirical Comparison of Statistical Pavement Performance Models." *Journal of Infrastructure Systems*, 14(2), 138-149.

CIA. (2012). "The World Factbook." Central Intelligence Agency (CIA), updated May 9, 2012, <https://www.cia.gov/library/publications/the-world-factbook/geos/us.html>, accessed May 12, 2012.

Clarke, T. A., Cooper, M., and Fryer, J. F. (1993). "An estimator for the random error in subpixel target location and its use in the bundle adjustment." *Optical 3-D measurement techniques II*, Pub. Wichmann, Karlsruhe, 161-168.

Cuhadar, A., Shalaby, A., and Tasdoken, S. (2002). "Automatic segmentation of pavement condition data using wavelet transform." *IEEE Canadian Conference in Electrical and Computer Engineering (CCECE2002)*, 2, 1009-1014.

Dierickx, B. (2000). "Cmos image sensors: concepts and limits." *A short course given at Photonics West 2000*.

Divinsky, M., Nesichi, S., and Livneh, M. (1997). "Development of a road roughness profile delineation procedure." *Journal of Testing and Evaluation*, 25(4), 445-450.

Dorsch, R., Hausler, G., and Herrmann, J. (1994). "Laser triangulation: fundamental uncertainty in distance measurement." *Applied Optics*, 33(7), 1306-1314.

El Gendy, A. and Shalaby A. (2008). “Using quality control charts to segment road surface condition data.” *International conference on managing paving assets (ICMPA2008)*, Calgary, AB.

FHWA. (2003). *Distress Identification Manual for the Long-Term Pavement Performance Program*, Federal Highway Administration (FHWA), Washington, D.C.

Forest Collado, J. (2004). "New Methods for Triangulation-based Shape Acquisition using Laser Scanners." Ph.D. Dissertation, Universitat de Girona.

Friedman, J. (1991). “Multivariate Adaptive Regression Splines.” *The Annals of Statistics*, 19(1), 1–67.

Gao, B. (2004). "A GIS-Enabled Multi-Year Pavement Rehabilitation Needs Analysis System." Ph.D. Dissertation, School of Civil and Environmental Engineering, Georgia Institute of Technology, Atlanta, GA.

GDOT. (2007). *Manual of Pavement Condition Evaluation System*. Georgia Department of Transportation (GDOT), Atlanta, GA.

Gey, S., and Lebarbier, E. (2002). “A CART Based Algorithm for Detection of Multiple Change Points in the Mean for Large Samples.” *Prépublication d’Orsay*, 2002(10), Université Paris d’Orsay, France.

Gisi, A. J. (2011). "2011 Kansas NOS Condition Survey Report." Kansas Department of Transportation, Topeka, KS.

Grondin, M., Leroux, D., and Laurent, J. (2002). “Advanced 3D Technology for Rut Measurements: Apparatus on Board of the Quebec Ministry of Transportation Multifunction Vehicle.” <http://pms.nevadadot.com/2002presentations/40.pdf>, accessed August 10, 2011.

Guidi, G., Russo, M., Magrassi, G., and Bordegoni, M. (2010). "Performance Evaluation of Triangulation Based Range Sensors." *Sensors*, 10(8), 7192-7215.

Haas, R., Hudson, W. R., and Zaniewski, J. (1994). *Modern Pavement Management*. Krieger Publishing Company, Malabar, Florida.

Hallett, J. and Robieson, P. (1996). “Trial of High Speed Data Collection Vehicle: 1996 Validation Report.” Beca Carter Hollings & Ferner Ltd., Auckland.

Hossain, K. V. M., Reigle, J., and Miller, R. (2002). "Comparison of 3-point and 5-point Rut Depth Data Analysis." *Pavement Evaluation 2002 Conference*, Roanoke, Virginia.

HTC. (2001). “Validation of ROMDAS transverse profile logger.” *Internal Report F003/1*, HTC Infrastructure Management Ltd., Auckland.

Huang, Y., Hempel, P., and Copenhaver, T. (2012). "Texas Department of Transportation 3D Transverse Profiling System for High Speed Rut Measurement." *Journal of Infrastructure Systems*, (accepted manuscript).

INO. (2010). *LCMS Data Processing Library: User Manual (Rev 1.3)*. INO, Pavemetrics Systems inc., Quebec City, Quebec, Canada.

INO. (2012). *LCMS Hardware and Software Installation Manual (Rev 2.0),* INO, Pavemetrics Systems inc., Quebec City, Quebec, Canada.

INO. (2012). *LRMS – Laser Rut Measurement System*. INO, Pavemetrics Systems inc., Quebec City, Quebec, Canada, <http://www.pavemetrics.com/en/lrms.html>, accessed May 10, 2012.

INO. (2012). *LCMS - Laser Crack Measurement System*. INO, Pavemetrics Systems inc., Quebec City, Quebec, Canada, <http://www.pavemetrics.com/en/lcms.html>, accessed May 10, 2012.

Jensen, R. E. (1969). "A dynamic programming algorithm for cluster analysis." *Operations Research*, 17(6), 1034–1057.

Jameson, G. W., Baran, E., and Sheldon, G. W. (1989). "Australian Experience with the Swedish Laser Road Surface Tester." *14th ARRB Conference*. Vermont South, Victoria, Australia.

Kamplade, J. (1990). “Analysis of Transverse Unevenness with Respect to Traffic Safety.” *Surface Characteristics of roadways: International research and technologies.* W. E. Meyer and J. Reichert, ed., American Society for Testing and Materials (ASTM), Philadelphia, PA, 198-210.

Ksaibati, K. (1996). “Comparison of Rut-Depth Measurements Obtained with Four Different Techniques.” *Road and Transport Research*, 5(2), 80-91.

Kerali, H. R., Robinson, R., and Paterson, W. (1988). “Role of the new HDM-4 in highway management.” *Proceedings of the 4th International Conference on Managing Pavements*, 2, 801–814.

Kim, S., Damnjanovic, I., and Gunby, M. (2010). “Effects of Pavement Spatial Variability on Contractor's Management Strategies.” *Journal of Infrastructure Systems*, 16(4), 231-240.

Kwang-Ho, B., Belton, D., and Lichti, D. D. (2009). "A Closed-Form Expression of the Positional Uncertainty for 3D Point Clouds." *IEEE Transactions on Pattern Analysis and Machine Intelligence*, 31(4), 577-590.

Latimer, D., Manoharan, S., Nata-Atmadja, A., and Robertson, N. (2004). “A Study of the Impact of Road Segmentation Schemas on Predicted Maintenance Investment Outcomes.” *Proceedings of the 6th International Conference on Managing Pavements, The Lessons, The Challenges, The Way Ahead*, R. Gordon, ed., Brisbane, Queensland.

Laurent, J., Talbot, M., and Doucet., M. (1997). “Road Surface Inspection Using Laser Scanners Adapted for the High Precision 3D Measurements of Large Flat Surfaces.” *IEEE Proceedings of the International Conference on Recent Advances in 3-D Digital Imaging and Modeling*, 303-310.

Laurent, J., Lefebvre, D., and Samson, E. (2008). "Development of a New 3D Transverse Laser Profiling System for the Automatic Measurement of Road Cracks." *Proceedings of 6th Symposium on Pavement Surface Characteristics (SURF 2008)*, Portoroz, Slovena, Europe, 20-22 October 2008.

Lebas, M., Peybernard, J., and Carta, V. (1981). “Méthode de traitments des enregistrements de mesure de densité en continu.” Bull. Liaison Labo. P. et Ch, 114, 8–10.

Li, F. and Tsai, Y. (2012). “An Optimal Solution for Benchmarking Homogeneous Pavement Rutting Segmentation Using Shortest Path Algorithm.” *Computer-Aided Civil and Infrastructure Engineering*, (Submitted).

Li, Q., Yao, M., Yao, X., Yu, W., and Xu, B. (2009). “A Real-time 3D Scanning System for Pavement Rutting and Pothole Detections.” *Proceedings of SPIE: Videometrics, Range Imaging, and Applications X*, 74470B-74479.

Li, Q., Liu, Y., and Mao, Q. (2009). "Design and Applications of an Integrated Multi-sensor Mobile System for Road Surface Condition Detection." *Geospatial Technology for Earth Observation*, D. Li, J. Gong, and J. Shan, ed., Springer-Verlag New York, LLC, 45-61.

Li, Q., Yao, M., Yao, X., and Xu, B. (2010). "A real-time 3D scanning system for pavement distortion inspection." *Measurement Science and Technology*, 21(1), 015702.

Linares, J. M., Bourdet, P., and Sprauel, J. M. (2000). “Quality measurement on CMM integrated design and manufacturing in mechanical engineering.” *Proceedings of Integrated Design and Manufacturing in Mechanical Engineering (IDMME’2000)*, Kluwer Academic Publishers, 219-226.

Mallela, R., and Wang, H. (2006). "Harmonising Automated Rut Depth Measurements - Stage 2." *Land Transport New Zealand Research Report 277*, Data Collection Ltd., New Zealand.

Shortis, M. R., Clarke, T. A., and Short, T. (1994). "Comparison of some techniques for the subpixel location of discrete target images." *Proceedings of SPIE: Videometrics III*, Sabry F. El-Hakim ed., 2350, 239-250.

Mavrinac, A., Chen, X., Denzinger, P., and Sirizzotti, M. (2010). “Calibration of dual laser-based range cameras for reduced occlusion in 3D imaging.” *Proceedings of the IEEE/ASME International Conference on Advanced Intelligent Mechatronics*, 79 – 83.

McGhee, K. (2004). "Automated Pavement Distress Collection Techniques: A Synthesis of Highway Practice." *NCHRP Synthesis 334*, National Coorperative Highway Research Program (NCHRP), Transportation Research Board, Washington, D.C.

Mishalani, R. and Koutsopoulos H. (2002). "Modeling the spatial behavior of infrastructure condition." *Transportation Research Part B: Methodological*, 36(2), 171-194.

Misra, R. and Das, A. (2003). "Identification of Homogeneous Sections from Road Data." *International Journal of Pavement Engineering*, 4(4), 229 - 233.

Naidu, D. K. and Fisher, R. B. (1991). "A Comparative Analysis of Algorithms for Determining the Peak Position of a Stripe to Sub-pixel Accuracy." In *Proceedings of the British Machine Vision Conference (BMVC)*, 217-225.

NCHRP. (2009). "Quality Management of Pavement Condition Data Collection: A Synthesis of Highway Practice." *NCHRP Synthesis 401*, National Coorperative Highway Research Program (NCHRP), Transportation Research Board, Washington, D.C.

Novick, B. (2009). "Norm statistics and the complexity of clustering problems." *Discrete Applied Mathematics*, 157(8), 1831-1839.

ODOT. (2010). *Oregon Department of Transportation - Distress Survey Manual*. Oregon Department of Transportation (ODOT), <http://www.oregon.gov/ODOT/HWY/CONSTRUCTION/docs/pavement/Distress_Survey_Manual.pdf?ga=t>, accessed November 07, 2010.

Pat Noyes & Associates. (1998). *Traffic Calming Primer*. <http://patnoyes.com/Library/Traffic%20Calming%20Primer.pdf>, accessed April 22, 2012.

Pathway Services Inc. (2012). *Pathway 3D Pavement Surface Imaging with Depth for Rutting, Cracking and Faulting*. <http://www.pathwayservices.com/3D_imaging.shtml>, accessed May 10, 2012.

PennDOT. (2010). *Automated Pavement Condition Survey Field Manual*. Pennsyvania Department of Transportation (PennDOT), Harrisburg, PA.

Phoenix Scientific Inc. (2010). *Unification of Roadway Surface Dimensional Measurements*. <http://www.phnx-sci.com/PPS/New_Paradigm_files/New%20Paradiam%202010_0121.pdf>, accessed May 10, 2012.

Phoenix Scientific Inc. (2004). *Pavement Profile Scanner White Paper*. <http://www.phnx-sci.com/PPS/Road_Condition_files/PPS%20Technology%20%282004%29.pdf>, accessed May 10, 2012.

Ping, W., Yang, Z., Gan, L., and Dietrich, B. (1999). "Development of Procedure for Automated Segmentation of Pavement Rut Data." *Transportation Research Record: Journal of the Transportation Research Board*, 1655(-1), 65-73.

Prozzi, J. A. (2001). "Modeling pavement performance by combining field and experimental data." Ph.D. Dissertation, Department of Civil and Environmental Engineering, University of California, Berkeley, San Francisco, CA.

Rao, M. R. (1971). "Cluster analysis and mathematical programming." *American Statistical Association*, 66, 622–626.

Rada, G. R., Wu, C. L., Bhandari, R. K., Shekharan, A. R., Elkins, G. E., and Miller, J. S. (1999). "Study of LTPP distress data variability." *Report No. FHWA-RD-99-074*, Volume 1, Office of Infrastructure Research and Development, FHWA, McLean, VA.

Rübensam, J., and Schulze, F. (1996). "Entwicklung einer Methodik zur zweckmäßigen Zusammenfassung maßnahmebedürftiger Abschnitte der BAB-Betriebsstrecken auf der Grundlage von Zustands- und Bestandsdaten." *Heft* 736, Bundesministerium für Verkehr, Abteilung Straßenbau, Bonn-Bad Godesberg, Germany.

Shahin, M. (1994). *Pavement management for airports, roads, and parking lots*. Chapman and Hall, New York.

Smith, A. (1975). "A Bayesian approach to inference about a change-point in a sequence of random variables." *Biometrika*, 62(2), 407–416.

Simpson, A. (2001). "Measurement of Rutting in Asphalt Pavements." Ph.D. Dissertation, Department of Civil Engineering, University of Texas at Austin, Austin, TX.

Simpson, A. (2001). "Characterization of Transverse Profile." *FHWA-RD-01-024*, FHWA, U.S. Department of Transportation, Washington, D.C.

Start, M., Kim, J., and Berg, W. (1998). "Potential Safety Cost-Effectiveness of Treating Rutted Pavements." *Transportation Research Record: Journal of the Transportation Research Board*, 1629(-1), 208-213.

Stoffels, S., Morian, D., Frith, D. J., and Larson, C. D. (2001). "Quality analysis methods for pavement distress data." *Proceedings of the Transportation Research Board Annual Meeting,*CD-ROM, Transportation Research Board, Washington, D.C.

Selezneva, O., Mladenovic, G., Speir, R., Amenta, J., and Kennedy, J. (2004). "National Park Service Road Inventory Program: Quality Assurance Sampling Considerations for Automated Collection and Processing of Distress Data." *Transportation Research Record: Journal of the Transportation Research Board,* 1889(-1), 106-105.

Tejeda, S. V., Tampier, H. D., and Navarro, T. E. (2008). "Proposal of a segmentation procedure for skid resistance data." *Arabian Journal for Science and Engineering*, 33(1B), 89-104.

TxDOT. (2009). *Pavement Management Information System Rater's Manual for Fiscal Year 2010*. Texas Department of Transportation, Austin, TX.

Thomas, F. (2001). "A Bayesian approach to retrospective detection of change-points in road surface measurements." Ph.D. Dissertation, Department of Statistics, Stockholm University, Stockholm, Sweden.

Thomas, F. (2003). "Statistical approach to road segmentation." *Journal of Transportation Engineering*, 129(3), 300-308.

Thomas, F. (2004). "Generating Homogeneous Road Sections Based on Surface Measurements: Available Methods." Proc*eedings of 2nd European Pavement and Asset Management Conference*, Berlin, Germany.

Thomas, F. (2005). "Automated Road Segmentation Using a Bayesian Algorithm." *Journal of Transportation Engineering*, 131(8), 591-598.

Trucco, E., Fisher, R., and Fitzgibbon, A. (1994). "Direct Calibration and Data Consistency in 3-D Laser Scanning." *Proceedings of the 5th British Machine Vision Conference* (*BMVC94)*, Edwin Hancock, ed., Sheffield, BMVA Press, 489-498.

Trinder, J. C. (1989). "Precision of digital target location." *Photogrammetric Engineering and Remote Sensing*, 55(6), 883-886.

Tsai, Y., Li, F., Kaul, V., and Wang, Z. (2010). "Characterizing Point-based Transverse Pavement Rut Measurement Errors Using Emerging 3D Continuous Profile-based Laser Technology." *Proceedings of 2010 NDE/NDT for highways and bridges conference: Structural Materials Technology (SMT)*, August 16-20, 2010, New York, New York.

Tsai, Y., Li, F., Purcell, R., and Rabun, J. T. (2012). "Reliable Statewide Pavement Performance Study Using a Confidence Evaluation System." *Journal of Transportation Engineering*, 138(3), 339-347.

Vinod, H. D. (1969). "Integer programming and the theory of grouping." *Journal of the American Statistical Association*, 64, 506–519.

Wang, I., Tsai, Y., and Li, F. (2011). "A Network Flow Model for Clustering Pavement Segments and Minimizing Total Maintenance and Rehabilitation Costs." *Computer and Industrial Engineering*, 60(4), 593-601.

Wang, K. C. P. (2011). "Elements of automated survey of pavements and a 3D methodology." *Journal of Modern Transportation*, 19(1), 51-57.

Wang, K. C. P., Li, L., Luo, W., and Larkin, A. (2012). "Potential Measurement of Pavement Surface Texture Based on Three-Dimensional Image Data." *Proceeding of the 91st Transportation Research Board Annual Meeting,* January 22-26, 2012, Washington, D.C.

West, G. A. W., and Clarke, T. A. (1990). “A survey and examination of subpixel measurement techniques.” *Proceedings of SPIE: Close Range Photogrammetry Meets Machine Vision*, Zurich, Switzerland, 1395, 456-463.

Whaite, P., and Ferrie, F. P. (1990). "From uncertainty to visual exploration." *Proceedings of Third International Conference on Computer Vision,* 690-697.

White, T. D., Haddock, J. E., Hand, A. J. T., and Fang, H. (2002). "Contributions of Pavement Structural Layers to Rutting of Hot Mix Asphalt Pavements." *NCHRP Report 468*, Transportation Research Board, Washington, D.C.

Wikimedia Foundation Inc. (2012). “Speckle pattern.” In *Wikipedia: The Free Encyclopedia*. ed. on May 2 2012, <http://en.wikipedia.org/wiki/Speckle_pattern>.

Xia, J., and Chen, M. (2007). “A Nested Clustering Technique for Freeway Operating Condition Classification.” *Computer-Aided Civil and Infrastructure Engineering*, 22(6), 430-437.

Yang, C., Tsai, Y., and Wang, Z. (2009), “Algorithm for Spatial Clustering of Pavement Segments.” *Computer-Aided Civil and Infrastructure Engineering*, 24(2), 93-108.

VITA

Feng Li

Feng Li was born on September 26, 1983, in Hunan, China. She received a B.S. in Civil Engineering in 2005 and a M.S., specialized in geotechnical engineering, in 2007 from Tsinghua University, Beijing, China. She joined the doctorate program at Georgia Institute of Technology, Atlanta, Georgia, in 2007.

Her primary research focus is on Asset Management, with emphasis on Pavement Management System and non-destructive pavement condition assessment. Apart from her primary research, her research interests include geotechnical engineering, operations research, signal processing, imaging processing, and statistical analysis. She is currently a member of the Institute of Transportation Engineers (ITE).